UCRL-ID-104556
PATC-IR 89-06

CONSTITUTIVE MODELS AND DYNAMIC BEHAVIOR OF SOILS UNDER IMPACT LOADING CONDITIONS

December 31, 1989

C. Y. Chang, J. A. Egan*, J. C. Chen

Prepared for
U.S. Nuclear Regulatory Commission

*Geomatrix Consultants, Inc.,
One Market Plaza, Spear Street Tower, San Francisco, California, 94105

DISCLAIMER

This work was supported by the United States Nuclear Regulatory Commission under a Memorandum of Understanding with the United States Department of Energy.

PATC-IR 89-06

CONSTITUTIVE MODELS AND DYNAMIC BEHAVIOR OF SOILS UNDER IMPACT LOADING CONDITIONS

December 31, 1989

C. Y. Chang, J. A. Egan*, J. C. Chen

Prepared for
U.S. Nuclear Regulatory Commission

*Geomatrix Consultants, Inc.,
One Market Plaza, Spear Street Tower, San Francisco, California, 94105

ABSTRACT

On December 7, 1987, PSA Flight 1771 crashed to the ground on a hillside southwest of Paso Robles, California. The crash impact created a crater-like indentation in the ground, displacing a large quantity of soil and rock in the process. Although a disastrous event, this plane crash nevertheless affords an opportunity to utilize a well-documented case history to evaluate the behavior of geologic materials under such impact loading and to verify and calibrate methods used to analyze and test the integrity of proposed air transport container designs for shipment of plutonium nuclear fuel. This study, which is part of the overall analysis and verification effort for plutonium air transport package designs, characterizes the "harder" (i.e., stiffer and stronger) response of soils to high rates of loading and high levels of stress such as imposed by the impact of an airplane or other projectile. Data available in the published technical literature, as well as some unpublished data, have been examined and interpreted to provide a basis for quantifying the response to high strain rates and stress levels of soils at the PSA crash site and other sites that may be used for testing the integrity under high-speed ground impact of proposed plutonium air transport package designs. Geotechnical characterization of the PSA crash site soils has been performed based upon extensive field exploration, field penetration testing, and laboratory testing. The soils at the crash site consist of colluvium and residual soils formed by in-place weathering of rock, and the engineering properties and behavior of these soils are consistent with those of other similar soils. The characterized engineering properties have been used to develop site-specific parameters for implementation of analytical modeling of airplane crash impacts using the computer program DYNA3D.

TABLE OF CONTENTS

TABLE OF CONTENTS
(continued)

TABLE OF CONTENTS
(continued)

LIST OF TABLES

LIST OF FIGURES

LIST OF FIGURES
(continued)

EXECUTIVE SUMMARY

The Plutonium Air Transport Certification Project is a study being carried out by the Nuclear Systems Safety Program of Lawrence Livermore National Laboratory for the U.S. Nuclear Regulatory Commission (NRC). Phase I of the study is to develop a set of draft test criteria to meet requirements of the public law established by Congress for certifying the safety of containers used in air shipment of plutonium through U.S. airspace by a foreign country. As part of the study, the NRC has chosen the crash of PSA Flight 1771 as the worst-case air transport accident to be used as the basis for developing the draft aircraft crash requirements. The soil characteristics of the PSA crash site must be studied for the development of crash site requirements for the draft aircraft crash test. Furthermore, constitutive relationships for the geologic materials at the PSA crash site must be established for conducting crash-impact analyses in support of appropriate development tests for design of plutonium air transport (PAT) packages that meet the legal requirements.

As part of the Phase I study, site characterization of the PSA crash site was conducted. This report presents the results of a study to characterize the near-surface soils encountered at the site. The study included laboratory tests on selected undisturbed soil samples recovered from borings made at the site to determine engineering properties, including stress-strain and strength properties, and index properties. In addition, a review was made of the literature on effects of loading rate and confining pressure on stress-strain and strength properties of geologic materials. Finally, model material parameters required as input to crash-impact analyses using computer program DYNA2D (or DYNA3D) were developed.

The results of the literature review are summarized as follows:

- The effect of strain rate varies considerably with soil types. Generally, the percentage change in the strength of sands is less than that for clays for the same change of loading rate.

- The effect of strain rate also appears to vary with the stress history of a given soil. It increases with increasing overconsolidation ratio.

- Strain rate affects stress-deformation behavior (modulus) of soil and soil strength in approximately the same proportion.

- An increase in strain rate causes a progressive stiffening of soils. Compressibility of soils decreases as the strain rate increases.

- An increase in effective confining stress results in a decrease in overconsolidation ratio and an increase in compressibility.

- An increase in effective confining stress results in a decrease in ratio of undrained shear strength to existing effective stress of clays (down to normally consolidated conditions) and in a decrease in effective friction angle of coarse grained soils.

The geotechnical characterization of the PSA Flight 1771 crash-site soils was performed for pre-crash and crash-impact conditions. The characterization study involved extensive field exploration, field penetration testing, and static laboratory testing of relatively undisturbed samples from the site to develop site stratigraphy and soil parameters for constitutive modeling and to determine penetrability of near-surface in-situ soil materials at the crash site.

Boreholes drilled at the site encountered a veneer of colluvial soil deposits overlying residual soils that were formed by in-place decomposition of the underlying bedrock materials. Distinction is drawn here between the surficial colluvium and the underlying residual soils because of the nature of their respective formation. Because of the relative thinness of the colluvium, it is not expected to play a significant role in the crash impact dynamics. Relatively, the engineering soil behavior characteristics of the colluvium observed from field and laboratory testing are interpreted to be not appreciably different from the residual soils; thus for the analytical modeling purposes of this study, it is concluded that the total zone of soils (colluvium and residual soil) may be treated as a unit.

The soils at the crash site are of low-to-medium plasticity with relatively low moisture content (below the plastic limit). At the time of drilling and sampling, the soils were in an unsaturated condition. Evaluations of apparent (or effective) stress history indicate the soils exist in a very heavily overconsolidated state, which in turn is associated with substantial shear strength, many times greater than a normally consolidated soil at these depths. The overall soil properties and behavior characteristics evaluated for the crash-site soils are consistent with those for other similar soils. Therefore it is expected that the dynamic soil behavior characteristics determined from the literature review are applicable to the crash-site soils for impact loading and that the analysis and verification study results provide an appropriate basis for extrapolations to other crash sites and/or candidate test sites.

ACKNOWLEDGMENTS

The work described in this report was carried out in support of the geotechnical study portion of the Plutonium Air Transport Certification Project. This project is currently being conducted by the Nuclear Systems Safety Program (NSSP) at LLNL for the U.S. Nuclear Regulatory Commission.

Valuable technical and administrative reviews of this report were provided by Larry Fischer, Garry Holman and Carl Walter of NSSP. C. K. Chou of NSSP provided administrative guidance and support. Dave Carpenter of the Earth Sciences Department reviewed the draft report and gave valuable comments. Gerald Goudreau, Monika Witte, and Jim VanSant, all of NSSP, provided technical guidance in selection of appropriate testing parameters. Zhi-Liang Wang of Geomatrix Consultants contributed to the literature review and assisted in report preparation. Laboratory soil testing was performed by Sam Capps of Woodward-Clyde Consultants. Carol Kumagai and Lilian DeCastro of Geomatrix Consultants typed the manuscript. Finally, Wally Clements and Lisa Hensel of NSSP provided final editing and publication services.

1.0 INTRODUCTION

1.1 Background

The Plutonium Air Transport Certification (PATC) Project, which is funded by the U.S. Nuclear Regulatory Commission (NRC), is currently being conducted by the Nuclear Systems Safety Program (NSSP) of the Lawrence Livermore National Laboratory (LLNL). The Phase I activity of this project is to develop a set of draft test criteria to meet the requirements of the public law established by Congress for the safety of containers designed for air shipment of plutonium through U.S. airspace by a foreign country. As part of the study, the NRC has chosen the PSA Flight 1771 crash that occurred on December 7, 1987, near Paso Robles, California, as the actual worst-case transportation accident to be used as the basis for developing the draft aircraft crash requirements. Thus, the PSA crash site must be studied. The study includes comprehensive field explorations of the crash site, laboratory tests on undisturbed soil/rock samples, dynamic penetration tests of the near-surface soil/rock formations at the site, and development of constitutive soil/rock models. In addition, a series of crash-impact analyses for plutonium air transport (PAT) package designs will be performed using the computer program DYNA2D (or DYNA3D) with implemented constitutive models in support of appropriate development tests for package design.

1.2 Objective and Scope

As a part of the input parameter requirements for the crash-impact analysis, the site geological materials need to be characterized in accordance with selected constitutive models available and implemented in DYNA3D. Testing and characterization of rock samples was performed by S. C. Blair, et al. (see Ref. 1). The objective of this study is to develop stress-strain and strength parameters for both the in-situ soils present at the crash site and other geological materials that are likely to be considered in the parametric impact study using DYNA3D. To achieve the objective of the study, the scope of work included the following:

1. Laboratory tests on selected soil samples recovered from holes drilled at the crash site to determine engineering properties including stress-strain and strength properties and index properties.

2. Review of literature on effects of loading rate and confining pressure on stress-strain and strength properties of geological materials.

3. Development of material parameters required as input to impact analyses using DYNA3D.

1.3 Report Organization

The organization of the remainder of this report is described briefly below.

Section 2.0 presents a brief review of the geological materials modeling. The geological materials' response to an impact loading is analyzed as a boundary value problem using the dynamic finite-element method. The two components of the modeling (the finite element code and the implemented constitutive relationships) are introduced in this section. Subsequently, a summary of parameters required for the selected constitutive model and the relationship of these to conventional soil characteristics are given.

Section 3.0 is concerned with the evaluations of dynamic soil behavior relevant to the airplane crash problem. A short literature review of loading-rate effects and high-pressure effects on soil properties is presented. These effects can be summarized with respect to compressibility and strength changes. The emphasis is on laboratory results for undrained loading conditions (i.e., where strain rates are high enough that any water in the pore spaces does not have time to drain away and hence is pressurized so that it adds to the effective stress state in the sample).

A major portion of the report, Section 4.0, is dedicated to characterization of the PSA crash site soils. Site description, the site characterization program, and soil properties obtained from current laboratory testing are interpreted. Based on these data, modeling parameters are developed for use in the finite element code, DYNA3D, to analyze the ground response to the crash impact of the PSA airplane.

Constitutive modeling parameters developed for soils other than those of the PSA crash site are presented in Section 5.0. These parameter values have been derived based on data from published papers and reports and our experience with other similar soils, and are intended to serve as preliminary input data when the present impact study is extended to sites with soil characteristics different from the PSA crash site.

The appendices to the report present information and data complementary to the study. Appendix A describes the details of the laboratory testing program and presents the test results. Appendix B presents the basic formulation of the selected constitutive model, which relates the model parameter definitions to the conventional Coulomb failure criteria.

2.0 GEOLOGICAL MATERIALS MODELING

2.1 General

2.1.1 Methodology

Analysis and verification of geological materials' response to impacts by penetrating projectiles (e.g., an airplane crash) requires characterization of various geological materials. Characterization of the PSA crash site materials has been accomplished through a field exploration program and laboratory testing performed on relatively undisturbed samples obtained from representative holes drilled at the crash site. The soil properties measured through conventional soil-testing procedures are intended to provide a data base for further two- and/or three-dimensional dynamic finite-element analyses.

Two analytical tools are extremely important in accomplishing this task and in proving the feasibility of the methodology by which the soil's response to an impacting projectile is analyzed. They are:

1. A powerful and efficient finite-element code capable of handling transient loading.

2. A constitutive model for geological materials, which, at the least, is capable of incorporating the pressure sensitivity and internal friction aspects of soils.

For practical application, the constitutive model should be relatively easy to use (i.e., have a limited number of parameters to determine), and the parameters should have definite physical meaning.

2.1.2 Description of DYNA3D

DYNA3D (Ref. 2) is an explicit three-dimensional finite-element code for analyzing large-deformation dynamic response. The code was originally developed in 1976 and then revised in 1979, 1981, 1982, and 1987. The 1981 version had the ability to model explosive/structure and soil/structure interactions, including the response of a structure to impact by a penetrating projectile. In the 1987 version, which is presently being used, 28 material models are implemented. The range of applicability and versatility is quite extensive.

2.1.3 Selection of Constitutive Models

Among the 28 models implemented in DYNA3D, there are 3 models designed for the constitutive modeling of geological materials and other pressure-sensitive materials (e.g., concrete):

1. No. 5 - Soil and Crushable Foam.
2. No. 16 - Pseudo TENSOR Concrete/Geological Model.
3. No. 25 - Inviscid Two-Invariant Geological Cap Model.

Model No. 5 is an elasto-plastic type of constitutive model originally developed by R. D. Krieg (Ref. 3). Six model parameters and a curve of mean pressure versus volumetric strain are required for utilization of the model. Model No. 16 was developed by S. J. Sackett (Ref. 4). A generalization of Model No. 5 takes into consideration reinforcement for concrete materials and loading rate sensitivity for both the principal material as well as the reinforcement. A damage scaling factor and a pressure hardening coefficient are other additional features. Model No. 25 is a well-known "cap-model" (J. C. Simo, et al., Ref. 5). Eleven model parameters are required. The yield surface and the cap have curved shapes in stress-invariant space. Other soil models not implemented in DYNA3D have not been considered for this study.

Model No. 5 has been selected as the choice for the present study because of its simplicity in comparison with the other two geological-material models. Model No. 5 will often be referred to as "Krieg's model" in subsequent discussions in this report.

2.2 Krieg's Model

A simple constitutive relationship for cellular concrete was developed and presented by R. D. Krieg (see Ref. 3). This relationship also provides a very simple yet useful constitutive model for foams and geological materials. The concepts of this model are quite familiar to many soil mechanics practitioners. Krieg's model is composed of four basic parts:

1. A pressure-dependent yield surface.
2. A flat cap.
3. A cut-off extension cap.
4. Elastic deformation moduli.

The pressure-dependent yield surface governs the deviatoric (shear) behavior of the material. The yield surface is given by the expression:

$$\Phi_s = J_2 - (a_0 + a_1 p + a_2 p^2)$$

in which p and J_2 are stress invariants, and a_0, a_1, and a_2 are yield function constants.

The stress-invariant parameters are given by:

$$p = (\sigma_{11} + \sigma_{22} + \sigma_{33})/3 = \text{mean normal stress},$$

$$J_2 = S_{ij}S_{ij}/2; \text{ with } S_{ij} = \sigma_{ij} - p\delta_{ij},$$

in which σ_{11}, σ_{22}, and σ_{33} are normal stresses and δ_{ij} is the Kronecker delta. For geological materials, especially soils, volumetric and shear behavior, including compressibility, strength, and shear modulus characteristics, is controlled by effective stress state (i.e., the net intergranular stress when pore fluid pressure is taken into consideration). Therefore, stresses referred to herein represent effective stresses unless otherwise noted.

For the yield surface to represent a cone-shaped surface, the yield function constants are to be defined by:

$$a_0 = \tau_0^2/3,$$

$$a_1 = 2/3\,\tau_0\,\mu,$$

$$a_2 = 1/3\,\mu^2,$$

in which τ_0 is the cohesive deviatoric strength and μ is the slope of the yield surface. The ultimate strength is defined by σ_u (i.e., $J_2 \le \sigma_u^2/3$).

The flat cap is governed by the compressibility of soil and is determined by the expression:

$$\Phi_p = p - f(\varepsilon_v) = 0,$$

in which $f(\varepsilon_v)$ is a relationship between volumetric strain and mean normal stress. This relationship is usually determined from the compression curve of a consolidation test (odometer or triaxial apparatus). For use in DYNA3D, this curve should be in tabulated format.

A cutoff extension cap defines the cutoff pressure, p_t, for tensile fracture. For all values of p in consideration, $p \ge p_t$.

Shear modulus, G, and volumetric rebound bulk modulus, k_e, are utilized to represent the elastic deformation characteristics.

The Krieg model may therefore be characterized by six parameters—G, k_e, a_0, a_1, a_2, p_t—and a curve of mean normal stress versus volumetric strain. In the following sections, τ_0, μ, and σ_u are selected as basic model parameters for evaluation instead of a_0, a_1, and a_2. A schematic state-space representation of Krieg's model is illustrated in Fig. 2-1.

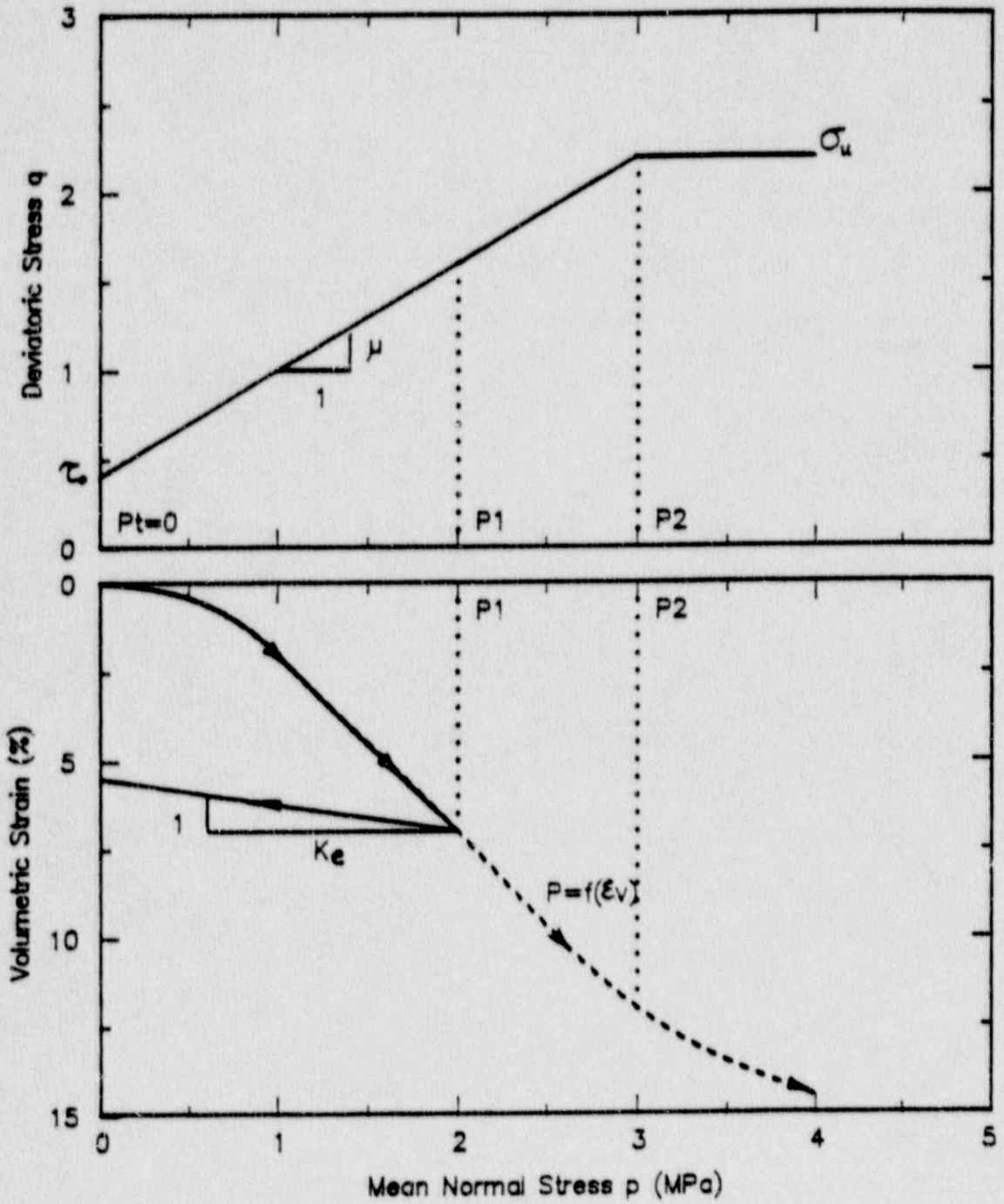

Fig. 2-1. State-space representation of Krieg's model.

It is worthy of mention that, as mean normal stress p increases, the flat cap is pushed farther from the origin of the state-space, and the yield surface and flat cap boundaries are expanded.

2.3 Summary of Model Parameter Requirement

As previously mentioned, six parameters and a compressibility curve are required for utilization of Krieg's model. In addition, mass density ρ of the material is needed for the dynamic numerical analysis. The merit of this set of parameters is that each has clear physical and mechanical meaning as stated in the previous section and all parameters can be characterized using conventional soil-testing results. In the present study, triaxial test and odometer test (one-dimensional consolidation) results are employed.

Some of the parameters are not directly the commonly used terms in conventional soil mechanics: e.g., cohesive strength τ_0 versus cohesion c, and slope μ versus friction angle Φ. A detailed formulation for deduction of model parameters from laboratory test results is presented in Appendix B. A correlation summary of model parameters and conventional soil-mechanics properties is listed in Table 2-1.

Table 2-1. Correlation between model parameters and conventional soil properties.

Parameters for Krieg's Model	Correlation	Soil Parameters
G = shear modulus	Need a proper estimate of confining pressure	G is shear modulus, pressure-dependent
K_e = unloading bulk modulus	Need a proper estimate of mean pressure change	K is bulk modulus, pressure-dependent
τ_0 = cohesive strength	$\tau_0 = (6c \cos \Phi)/(3 - \sin \Phi)$	c is cohesion
μ = slope of σ_y-vs-p curve	$\mu = (6 \sin \Phi)/(3 - \sin \Phi)$	Φ = friction angle in Mohr-Coulomb failure envelope
p_t = pressure cutoff for tensile fracture		

3.0 DYNAMIC SOIL BEHAVIOR CONSIDERATIONS

3.1 General

At the instant that a falling object such as an airplane or fuel storage canister impacts the ground surface, high levels of shear and compressive stresses are imposed on the contacted geologic material at very rapid rates of loading, at least relative to conventional geotechnical evaluations and applications of stress-strain-strength characteristics. For example, the crash impact velocity of the PSA Flight 1771 airplane has been estimated to be approximately 280 m/s (925 fps). The significance of such rapid rates of loading is that geologic materials (i.e., soil and rock) will behave in a "harder" fashion; in other words, strength and stiffness responses of soils are greater for rapid loading than for conventional static loading conditions.

Early studies pertaining to rate of loading effects, in which increases of soil strength with higher loading rates were observed, may be traced to the nineteenth century (see Refs. 6 and 7). Using a double-shear device, A. Collin observed that the permanent (under slow loading rate) strength of a clay may be in the range of 1/4 to 1/3 of the instantaneous (under one pulse at rapid loading rate) strength. Over the last four decades, 1948 to present, numerous investigators have studied the effects of rate of loading on soil behavior; in fact, during the course of this study, sixty-plus available reports and papers dealing with this subject have been reviewed to obtain both qualitative and quantitative understanding of the phenomenon.

Interest in the effects of loading rate on soil behavior is derived from developments in many areas of soil dynamics, including earthquake loading, machine vibrations, pile driving, explosion, impacts, etc. A major area of research in this topic has been response of soils subjected to explosive-induced loading and/or impact loading from projectiles (the dynamic penetration problem). The characteristics of such loading are high pressure and short duration, namely, rapid loading. Corresponding strain-rates induced by such loading in soils can be 10% or more per millisecond.

The term "strain-rate effect" was coined by R. V. Whitman (see Refs. 8 and 9) to indicate the relationship between shearing strength and rate of loading. Review of the available literature has indicated that this relationship has been the primary interest of a majority (more than 70%) of investigators. A by-product, or side-observation, of many of these strength studies was information and/or data regarding effects on shear modulus characteristics. Recent laboratory studies have also focused on the important aspect of uniaxial compressibility under rapid loading for simulating loading conditions in which an airblast sweeps out over a soil surface and large areas are effectively loaded instantaneously. One-dimensional compression or uniaxial strain tests are commonly used to approximate these conditions, and several researchers have studied the phenomenon in detail (see Refs. 10 through 15).

As for high pressure effects, the significant influence of confining stress on the behavior of not only "cohesionless" granular soils, but "cohesive" fine-grained silt and clay soils and other geological materials as well, has been recognized since the earliest days of soil mechanics. Changes to geologic stress history, strength, saturation, and a soil's physical properties (grain crushing) are all important results associated with higher confining stresses. The basis of knowledge, however, has been and generally remains limited to observations at stress levels that can be achieved in a conventional triaxial apparatus and odometer device. Behavior for impact loading levels of stress requires extrapolation from that basis.

A more direct approach to solving individual soil-dynamics problems is in-situ testing. For the impact problem, numerous studies have now been made toward understanding projectile penetration into earth materials (see Refs. 16 and 17). Based on the gathered in-situ test data, empirical formulations for estimating penetration have been proposed which correlate shape, size, velocity, and material properties of projectiles with density, strength, or other parameters of soils at a test site (Ref. 18). Although these studies are quite useful for simulating individual impact problems and for the characterization of in-situ properties of soils in terms of penetrability of certain projectiles, their applicability to the general impact problem is still limited (for example, their applicability to the airplane crash problem).

3.2 Rate-of-Loading Effects

3.2.1 Shear Strength and Stress Deformation

The shear behavior that a soil will exhibit (e.g., strength and stress deformation) is controlled by the effective stress state of the soil and therefore depends upon the level of pore water pressure generated by the loading regime under consideration. If the rate of shear is sufficiently slow to allow simultaneous pore pressure dissipation, effective stress is not influenced by excess pore pressure and the soil behaves in a "drained" manner. However, for higher rates of loading, such as those associated with an airplane crash, there is typically not enough time for pore water to be expelled from the soil via drainage; therefore, shearing of the soil will occur under undrained conditions.

At this point, differentiation needs to be made between:

1. Soils whose pore space is relatively dry or contains only a small proportion of water.

2. Soils whose pore space is saturated with water or contains a large proportion of water.

In the former category, there is no water or very little water in the soil in proportion to void space; even though undrained (i.e., high strain rate) conditions exist, no excess pore water pressure is generated during shear that could affect the effective

stress state and hence the strength and deformation behavior, and so the soil will behave essentially in accordance with drained characteristics. A. W. Bishop, et al. (Ref. 19) and T. W. Lambe and R. V. Whitman (Ref. 20) discussed the relationships of effective stress to pore air pressure development. They indicated that because of the relatively high compressibility of air, its presence in the void spaces has very little effect on effective stress; until the degree of saturation is on the order of 0.85 to 0.90, pore pressure effects are in general not significant to the effective stress state. Because shear deformation of soil is a rate process (Refs. 21 and 22), some effect on shear strength and modulus characteristics may be expected for rate-of-loading increases; but results from laboratory studies have indicated that rate-of-loading effects on dry soils (typically sands) are quite small, on the order of 10 to 15 percent over a 10,000-fold or more increase of strain rate (Ref. 11).

For soils in the latter category, excess pore-water pressures may be generated that change the effective stress and thus affect the strength and stress-deformation behavior accordingly. Traditionally, undrained soil behavior has been determined using loading rates low enough to allow full development and equalization of excess pore-water pressure throughout the soil sample. Those loading rates are proportional to the soil permeability so that rates for coarse-grained soils can generally be greater than for fine-grained soils (see Ref. 23). If, however, the rate of loading is so high that the full equalization of excess pore-water pressure cannot develop, the shear stress must increase to attain the failure principal stress ratio defined by the friction angle for the soil, leading in turn to higher strength. The remainder of the discussion in this section addresses such rate-of-loading effects on undrained behavior of saturated soils, inasmuch as the PSA crash occurred during the rainy season and the soils were likely in a high degree of saturation.

Most early data were obtained using unconfined compression tests on cohesive soils. These tests commonly showed strength increasing by factors of 1.5 to 2 (with some factors as high as 4) when the rate of strain was increased by a factor of about 10^4. R. V. Whitman (Ref. 11) discussed much of this early data and presented the information summarized in Table 3-1. As one might expect, a decrease of strain rate (i.e., creep tests) produces opposite effects, reducing strength by similar amounts. Figure 3-1 illustrates this continuum of behavior through typical results for Cucaracha clay-shale (see Ref. 24) in both ranges of strain rate.

R. V. Whitman (Refs. 8 and 9) made the observation that strain-rate effect was greater for specimens tested without confinement than for those tested with confinement, such as in unconsolidated- and consolidated-undrained triaxial tests. He suggested that more representative estimates of strain-rate effect could be obtained using confined specimens and recommended using a test such as the triaxial test.

Table 3-1. Summary of transient-loading triaxial tests on cohesive soils (Ref. 11).

Soil	PI %	PL %	w %	Chamber Pressure psi	Static Compressive Strength psi	Strain-Rate Effect* At Low Stress (1/2 to 4%)	Strain-Rate Effect* At Peak Stress
Medium-soft, slightly sensitive clay, undistributed	24	26	27	0	10	2.0	4.0
Compacted silty sand	17	11	12	0	25	1.8	2.7
Normally consolidated, sensitive ocean sediment, undisturbed	63	49	92	0	0.3	2.0	2.4
Tough compacted fill	41	21	26	42	35	2.0	2.0
Slightly organic silty clay; undisturbed, saturated	21	22	35	0 85	22 54	1.6 1.7	1.9 1.7
Compacted silty sand	17	11	16	0	10	1.7	1.7
Plastic clay, remolded	27	38	44	0	15	1.6	1.8
Plastic clay, remolded	27	38	48	0	7	1.6	1.8
Plastic clay, remolded, saturated	38	24	30	60	36	1.6	1.8
Stiff dray clay, undisturbed	23	30	20	0 30	250 330	1.4 1.4	1.6 1.4
Slightly organic silty clay; undisturbed, saturated							1.6
Compacted silty clay (also sedimented specimens of same soil)			20 20	0 15	30 40		1.3 1.2
Compacted plastic clay	38	24	25	0 15	25 40		1.4 1.5
Compacted clay loam	23	22	21	0 30	13 15	1.5 1.5	2.5 1.7

* Ratio of resistance at 1000%/sec to resistance at 0.03%/sec.

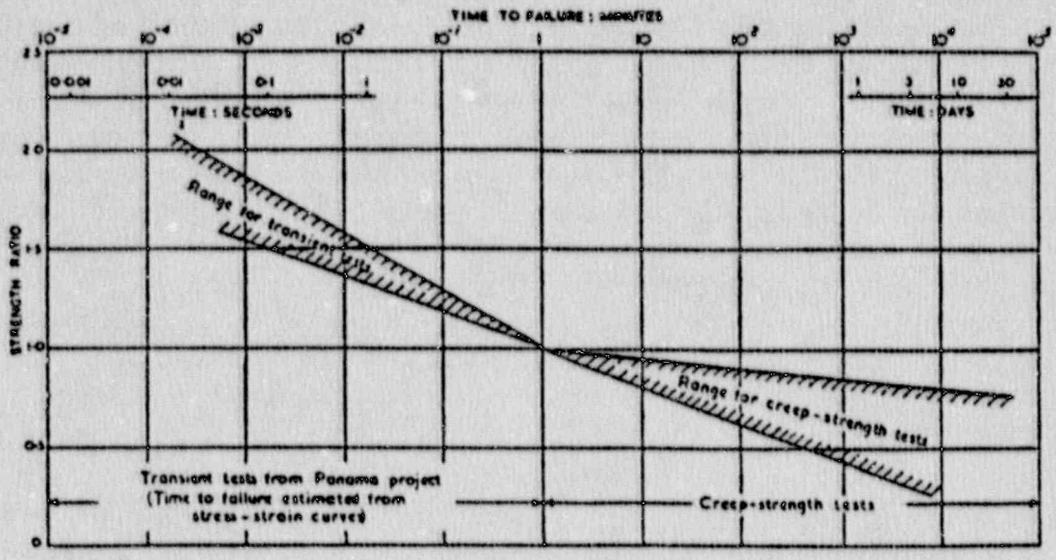

Effect of rate of loading on the compressive strength of Cucaracha clay-shale

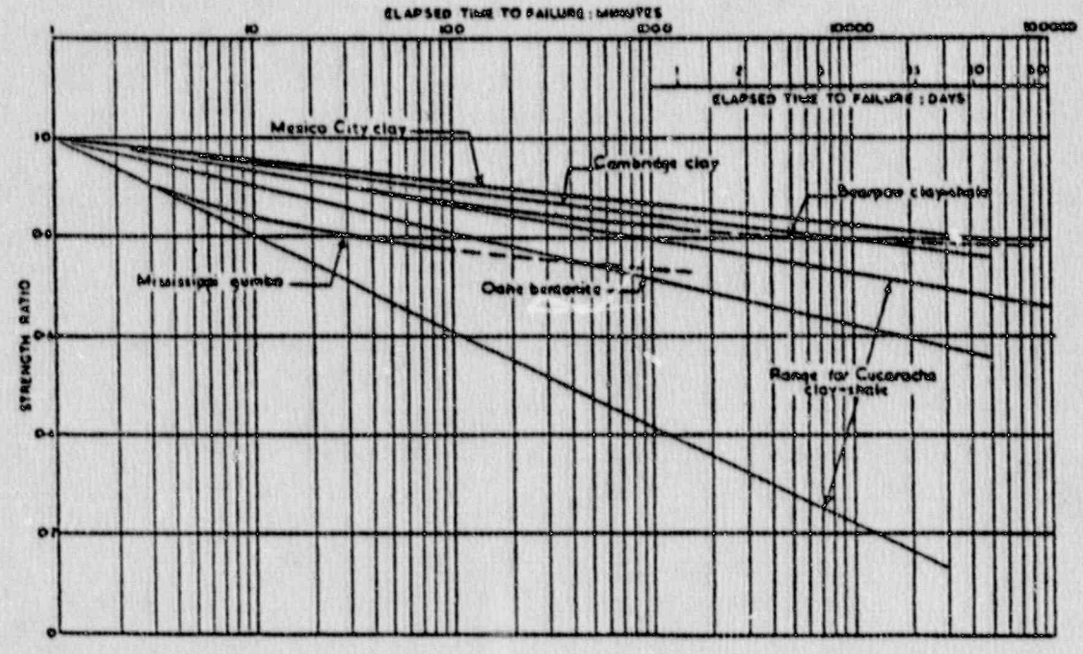

Strength ratio/elapsed time to failure: creep-strength tests
at constant water content on six undisturbed soils

Fig. 3-1. Comparison of transient and creep strain-rate effects on soil strength (see Ref. 24).

L. Bjerrum, et al. (Ref. 25) and C. B. Crawford (Ref. 26) made significant contributions to the understanding of the strain-rate phenomenon. Their tests, performed on two different normally-consolidated-to-lightly-overconsolidated marine clays, demonstrated that excess pore-water pressure generated during shear was considerably less for shorter times to failure than for slower rates of loading. Figure 3-2 illustrates a comparison of strain-rate effects on pore water pressure and strength observed in these two studies, and demonstrates the direct relationship between pore water pressure decrease and strength increase. As previously noted, this may be interpreted to mean that to achieve the failure envelope, a soil loaded rapidly must attain a larger shear stress than a soil loaded slowly because the excess pore-water pressure is lower. Stress paths for this concept are illustrated in Fig. 3-3 for Crawford's Leda clay data. Responses of this kind are very much in line with the time-dependent nature of soil behavior. Although these tests were performed at moderate strain rates, not appropriate for impact-type problems, the trend of behavior can be extrapolated to those higher strain-rate ranges, as is supported by the A. Casagrande and S. D. Wilson (Ref. 24) data presented in Fig. 3-1.

During the early 1960s, several studies were performed at MIT which examined the strain-rate effect phenomenon within a range of higher rates of loading. The results of those studies for a variety of soil types—including sands, silty sands, clayey silt, silty clay, and fat clay—indicated trends of response very similar to the data published by L. Bjerrum, et al. (Ref. 25) and C. B. Crawford (Ref. 26). For example, test results presented by R. V. Whitman and K. A. Healy (Refs. 27 and 28) for saturated Ottawa sand confirm that behavior patterns observed by L. Bjerrum and C. B. Crawford for clay soils apply to sands as well. Typical results for loose Ottawa sand specimens presented in Fig. 3-4 illustrate the decrease of pore-water pressure and increase of stress associated with strain-rate increase. Other results may be found in A. M. Richardson (Ref. 29), K. A. Healy (Ref. 30), R. V. Whitman, et al. (Refs. 27 and 28), K. A. Healy (Refs. 31 and 32), and A. M. Richardson, Jr. (Refs. 33 and 34).

Considering all of the available data collectively rather than individually, the following observations may be made:

- Strain-rate effect varies considerably with soil types. Generally, the percentage change in the strength of a sand is less than that for a clay for the same change of loading rate. Figure 3-5 illustrates this in a comparison between Leda clay (Ref. 26) and Ottawa sand (Refs. 27 and 28). The strain-rate effect for the Leda clay is approximately fifteen percent greater than that for the Ottawa sand at relative strain-rate changes of 100 times. As implied previously, rate-of-loading effects are inversely proportional to soil permeability; thus the more plastic a soil (lower permeability) the greater the expected strain-rate effect. Varying degrees of strain-rate effect occur among the wide variety of soil types and characteristics.

- Strain-rate effect appears to also vary with the stress history of a given soil. Figure 3-5 qualitatively illustrates the influence of over-consolidation on strain-rate effect. R. V. Whitman, et al. (Refs. 27 and 28) and A. M. Richardson, Jr. (Refs. 33 and 34) present results for a remolded fat clay with varying degrees of overconsolidation (1, 8, and 16) which similarly indicate that there is an increase of strain-rate effect with increasing overconsolidation ratio. This may explain the greater effects observed for unconfined tests, because the unconfined stress state can create the equivalent to a high degree of overconsolidation condition in a specimen through pore-water tension.

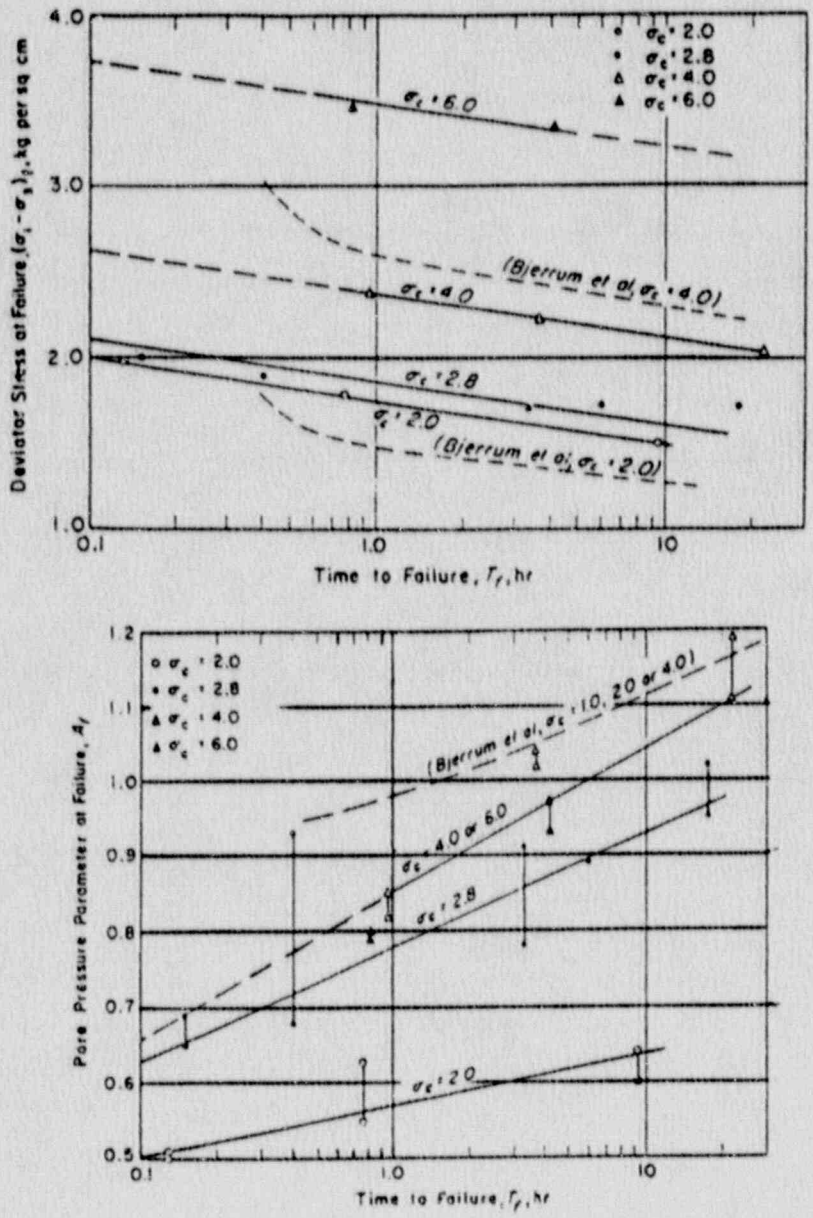

Fig. 3-2. Strain-rate effect on deviator stress and pore pressure at failure for Fornebu Clay (Ref. 25) and Leda Clay (Ref. 26).

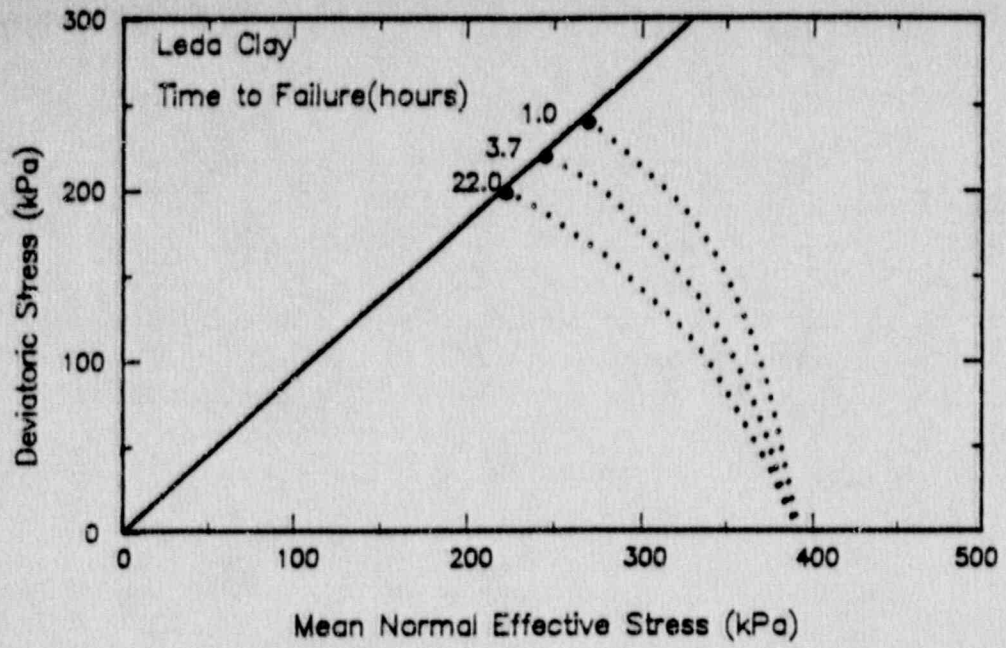

Fig. 3-3. Strain-rate effect on stress path response of Leda Clay (Ref. 26).

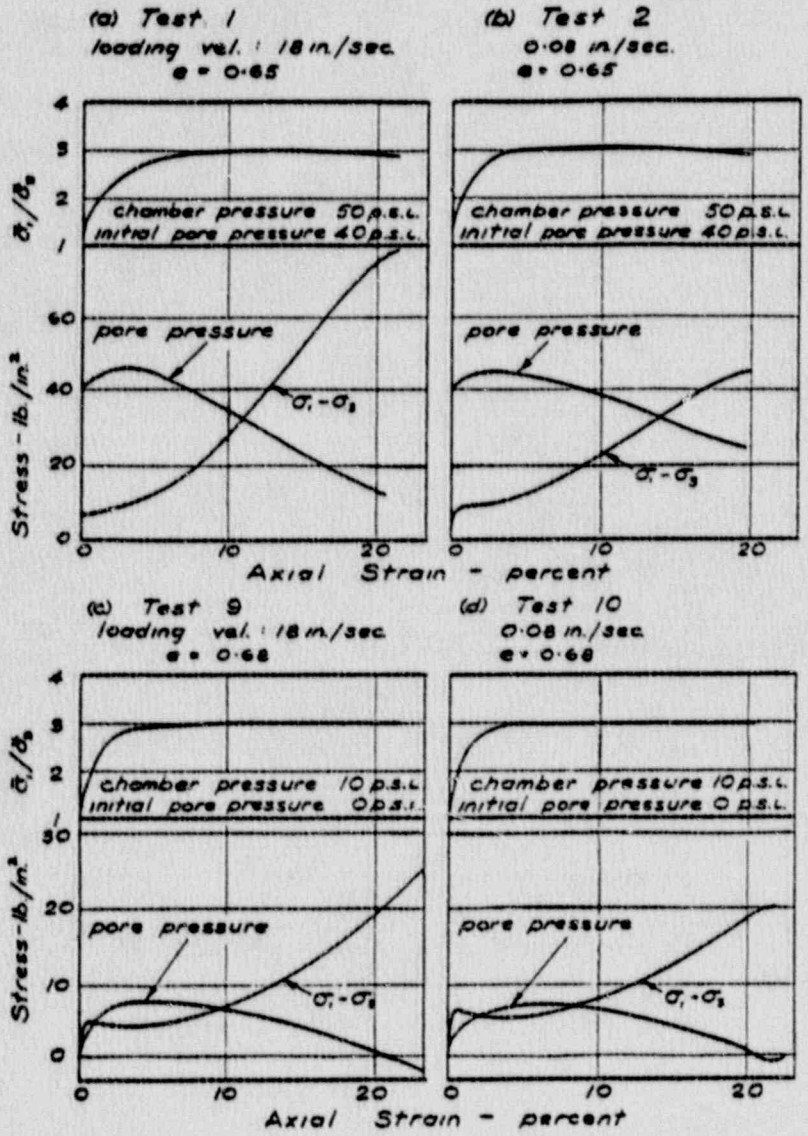

Fig. 3-4. Strain-rate effect on deviator stress and pore pressure response for loose Ottawa Sand (Refs. 27 and 28).

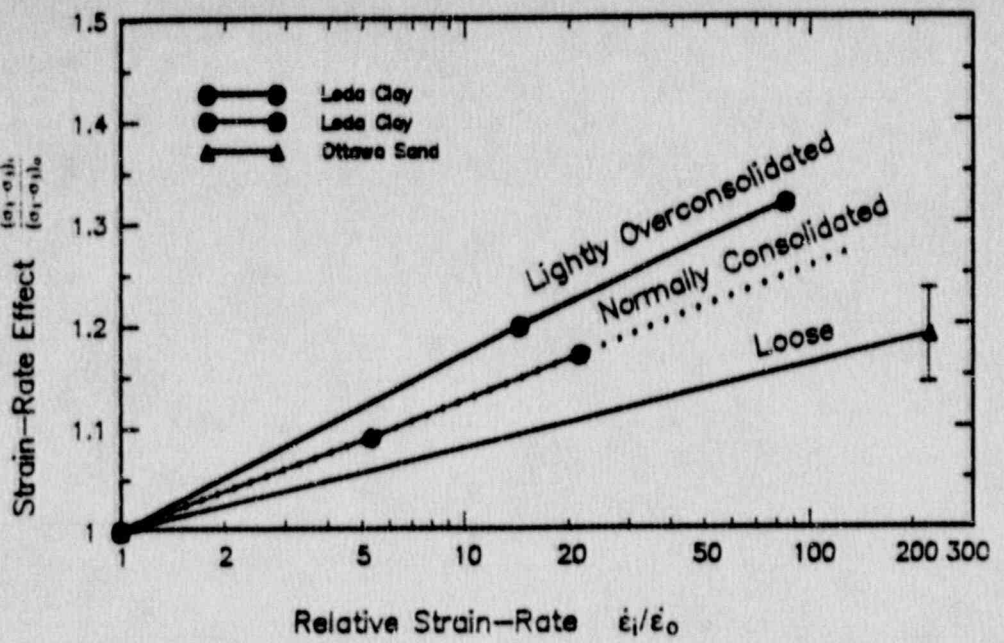

Fig. 3-5. Typical strain-rate effect differences between clay and sand and influence of soil stress history.

Subsequent to the MIT studies, there were many investigators who undertook similar work on the effects of strain rate on strength. Some of the more notable include B. B. Schimming, et al. (Ref. 35), R. N. Yong and R. D. Japp (Ref. 36), K. L. Lee, et al. (Ref. 37), M. Perlow, Jr. and A. F. Richards (Ref. 38), Y. P. Vaid and R. G. Campanella (Ref. 13), and Y. P. Vaid, et al. (Ref. 39). The results of these studies were similar to the results previously described and do not warrant further discussion here. They did, however, add data and validity to the existing behavior trends.

Effects of strain rate on stress-deformation behavior (modulus) are also important considerations for modeling dynamic response of a soil mass. Discussion of strain-rate effect thus far in this section has focused on changes of shear strength associated with rate-of-loading changes. And with good reason; the increase of soil stiffness, as measured by shear modulus, is approximately in the same proportion as soil strength increase. Stress-strain response to strain-rate changes have been discussed by a number of authors, including A. Casagrande and W. L. Shannon (Refs. 40 through 42), A. Casagrande and S. D. Wilson (Ref. 24), R. V. Whitman and K. A. Healy (Refs. 27 and 28), R. J. Krizek (Ref. 43), Y. P. Vaid and R. G. Campanella (Ref. 13), and Y. P. Vaid, et al. (Ref. 39).

Figure 3-6 illustrates test results for Haney clay (see Ref. 13) at three different strain rates separated by an order of magnitude each. Comparison indicates very similar stress-strain (modulus) characteristics, but differentiated by the respective strength changes. The stress-strain curves for Ottawa sand tests presented in Fig. 3-4 appear similar as well. The proportionality of changes in modulus and strength with changing strain rate are readily demonstrated by the test results for East Breaks clay illustrated in Fig. 3-7. Panel (a) of the figure shows the measured stress-strain curves for three strain rates and indicates similarity of curve shape and illustrates the change of strength with strain rate as expressed in panel (b); but in panel (c), the stress-strain curves have been normalized by their respective undrained shear

strength values and very clearly demonstrate the proportionality of strength and stress-deformation changes due to strain-rate effect.

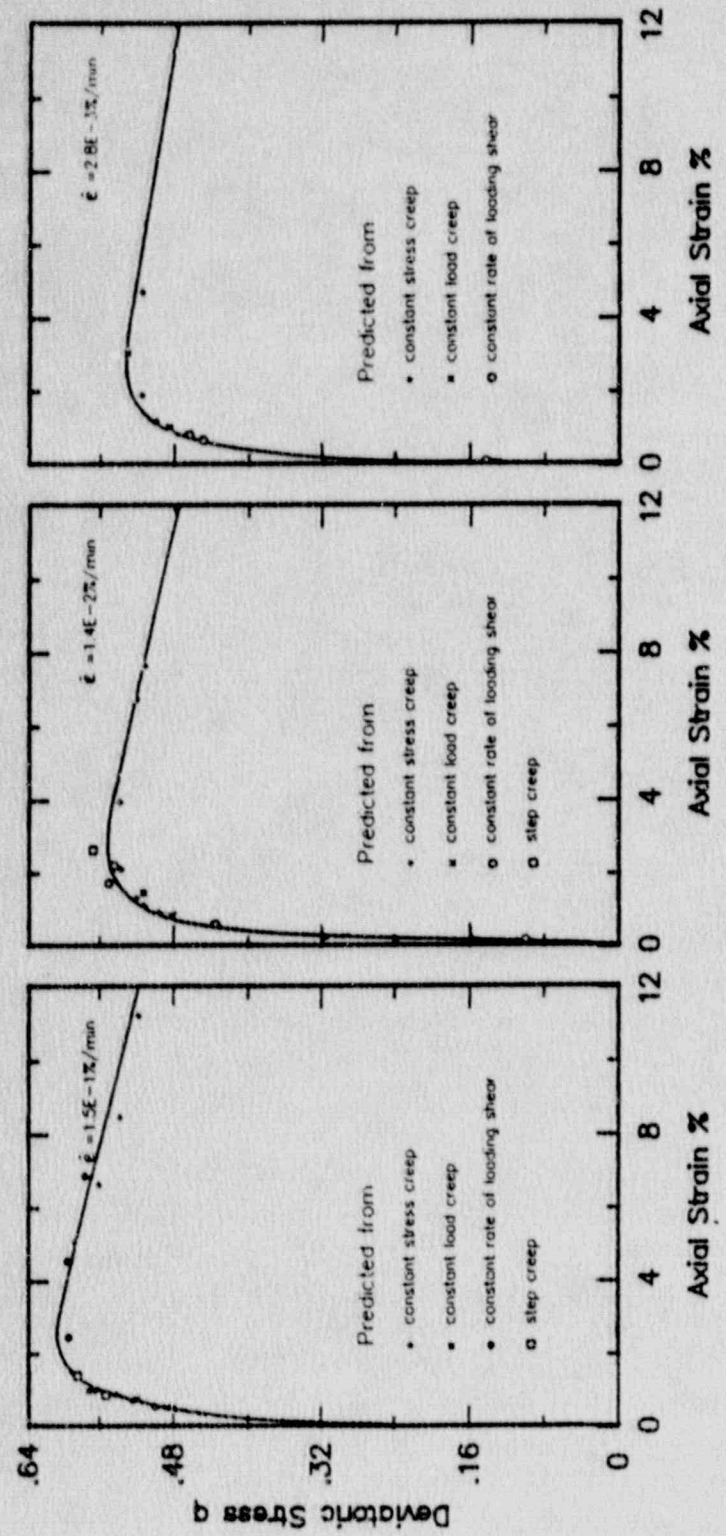

Fig. 3-6. Comparison of stress-strain response at three strain rates for Haney Clay (from Ref. 39).

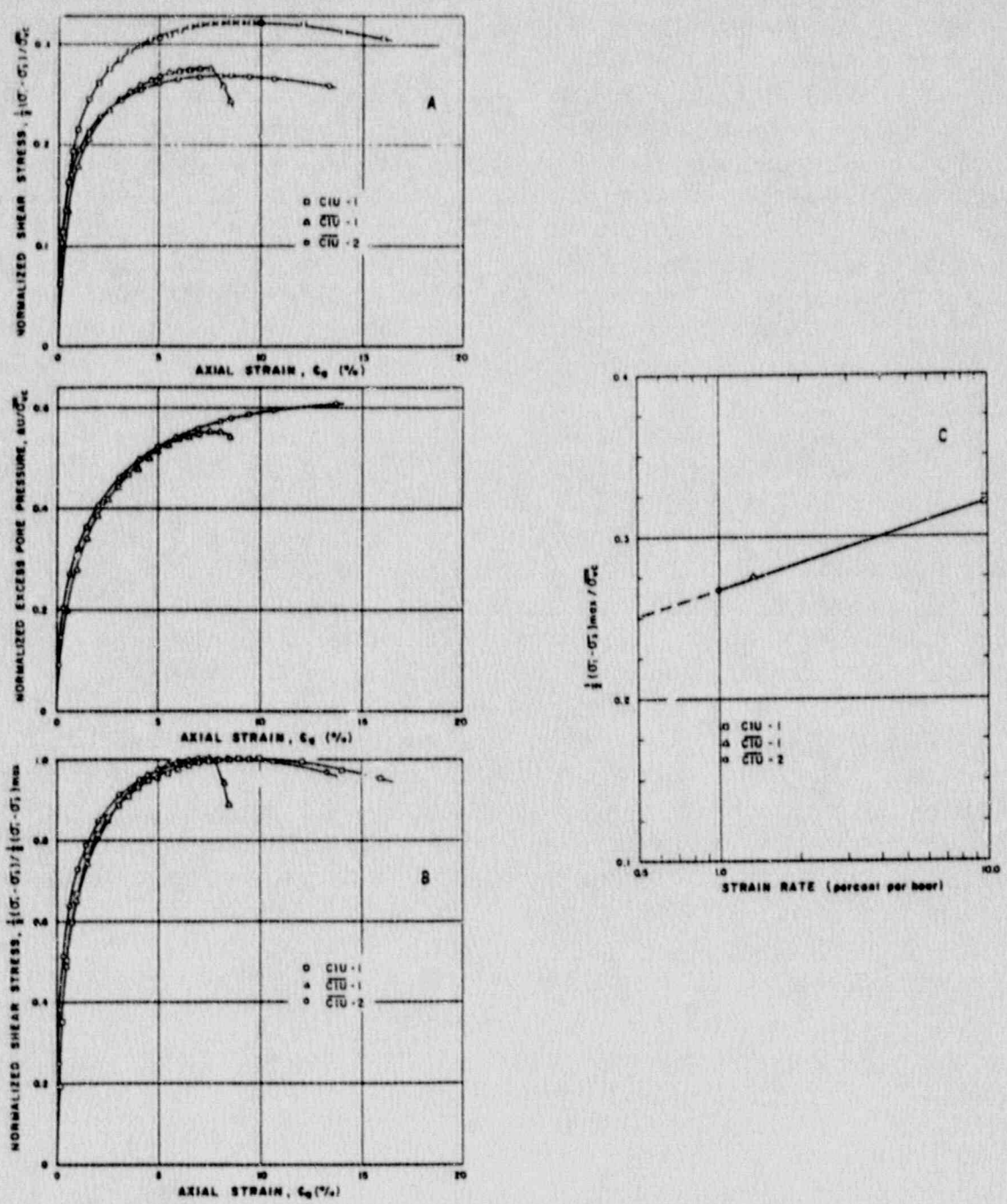

Fig. 3-7. Strain-rate effect on undrained strength and stress-strain response of east breaks clay (Ref. 44).

To be able to quantify the possible "strain-rate effect" for a given soil, it is first necessary to recognize that, as pointed out in the first observation above, the effect varies from soil type to soil type, generally in a fashion related to permeability (more simply, plasticity). Close examination of the response observations from a variety of soils has led to an empirical correlation by which strain-rate effect on strength and modulus could be approximated. To make the expression general for a wide range of soils, it was necessary to non-dimensionalize the data. The first step was to recognize that some of the differences of strength change observed are simply a result of the differences in the normal or static shear strength level to which other strain-rate strengths are compared. Thus it was found to be appropriate to consider the logarithmic change of shear strength that occurred as a function of logarithmic change of strain rate. Because shear strength is a function of normal stress, this change was related to the effective consolidation stress, σ_v', which becomes important in consideration of stress-history effects. In this way, the change of shear strength could be related as a ratio per log cycle of strain-rate change, rather than to an absolute static shear strength value which is dependent on some arbitrary strain rate.

Figure 3-8 illustrates data accumulated for tests on seven undisturbed natural soils. As may be seen, the slopes of the lines are different among the soils, and the data for all the soils collectively indicate a decrease of the amount of strength change as the plasticity decreased. Figure 3-9 illustrates a relationship derived from the data in Fig. 3-8 between the slope of the strength change relationships (designated as coefficient A) for each soil and the respective soil's Plasticity Index. The line indicated is a best fit to the data for normally consolidated (OCR = 1) soils. For the case of overconsolidated soils, mentioned in the second observation above, the limited data indicated that the change of shear strength per log cycle change of strain rate was related to the maximum past effective consolidation stress and thus proportional to OCR. Trend lines for other overconsolidation conditions are parallel to the normally consolidated line, but at abscissa values that are a function of OCR times the values for the normally consolidated line plotted. Strain-rate effect may therefore be described using the expression:

$$S_1/S_0 = (\varepsilon_1/\varepsilon_0)^{A*OCR},$$

in which S_0 and S_1 are soil strength at strain rates ε_0 and ε_1, respectively, OCR is the overconsolidation ratio of the soil, and A is the empirical coefficient determined from Fig. 3-9.

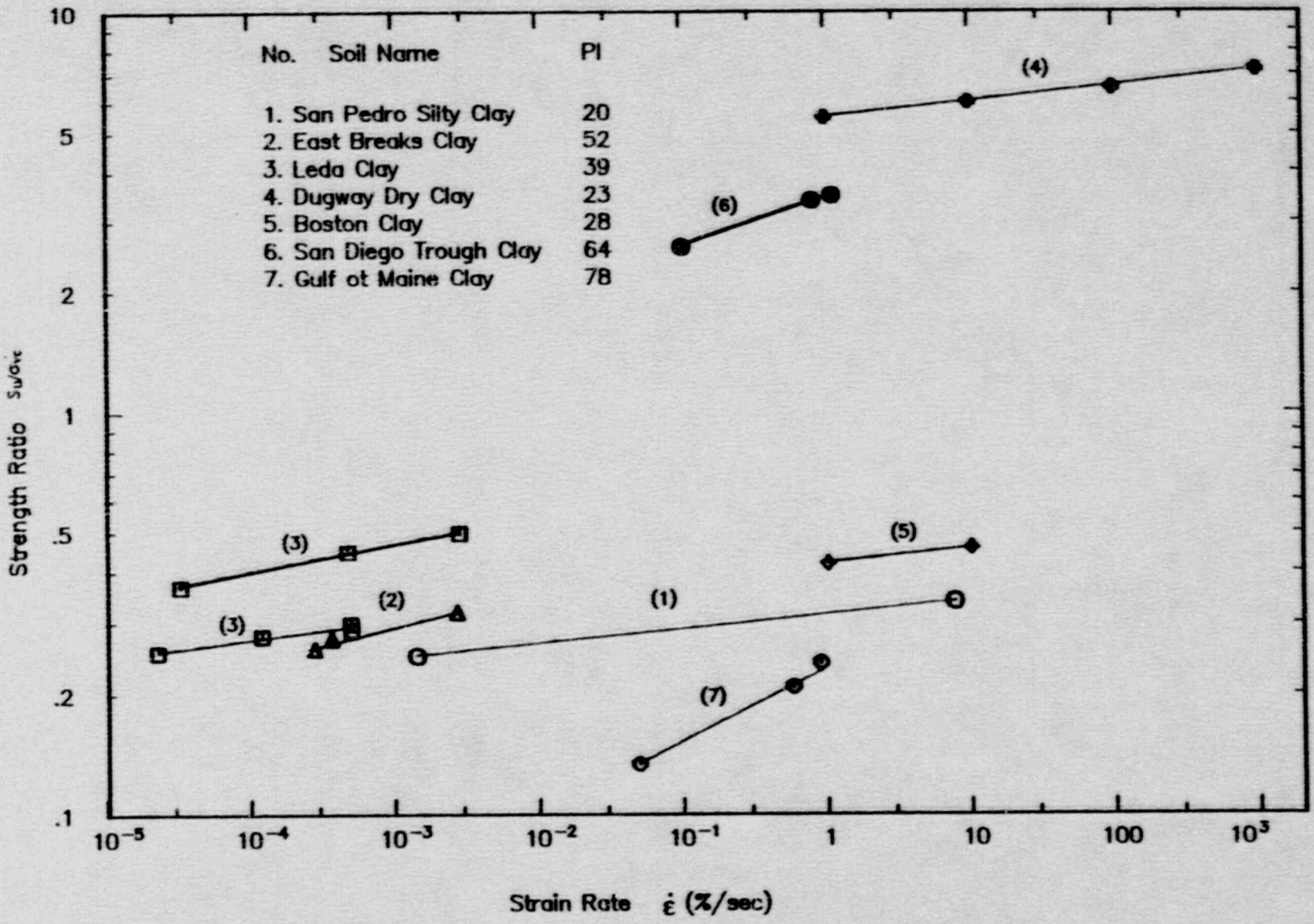

Fig. 3-8. Comparison of strain-rate effect on undrained strength for natural clay soil.

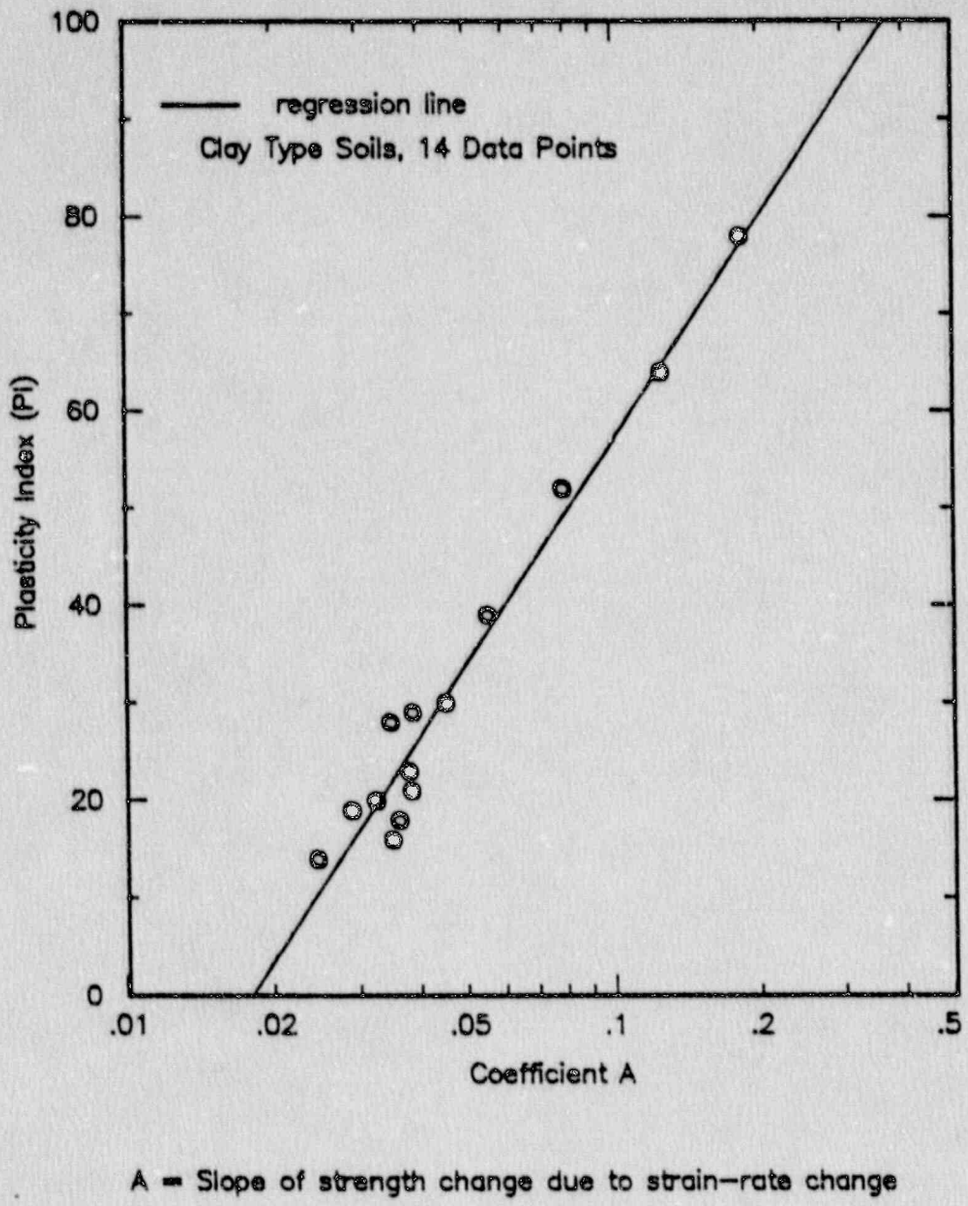

Fig. 3-9. Relationship between soil plasticity and strain-rate effect.

3.2.2 Compressibility

Similar to shear behavior, uniaxial strain response of most geotechnical materials subjected to high-intensity transient loading differs from the response measured under static conditions. R. V. Whitman (Ref. 10) pioneered the use of the uniaxial strain device for high-pressure testing of unsaturated soils. As the time to peak pressure decreases, most materials exhibit a stiffening of the loading stress-strain response. Y. P. Vaid, et al. (Ref. 39) have presented results for one-dimensional consolidation of Saint-Jean-Vianney clay which indicate that the effect of increasing the loading rate is an increase of the apparent maximum past consolidation stress, as illustrated in Fig. 3-10. In a mean-stress-versus-volumetric-strain response for rapid loading, this behavior would be manifested as a stiffening of the soil. Some researchers (see Refs. 11 and 45) have speculated that as the time to peak pressure approaches the submillisecond range, the time-dependent effects may be very important for large stress changes, especially for unsaturated granular soils. Using an explosive-loaded uniaxial strain device at Waterways Experiment Station (WES), J. G. Jackson, Jr., et al. (Ref. 45) observed increases on the order of 10 within the 1-msec to 0.1-msec decrease rise time for the dynamic-to-static modulus for a partially saturated clean quartz sand under unconsolidated-undrained condition. However, other test results (Ref. 46) obtained using a split Hopkinson bar showed no loading rate effects for a quartz sand under similar conditions.

Since the 1979 work of J. G. Jackson, Jr. and others, the device at WES has been improved both in electronic measuring systems and analysis techniques of recording and interpreting test results (Refs. 14 and 15). This second generation device is capable of producing submillisecond times to a maximum peak pressure of about 138 MPa (20,000 psi), which is used at WES in research programs to study loading rate effects on a variety of earth materials. J. V. Farr's test results obtained in this new device and in a conventional uniaxial strain device show that progressive stiffening of the uniaxial strain response occurs as the time to peak pressures decreases, but not a drastic stiffening. Results for four soils presented by J. V. Farr (Ref. 14) may be summarized as follows:

1. Enewetak Beach Sand. Twenty-five uniaxial strain tests were performed on remolded samples of Enewetak beach sand at constant initial conditions for various loading rates. Figure 3-11 summarizes the effects for six loading rates upon the uniaxial strain response of Enewetak beach sand. These tests are representative of the average uniaxial strain response for the various loading rates. Figure 3-12 illustrates the results presented in Fig. 3-11 in the more conventional semi-logarithmic compression curve format. Note that the virgin compression portions of the curves are parallel and at higher stresses for higher strain rates. These results are thus consistent with the interpretations of Y. P. Vaid, et al. (Ref. 38). As shown in Fig. 3-13, a significant rate effect exists for this material. It is important to note from these results that a drastic stiffening of the measured responses

does not occur in the submillisecond range, but that progressive stiffening occurs continuously as the rise time to peak pressure decreases.

2. Flume Sand. Eighteen uniaxial strain tests were performed on remolded samples of flume sand to investigate loading rate effects. The results of the flume sand testing program are summarized in Fig. 3-14. As shown in this figure, a small rate effect exists; however, it does not approach the magnitude of that measured for the beach sand. As with the beach sand, the submillisecond loading did not produce a drastic stiffening of the material response.

3. Yuma Clayey Sand. Sixteen uniaxial strain tests were performed on remolded samples of Yuma clayey sand to investigate loading rate effects. Results from the study on Yuma clayey sand are summarized in Fig. 3-15. As shown in this figure, a rate effect does exist; it is not as large as the effect measured for the beach sand, but it is greater than that measured for the flume sand.

4. Vicksburg Loess. Two testing programs were performed using Vicksburg loess; they are designated as the D- and V-series. The D-series testing program was similar to those performed for Enewetak beach, flume, and Yuma clayey sands. Fixed water content and dry density were maintained and the loading rate varied. Seventeen uniaxial strain tests were performed on remolded samples of Vicksburg loess under the D-series test program at a wide variety of loading rates. Figure 3-16 summarizes the effects of various loading rates upon the uniaxial response of Vicksburg loess. The rate effects for this material are similar to those for the flume and Yuma materials. Like the other three materials, drastic stiffening of the uniaxial response did not occur in the submillisecond range. A series of tests was also performed to study how water content, dry density, and loading rate effects are interdependent; this series is designated as the V-series of tests. Results of five static tests at approximately the same dry density but with the water content varied indicate that as the water content increases (i.e., higher degree of saturation) the response becomes softer.

Based on the results of the laboratory tests and on comparisons with field tests, J. V. Farr (Ref. 14) concluded that an order of magnitude stiffening of soil uniaxial strain loading moduli does not occur under large impulse-type loading with times to peak pressure of less than a millisecond, as speculated by some researchers (see Ref. 45). Increases in moduli ranging up to 125% were determined for the soils tested at their field values of water content and density.

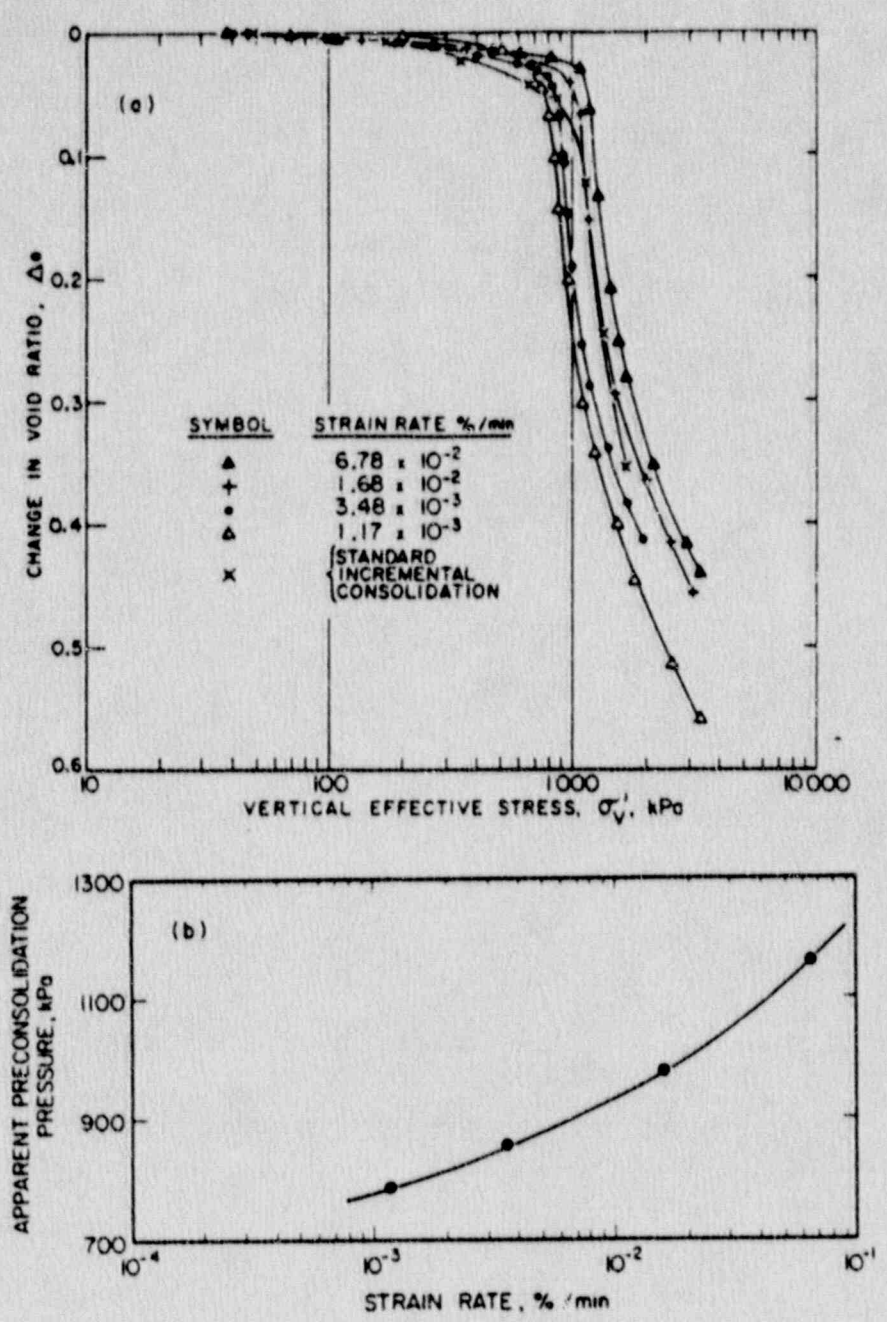

Fig. 3-10. Strain-rate effects on one-dimensional compression characteristics of Saint-Jean Vianney clay (Ref. 39).

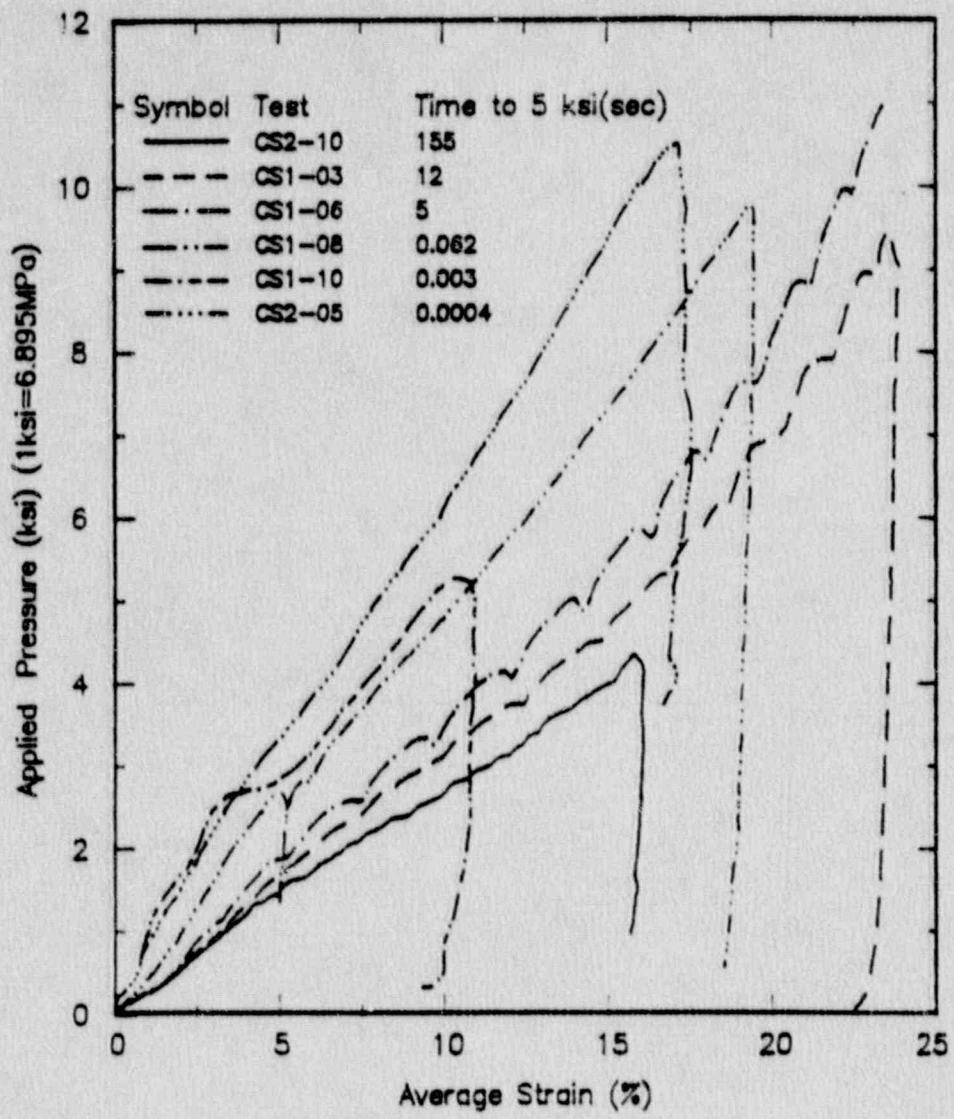

Fig. 3-11. Loading-rate effects on uniaxial compression characteristics of Enewetak beach sand (Ref. 14).

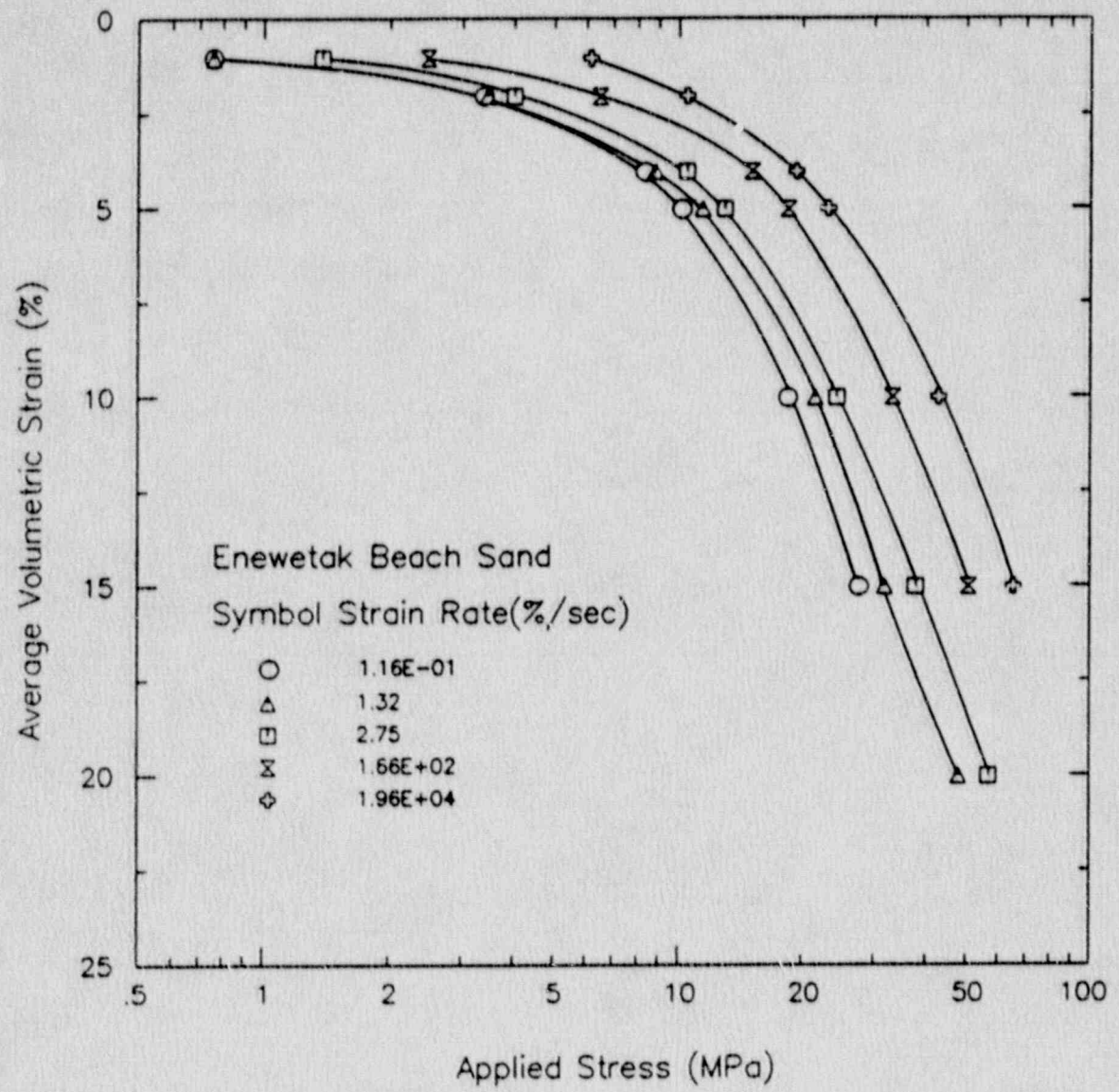

Fig. 3-12. Alternative representation of uniaxial compression data for Enewetak beach sand.

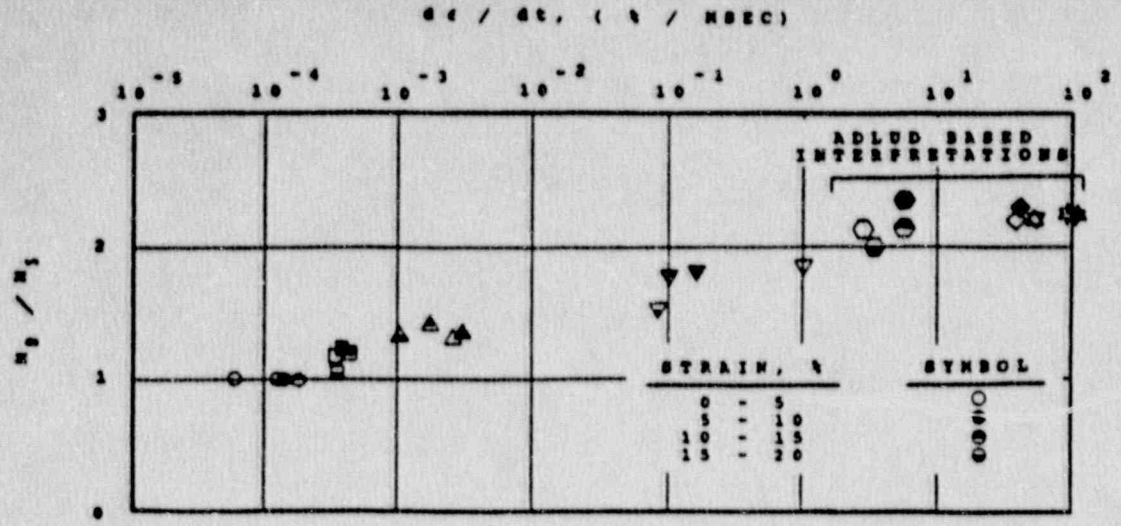

Fig. 3-13. Strain-rate effect on uniaxial modulus for Enewetak beach sand (Ref. 14).

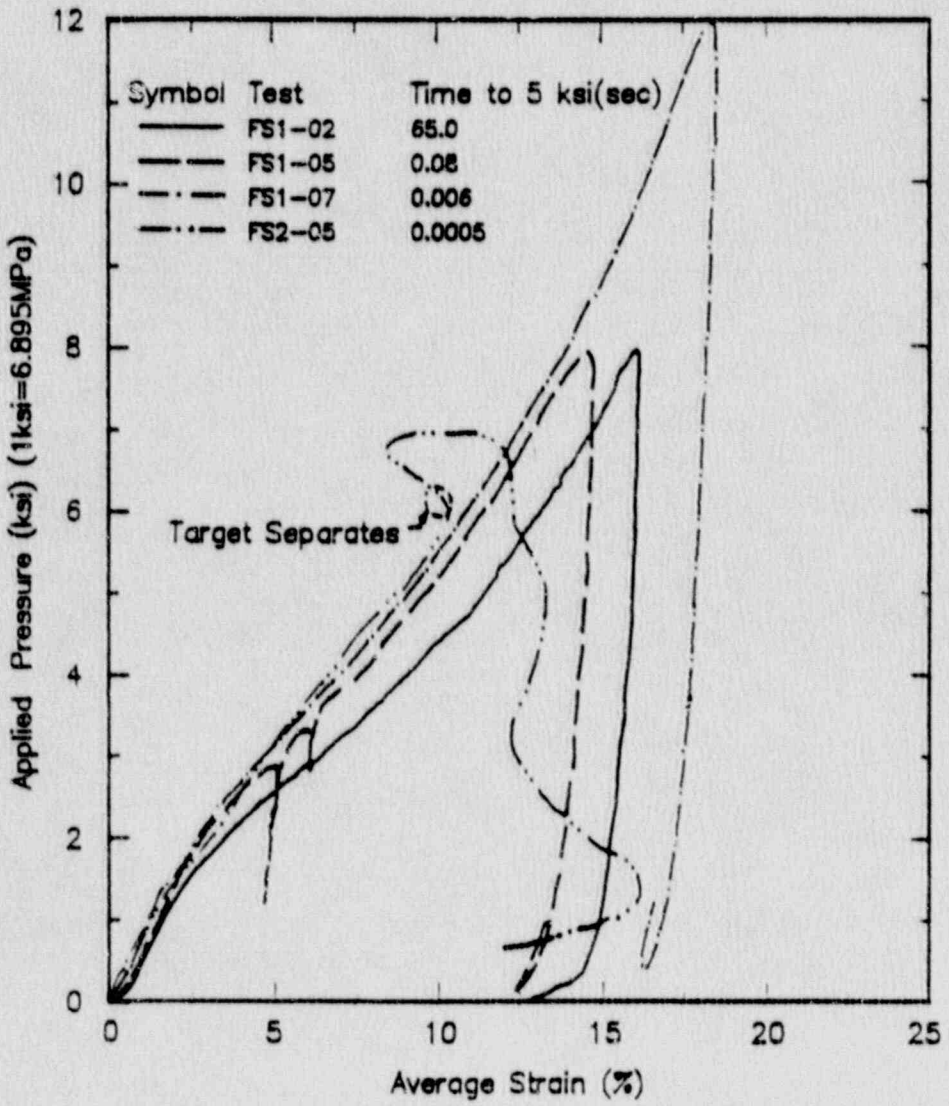

Fig. 3-14. Loading-rate effects on uniaxial compression characteristics of flume sand (Ref. 14).

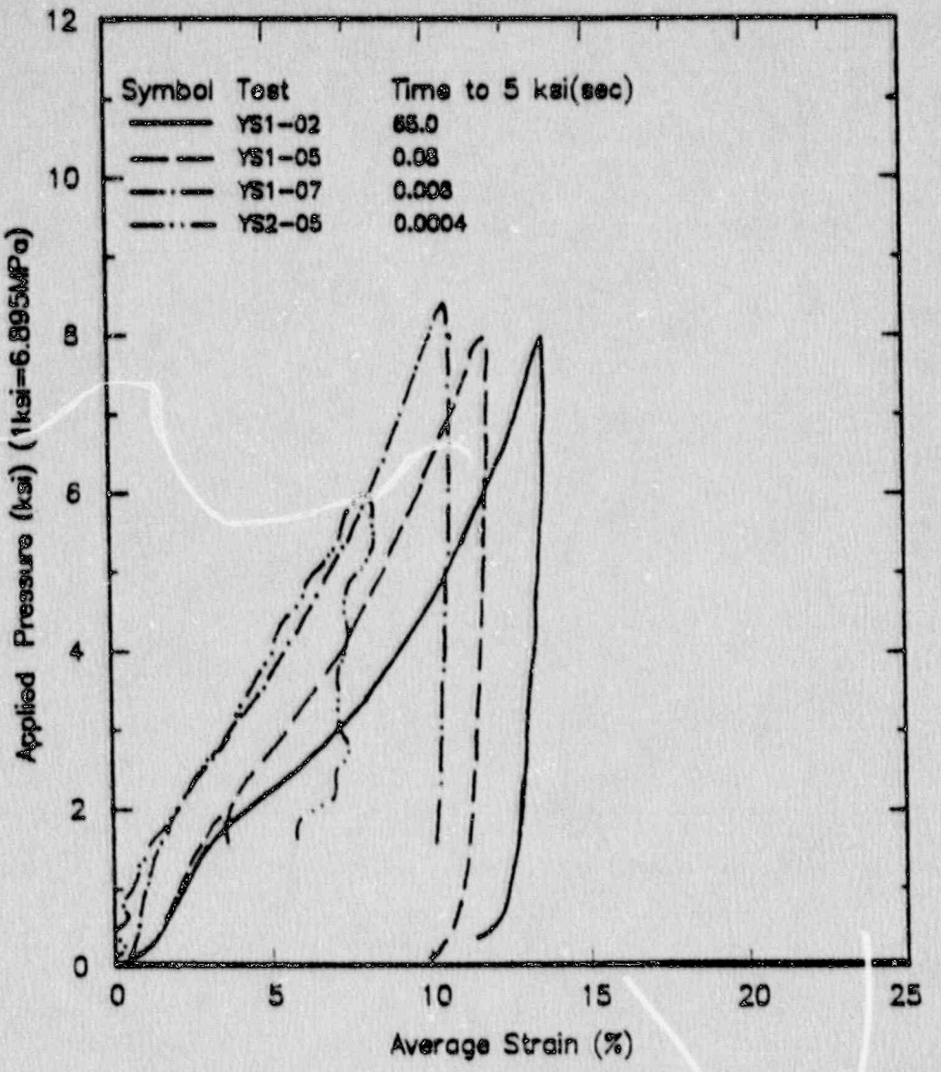

Fig. 3-15. Loading-rate effects on uniaxial compression characteristics of Yuma clayey sand (Ref. 14).

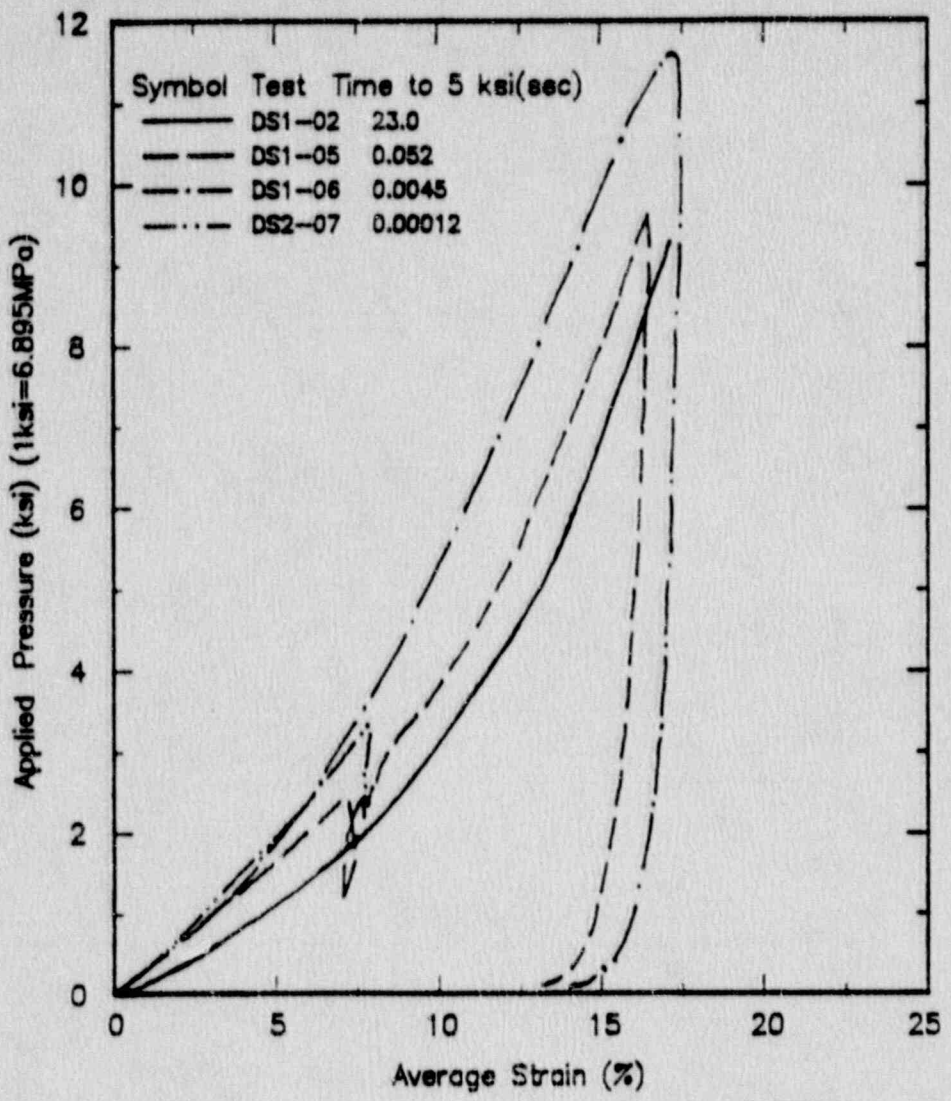

Fig. 3-16. Loading-rate effects on uniaxial compression characteristics of Vicksburg loess (Ref. 14).

3.3 Confining Stress Effects

As mentioned previously, imposition of high confining stress can modify the geologic stress history, degree of saturation, strength, and compressibility characteristics. In fact, all of these items tend to be interrelated.

Stress history is the most directly affected by high confining stress and is discussed first. Most soils exist in a state of overconsolidation to some degree, ranging from lightly overconsolidated (OCR = 1+ to 3) to heavily overconsolidated (OCR > 8); the overconsolidation ratio, OCR, is the ratio of the maximum past effective consolidation (sometimes referred to as preconsolidation) stress to the presently existing effective stress (i.e., OCR = $\sigma_{vmax}'/\sigma_{v0}'$). It is evident, therefore, that as effective confining stress is increased from the existing stress, OCR decreases. That continues until the increased stress achieves the maximum past effective stress; at which point and beyond, the increased stress and maximum stress levels are the same and the soil is in a normally consolidated (OCR = 1) state.

This change of stress history has important implications to compressibility characteristics (i.e., compressibility increases as OCR decreases). Consider, for example, the one-dimensional consolidation characteristics of Saint-Jean-Vianney clay illustrated in Fig. 3-10 and/or Enewetak beach sand illustrated in Fig. 3-12. Both of these soils exhibit relatively low compressibilities at stress levels less than the past maximum pressure (OCR > 1), then experience a sharp increase of compressibility at and beyond the maximum past pressure as the soil is strained in virgin compression (OCR = 1).

As discussed by many authors, shear strength is strongly affected by effective confining stress and stress history, as indicated by the expressions

$$S_u = \beta\,(OCR)^m\,\sigma_0',$$

$$S_d = \sigma_0' \tan \Phi',$$

in which the subscripts u and d designate undrained and drained shear strength, respectively. In both situations, strength is directly proportional to effective confining stress and therefore to increases of confining stress. Strengths are also affected by stress history, although the effect is generally different for clayey and sandy soils. The undrained strength expression, commonly used for clayey soils, contains a term, β, which is the strength ratio for normally consolidated conditions and typically has a value in a range of 0.25 to 0.35 and a term for OCR with an exponent, m, which typically has a value of about 0.8. For drained strength, typically used for sandy soils, stress history is most commonly reflected by relative density and in corresponding changes of friction angle, Φ'. In either case, OCR values greater than one are responsible for observed curvature of the failure envelope at low effective stress levels.

Degree of saturation also increases in response to the increased confining stress. The soil density increases as a result of compression of air in the void spaces and intergranular effective stresses are increased according to the compressibility characteristics of the soil. When all void space containing air has been compressed, the air has either been expelled or has been taken into solution by pore water and the soil is then considered to be in a saturated state and to behave accordingly.

4.0 CHARACTERIZATION OF PSA FLIGHT 1771 CRASH SITE SOILS

4.1 Site Description

As mentioned in Section 1.0, the analysis verification study is based upon the crash of PSA Flight 1771 on December 7, 1987. The crash site information and test data for the site's geological materials are being utilized in the study's dynamic soil-rock-structure interaction analysis.

The PSA Flight 1771 crash site is located 17.6 km (11 miles) northwest of Atascadero, California. Figure 4-1 illustrates the mapped geology and topography in the vicinity surrounding the crater created by the airplane's impact. From this plan view, it may be observed that:

1. The PSA airplane crashed part-way up a hillside with a top elevation of about 410 m (1347 ft). The elevation of the impact point is about 404 m (1325 ft).

2. The topography in the crash site vicinity is moderately sloping. The overall hillside slope gradient is about 21 degrees downward to the east, with localized gradients as steep as about 28 degrees. Through the crash impact crater, the slope gradient is about 23 degrees.

3. The geology mapped for the crash site vicinity consists of a surface veneer of Quaternary colluvial soils underlain by late Mesozoic marine sedimentary rocks.

4. Ground cover in the crash site vicinity reportedly consisted of grasses and a few scattered trees. A wooded area lies adjacent to the crash impact location.

5. The crash-impact crater is essentially elliptical in shape with dimensions of about 20 m by 7.5 m (65 ft by 25 ft), elongated in a north-south direction. The maximum depth of the crater was reportedly about 3.5 m (11 ft).

Details regarding the local crash site geology and subsurface geological materials are described in Ref. 47. Geotechnical characteristics of these materials were investigated through a program of field exploration and laboratory testing. Characterization of geotechnical properties for the colluvial soils and residual soils (the decomposed upper portion of the sedimentary rock sequence) is described in the remaining portions of this section. Characterization of properties for the rock materials is described in Ref. 1.

4.2 Site Characterization Program

4.2.1 Field Exploration Overview

Subsurface geological conditions in the crash site vicinity were investigated by drilling and sampling five exploratory holes. The approximate locations of these holes are shown in Fig. 4-1. The deepest penetration among the holes was 21.3 m (69.9 ft) in hole DH-1, drilled within the limits of the crash impact crater. The other four holes, DH-2 through DH-5, were drilled outside the crater boundary in an effort to characterize the pre-crash conditions of the materials. Penetration depths of these holes ranged between 14.9 m (48.9 ft) and 15.6 m (51.2 ft). Each of the holes encountered a veneer of colluvial soil deposits and/or residual soil materials (decomposed rock) overlying rock, grading from intensely weathered to unweathered. Drive samples of the soil materials and core samples of the rock were obtained for laboratory testing. In addition, geophysical measurements (shear and compression wave velocities) were obtained for the zone of weathered rock. Hole logs describing the conditions encountered in each hole are presented in Ref. 47.

4.2.2 Laboratory Testing Overview

The laboratory testing portion of the site soil characterization program was intended to provide information regarding the identification and classification, volumetric compressibility, and shear strength and shear stress-deformation characteristics of the soils. The testing program consisted of visual classification, water content, plasticity, and unit weight evaluations to provide indices to identify and classify the soils; one-dimensional consolidation tests to provide volumetric stress-strain characteristics, as well as a means to estimate the apparent existing soil-stress history; and unconsolidated undrained triaxial tests to provide measurements of undrained shear strength and shear stress-deformation characteristics.

The seven soil samples selected for testing involved a variety of soil types and conditions. Only samples from holes outside the crash impact crater were tested. Test sample depths ranged between 0.075 m and 1.8 m (0.25 ft and 6 ft) below the ground surface. Details of the laboratory testing program are presented in Appendix A.

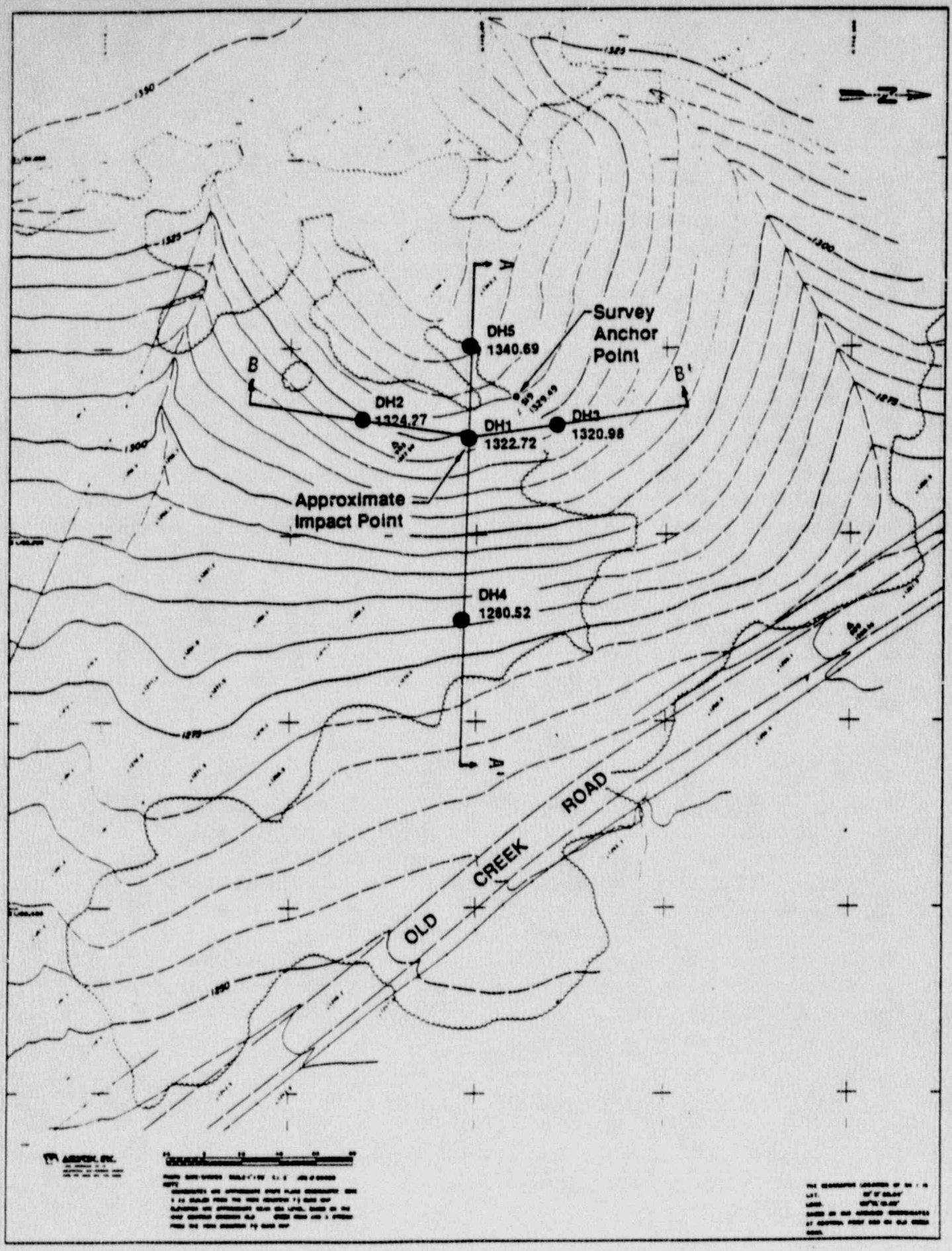

Fig. 4-1. PSA Flight 1771 crash site vicinity map.

4.3 Crash-Site Soil Properties Interpretation

4.3.1 Stratigraphic Conditions

Mapped geological conditions at the crash site indicated that a veneer of Quaternary colluvial deposits is underlain by late Mesozoic marine sedimentary rock materials. Within the vicinity of the crash impact location, but outside of the crater, field exploration encountered the colluvial deposits at the ground surface with thicknesses up to 0.2 m (0.7 ft) and consisting variously of sandy silt, clayey silt, and silty clay. The sedimentary rock materials are interpreted to be Great Valley Sequence and consist primarily of interbedded clay shales and silty sandstones with occasional seams of siltstone and claystone. The upper portion of this sequence, immediately underlying the colluvium, has been decomposed through weathering to a residual soil condition. These residual soils, although formed from rock decomposed in place, have properties and behavior characteristic of soils rather than rock and will be treated as such herein. The residual soils consist of lean silty sandy clay, decomposed from the shale, and silty sand, decomposed from the sandstone. The residual zone varies in thickness from about 0.3 to 3 m (1 to 10 ft), with greatest thickness at about mid-slope height (i.e., approximately the elevation of the crash impact crater). Thus, the zone of soils considered in this report appears to have a maximum thickness of about 3.5 m (11 ft); the remainder of the rock sequence, grading with depth from intensely weathered to unweathered, is not addressed herein. Geologic cross sections through the site (section locations shown in Fig. 4-1) are illustrated in Fig. 4-2.

4.3.2 Geotechnical Properties

Observations made during the field exploration indicate that the residual soil materials encountered were typically very stiff to hard (clays) or very dense (sands). The colluvium, although not appearing as strong because of its ground surface location, is also interpreted to be quite competent based upon blow count information. Measured blow count data, corrected for overburden effects, are illustrated in Fig. 4-3. Note that the colluvium and in-place residual soils have penetration resistances (blow counts) that are quite similar. Laboratory measurements of moisture content, density (unit weight), strength, and apparent stress history characteristics are consistent with the field observations.

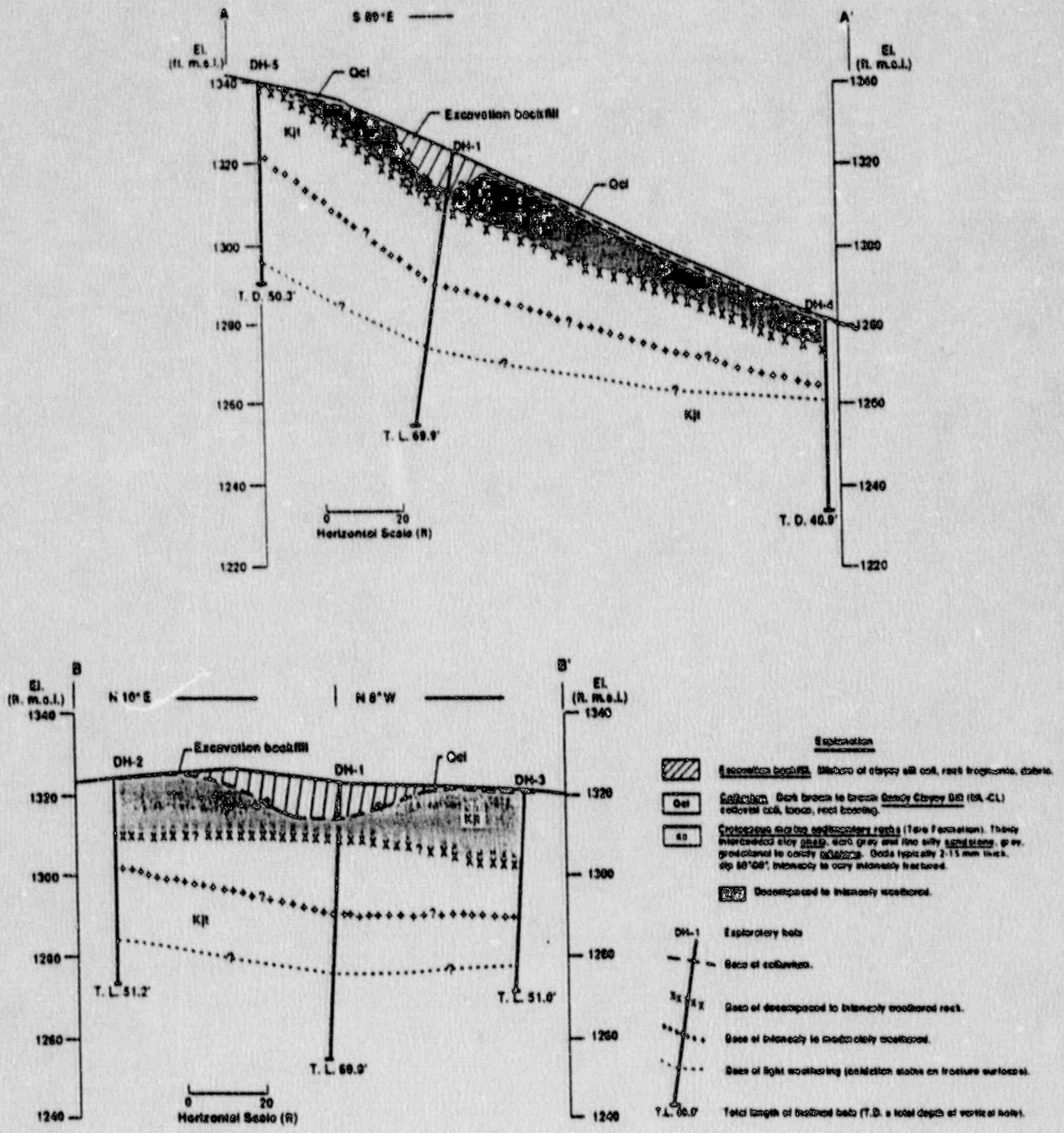

Fig. 4-2. Geologic cross-sections through crash site.

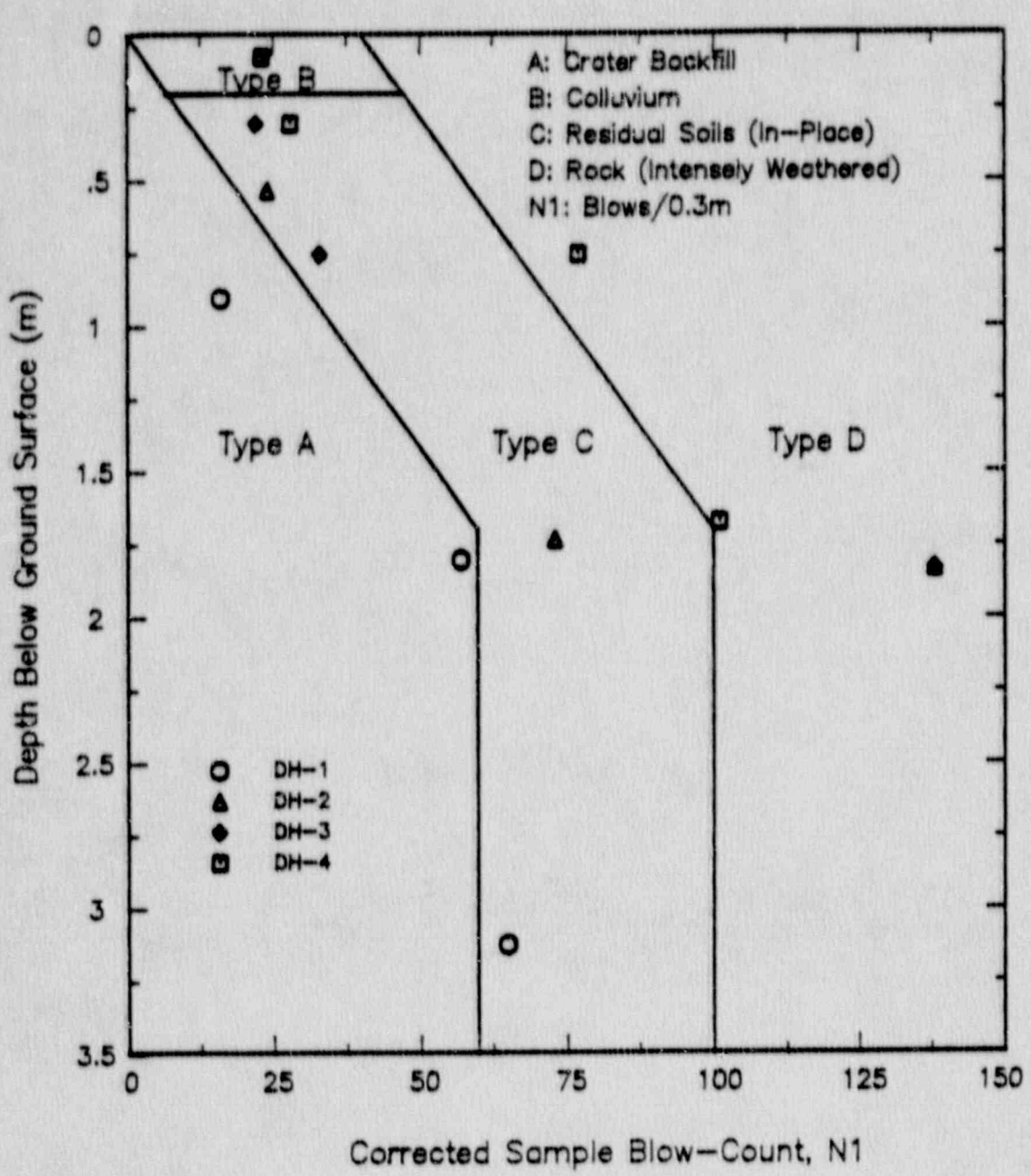

Fig. 4-3. Corrected blow-count data from field exploration drilling and sampling program.

4.3.2.1 *Classification and Index Properties*

Soil unit weights (total, γ_T, and dry, γ_D) are important characteristics for determining in-situ effective confining stress conditions and for estimating anticipated volumetric strains due to effective stress changes (γ_D is a measure of the structural density of a soil and therefore is directly linked to void ratio changes and volumetric strains). Figure 4-4a illustrates the unit weights measured for the site soils. The data indicate a trend of unit weight increasing with depth at a rate of about 150 kg/m^3 per meter (3 lb/ft^3 per foot) for both γ_T, and γ_D, although γ_T, has surface intercept of about 1850 kg/m^3 (117 lb/ft^3), whereas the intercept for γ_D is about 1570 kg/m^3 (98 lb/ft^3). The relationship between γ_T and γ_D is given by the expression:

$$\gamma_T = (1 + w_c)\,\gamma_D,$$

in which w_c is the moisture content of the soil. It should be noted here that the soils at the site exist in an unsaturated condition, and thus measured γ_T reflects the in-situ moisture conditions as encountered during drilling and sampling. The degree of saturation and corresponding volumetric proportion of air-filled void space for the soils at the time of sampling have been estimated from the tested specimens, and these estimates are presented in Fig. 4-5. Moisture conditions and therefore γ_T may be seasonally dependent and vary as rainfall percolates into and through the ground, replacing air in void spaces with water. The upper limit for values of γ_T is given by the saturated condition, with or without a groundwater table (i.e., all void spaces filled with water).

Moisture contents measured for the soils at the site are illustrated in Fig. 4-4b and are shown to be in the range of 16 to 21 percent. Also illustrated are liquid and plastic Atterberg limits (LL and PL, respectively) determined for three of the residual soil clay samples. (Atterberg limits are the limiting water contents of a clay-water mixture that define physical states of the clay. Above the liquid limit, the soil-water mixture is a suspension. Below the liquid limit and above the plastic limit the soil-water mixture is said to be in a plastic state. The limiting water content serve as index properties useful in the classification of clays.) The Atterberg limits indicate these clays to be of low to medium plasticity, with Plasticity Indices (PI = LL – PL) between 8 and 15. As is illustrated by Fig. 4-4b, moisture contents are below the PL for each case determined. Liquidity index (LI), given by the expression:

$$LI = (w_c - PL)/PI,$$

is a measure of the relative "wetness" of a soil and is a useful index that is indicative of shear strength and stress history conditions. As would be expected from an examination of Fig. 4-4b, LI is negative for these soils, indicating relatively high shear strengths and/or high degrees of overconsolidation (see Ref. 22).

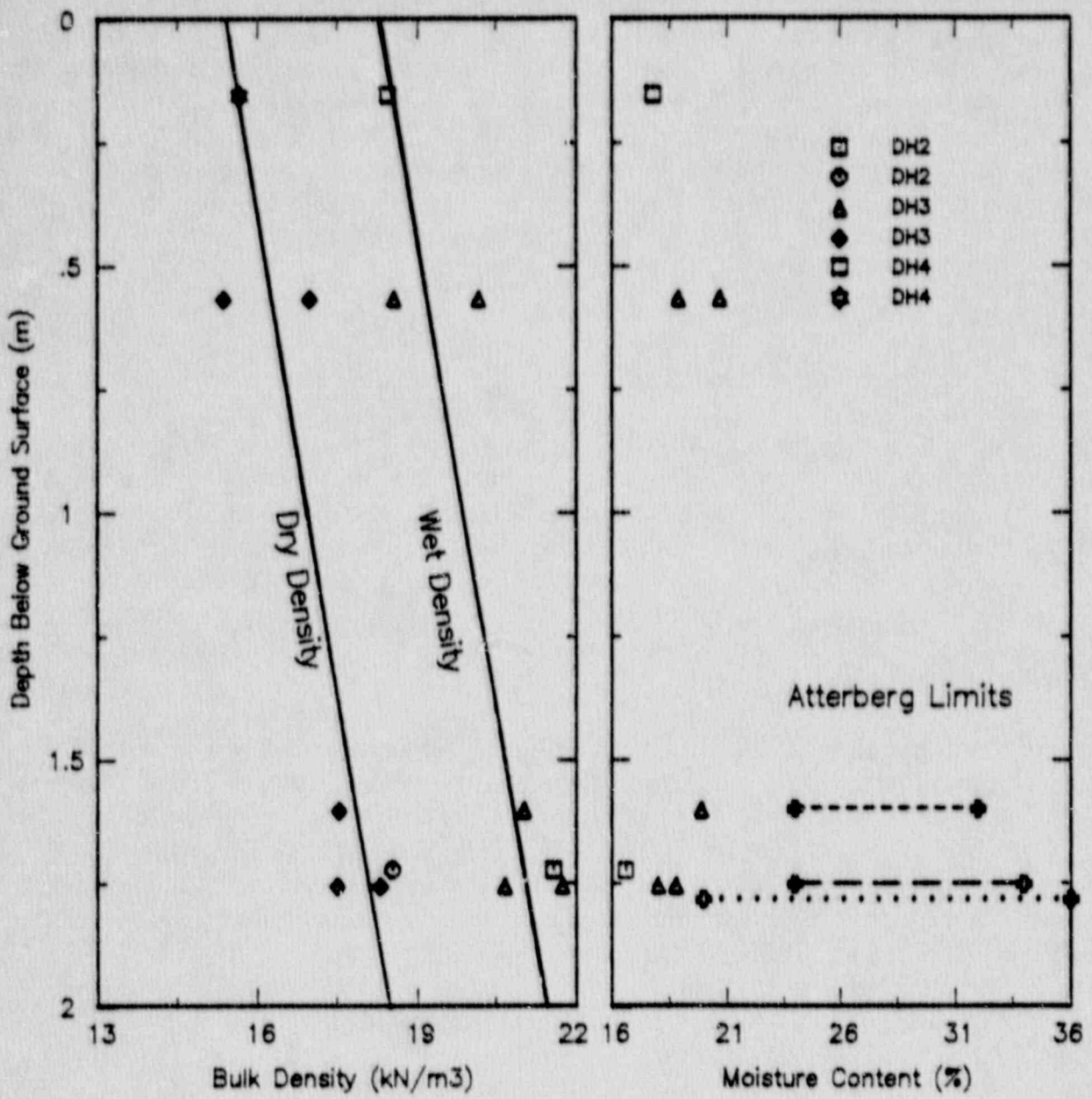

Fig. 4-4. Depth variation of bulk density, water content, and plasticity characteristics.

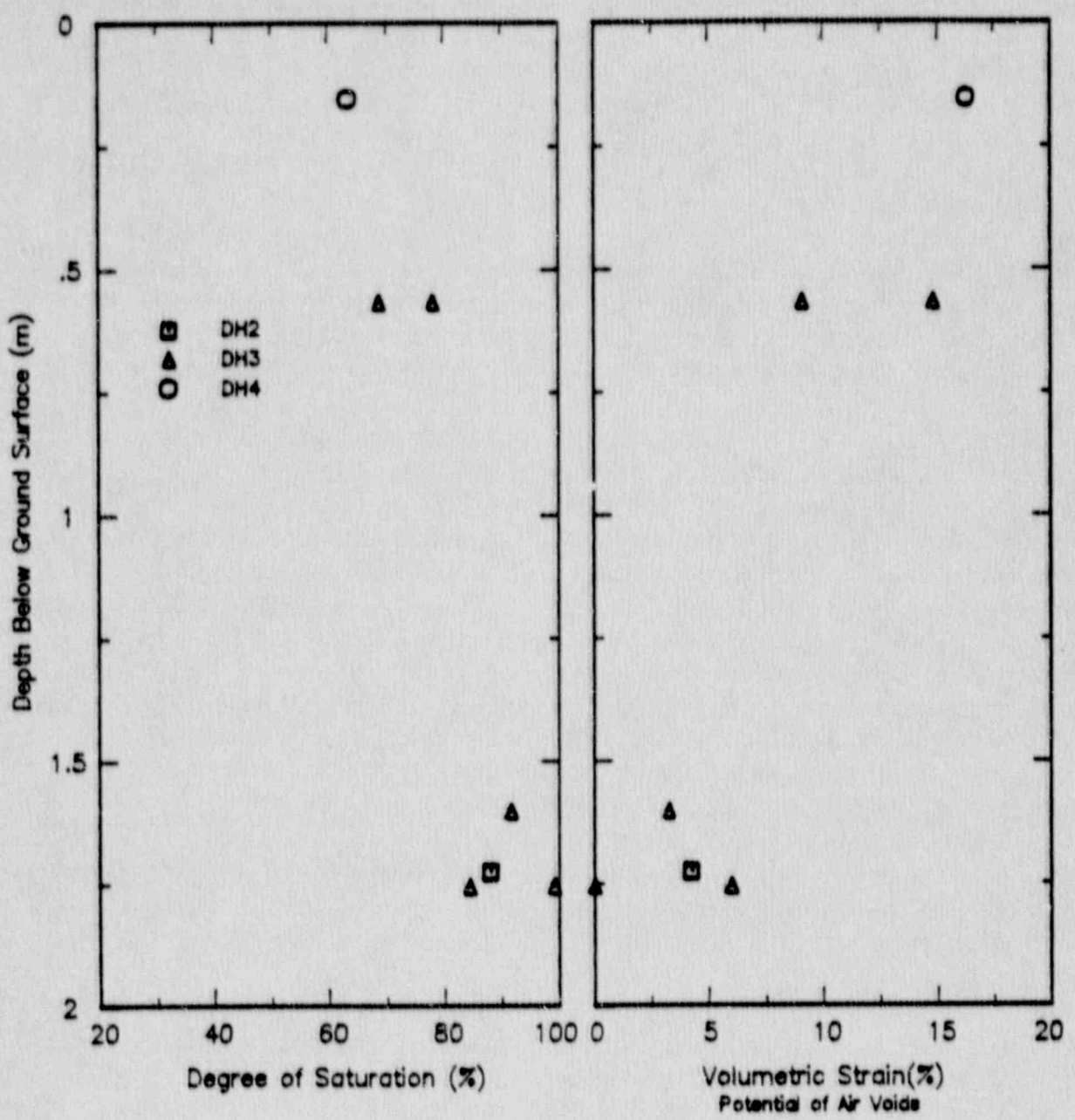

Fig. 4-5. Depth variation of degree of saturation and volumetric strain potential of air voids.

4.3.2.2 *Volume Change and Stress History Characteristics*

One-dimensional consolidation tests were utilized to investigate volume change and stress history characteristics for the crash site soils. Results from those tests are presented in Appendix A. At first examination of those results, significant differences of compressibility appear to be represented among soils at the site, with a ratio of about two between volumetric strains for the near-surface colluvium sample and the residual soil sample tested from a depth of about 1.8 m (6 ft). Distinction is drawn here between the surficial colluvium and the underlying residual soils because of the different natures of their respective formation. The colluvium by its nature may be expected to exhibit greater compressibility than the residual soils. Given such anticipated differences, however, there is an overall trend of decreasing compressibility with depth in the soil profile. The marked differences in measured volumetric strains, however, are a product of the variations with depth of initial dry density, existing in-situ effective stress, and past maximum effective stress. When these aspects are taken into consideration and the soil profile examined as a unit, a consistent pattern of behavior emerges. As previously mentioned, volumetric strain and changes of dry unit weight are directly related; therefore the volumetric strains from the consolidation test results were evaluated in terms of dry unit weight and the compression relationships for the three samples were recompared, as illustrated in Fig. 4-6. This figure indicates that the characteristics controlling volume change (i.e., virgin compression curves and rebound curves) are quite similar within this soil profile among the samples tested. Examination of Fig. 4-6 illustrates the similarity and difference of the dry-density-versus-mean-effective-stress relationships for this soil profile among the colluvium and residual soil samples tested. The two residual soil curves converge to the same virgin compression line, whereas the colluvium curve lies outside of, but essentially parallel to, the residual soil curves.

Estimates of stress history characteristics for the soils at the site were evaluated using the measured unit weight properties and the one-dimensional consolidation test stress-strain results presented in Appendix A. Existing in-situ vertical effective stress conditions were approximated using the variation of total unit weight with depth illustrated in Fig. 4-4a, which produced the relationship illustrated in Fig. 4-7. Estimates of maximum past consolidation stress (σ_{vmax}') were derived from the consolidation test results using a modified form of the J. H. Schmertmann (Ref. 48) approach and employing the measured virgin and rebound compressibility characteristics. Combining the estimates of maximum past consolidation stress and existing in-situ effective stress, values for overconsolidation ratio (OCR) were developed. These values are illustrated in Fig. 4-7; they are presented as "apparent" because the mechanism that produced the overconsolidation is not clearly evident, although it is well known that weathering and desiccation of soils and decomposition of rock can create overconsolidated behavior such as observed for the crash site soils. Finally, given the values of OCR and σ_v' (effective overburden

pressure), in-situ mean normal effective stress σ_m' was estimated from the expression:

$$\sigma_m' = (1 + 2K_0)\,\sigma_v'/3,$$

in which K_0 is the at-rest lateral earth pressure coefficient and was estimated using relationships between K_0 and OCR appropriate for soils with similar characteristics (see Ref. 49). Estimated existing in-situ mean normal effective stress for the crash site is illustrated in Fig. 4-7.

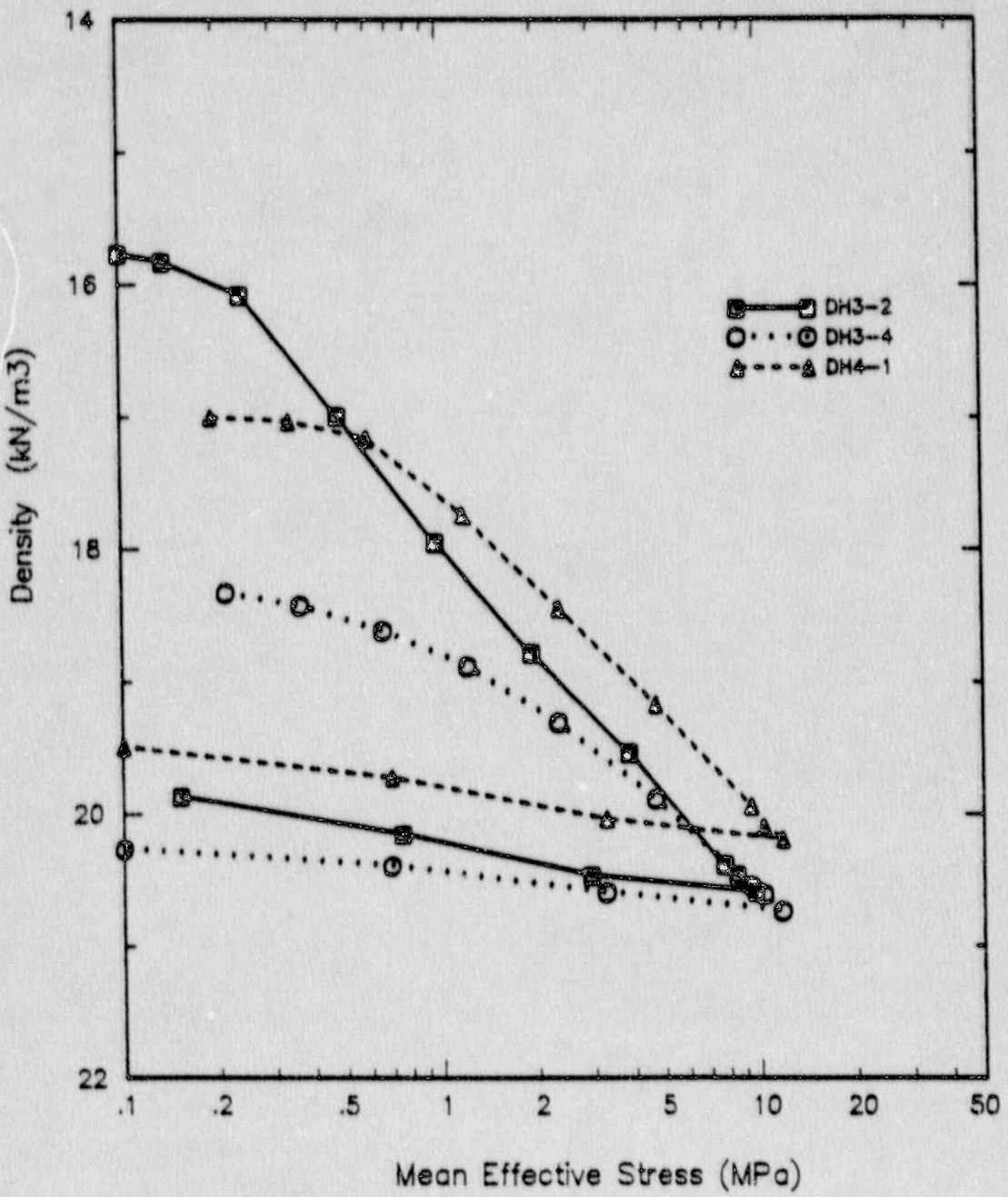

Fig. 4-6. Relationship between dry bulk density and mean effective stress.

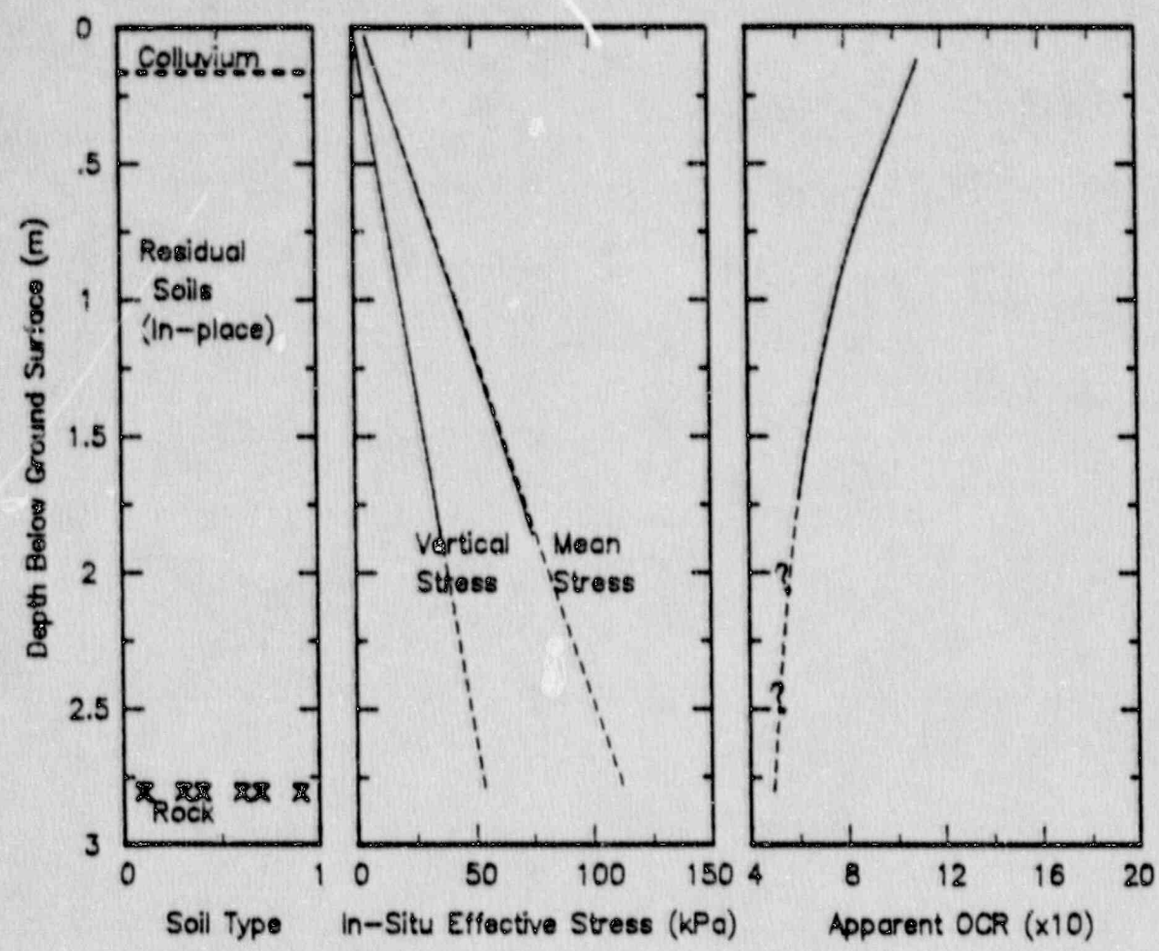

Fig. 4-7. Depth variation of effective stress and stress history characteristics.

4.3.2.3 *Strength and Modulus Characteristics*

Relatively undisturbed, intact specimens were tested "as-is" under unconsolidated-undrained (UU) conditions in triaxial compression to examine the shear characteristics of the soil, specifically strength and stress-strain properties. Thus, as indicated previously, the soil specimens were unsaturated to varying degrees at the outset of the tests. This fact has important significance to interpretation of the test results. Prior to beginning shear, volumetric strain measurements were obtained during the incremental application of the triaxial confining stress, and the stress-strain curves from these measurements are presented in Appendix A. By comparing the volumetric strain induced in a specimen by the test's confining stress

with the available volumetric strain potential of the air voids for that specimen, we have deduced that three of the specimens tested (DH3-2, -3, and -4) remained unsaturated at the beginning of shear and during shear; therefore, all of the applied confining stress and shear stress contributed to intergranular effective stress, and the specimen behaved in a "drained" fashion. The fourth specimen (DH2-2) is interpreted to have compressed to a saturated condition at or near its test's confining stress and therefore to have behaved in an undrained manner. Stress paths representing the response of the respective specimens are illustrated in Fig. 4-8. Because pore pressures were not measured, the actual stress path for specimen DH2-2 is unknown, but it is assumed to have achieved the same failure envelope as the other three specimens. The failure envelope demonstrated by the specimens corresponds to an effective stress friction angle (Φ') of about 20°. As is indicated by the relationship illustrated in Fig. 4-9, the observed individual test friction angles agree quite well with friction angles for other residual soils with similar plasticity characteristics (see Refs. 50 and 51).

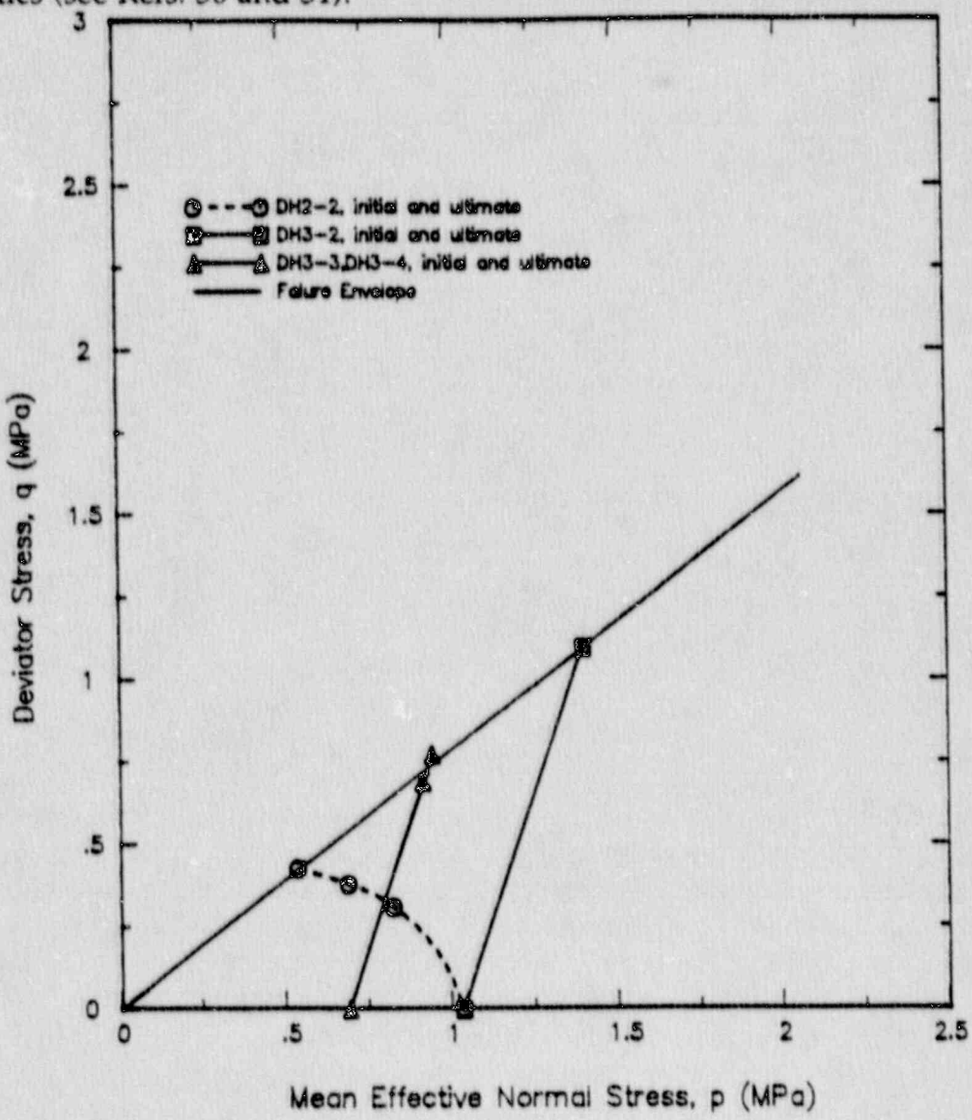

Fig. 4-8. State-space characteristics determined from triaxial test results.

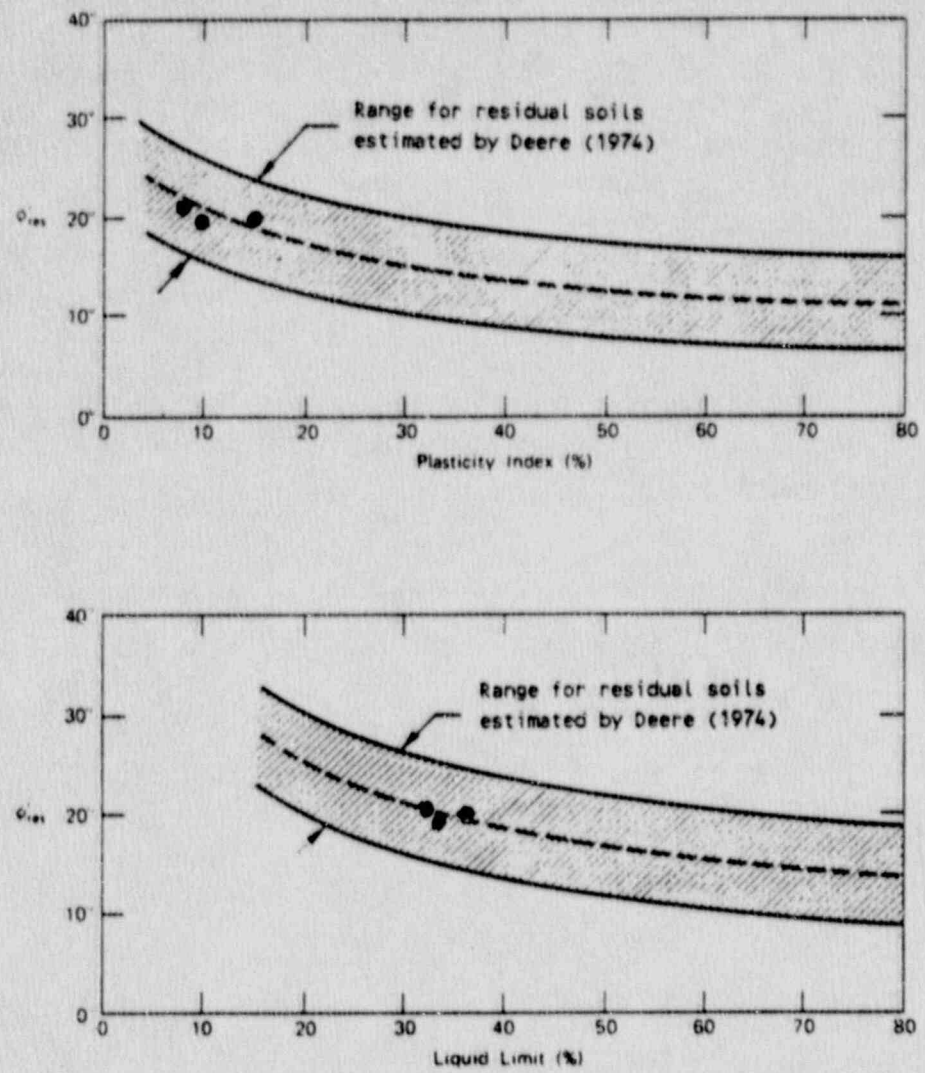

Fig. 4-9. Comparison of crash-site soil friction angle to other residual soil friction angles.

As may be seen by the stress path (Fig. 4-8) and stress-strain responses (Appendix A), there are dramatic differences between the drained and undrained behavior. If the soil remains unsaturated and behaves in a "drained" manner during shearing, strength may be estimated by an equivalent μ of 0.78, whereas if saturated undrained conditions occur, strength is given by an equivalent μ of 0.37.

Variation of shear modulus (G) with applied stress level has also been examined for the site soils. These shear modulus results, illustrated in Fig. 4-10, indicate a difference of response between the saturated undrained specimen and the specimens interpreted to be "drained."

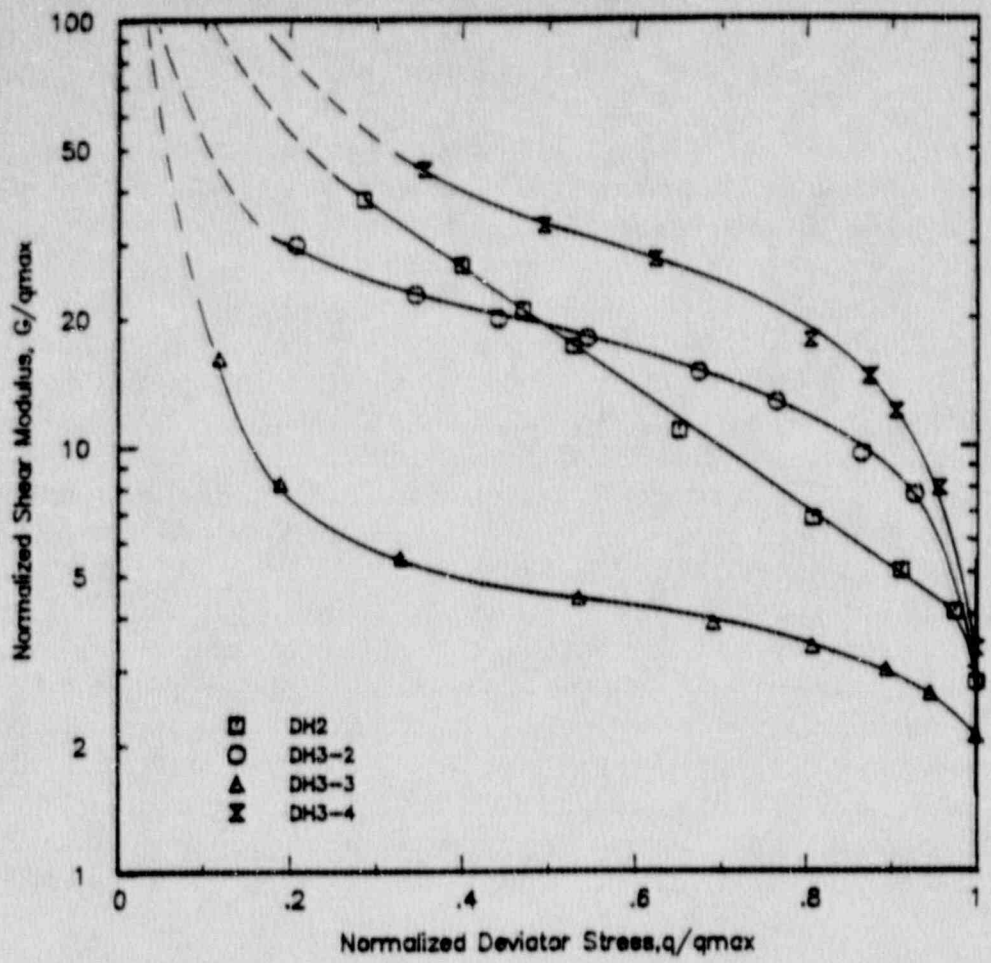

Fig. 4-10. Variation of normalized shear modulus with relative deviator stress level.

4.4 Crash-Impact Soil Behavior

During the moments of airplane impact and penetration into the soil, a number of phenomena are occurring simultaneously:

- The high impact stress states very rapidly impose increased confining stress conditions within the soil mass.
- In response to the increased confining stress, the soil density increases as a result of compression of any air in the void spaces, and intergranular effective stresses are increased accordingly. If the soil is saturated with water, no increase of density is manifested because of the relative incompressibility of the water, and the net effective stress state remains unchanged.
- The presence of the crashing airplane induces shear stress in the soil at a very high rate, with resultant shear deformation and failure response of the soil in accordance with the loading-rate-compatible modulus and strength characteristics of the soil.

To enable proper analytical modeling of the airplane-impact problem, effects of the phenomena cited above on the geotechnical characteristics of soils at the crash site must be accounted for. Those effects are described in the following paragraphs.

Changes of soil density and intergranular effective stress are controlled by the volumetric compressibility characteristics of the soils and by the degree of saturation existing for the soils at the time of the crash. A volumetric compressibility curve may be developed for any depth of interest in the soil profile by utilizing the dry-unit-weight-versus-mean-effective-stress relationship illustrated in Fig. 4-6, the γ_D variation with depth illustrated in Fig. 4-4a, and the existing in-situ mean effective stress conditions illustrated in Fig. 4-7. To develop a curve, one first selects the average unit weight and mean effective stress appropriate to the depth for which the curve is being developed. That pair of values serves as the initial conditions for evaluating volumetric strain. Enter Fig. 4-6 at the point of those initial conditions and construct a line with the same slope as the rebound curves between the initial point and the virgin compression curve. The combination of constructed line and the virgin compression curve forms the basis for the volumetric compressibility curve being developed. Identify dry unit weight values for a number of mean effective stresses along those two curves (rebound and virgin compression curves), then evaluate the corresponding volumetric strain value using the expression:

$$\varepsilon_{vi} = 1 - (\gamma_{D0}/\gamma_{Di}),$$

where γ_{D0} = initial density and γ_{Di} = density at mean effective stress of interest. The volumetric compressibility curve is then developed from the mean effective stress and volumetric strain pairs. Curves developed for depths of 0.75 m (2.5 ft) and 1.5 m (5 ft) below the ground surface are illustrated in Fig. 4-11.

The second aspect controlling volumetric strain and effective stress is the degree of saturation, as reflected in the volumetric strain potential due to the air voids. During the crash impact, volumetric strain and effective stress increases can occur up to the point where the soil becomes saturated, after which it responds according to the description above. That limit may be identified from the variation of volumetric strain potential with depth given in Fig. 4-5. The saturation limits for the depths of 0.75 and 1.5 m are shown on the curves illustrated in Fig. 4-11. As is indicated in that figure, the volumetric strains induced by the crash impact are anticipated to be sufficient in this case for the mean effective stress to increase beyond the apparent past maximum consolidation stress to an essentially normally consolidated state. The soil is therefore expected to behave under shear according to characteristics for normally consolidated saturated-undrained conditions.

Given then a volumetric strain and a corresponding increased mean effective stress state defined by the compressibility curve, the undrained soil strength and modulus may be determined from the characteristics given in Section 4.3 and appropriately adjusted for strain-rate effects based upon the considerations described in Section 3.0. As mentioned, it is expected that saturated undrained conditions will prevail in the

PSA crash modeling, therefore strength should be evaluated using a value for μ of 0.37. Therefore, and with account taken of the increases in mean effective stress, the ultimate "static" strength variation with depth is expected to be similar to that illustrated in Fig. 4-12. By then applying strain-rate effect to that strength, the ultimate strength expected to be mobilized during the airplane crash impact is given by the band in Fig. 4-12 labeled "strain-rate effect". This band represents an increase of strength due to rapid loading on the order of 35 to 50 percent. This effect was evaluated using values from Fig. 3-9 appropriate to the range of Plasticity Index for soils at the crash site and the difference between the crash impact velocity and the laboratory rate of shear deformation.

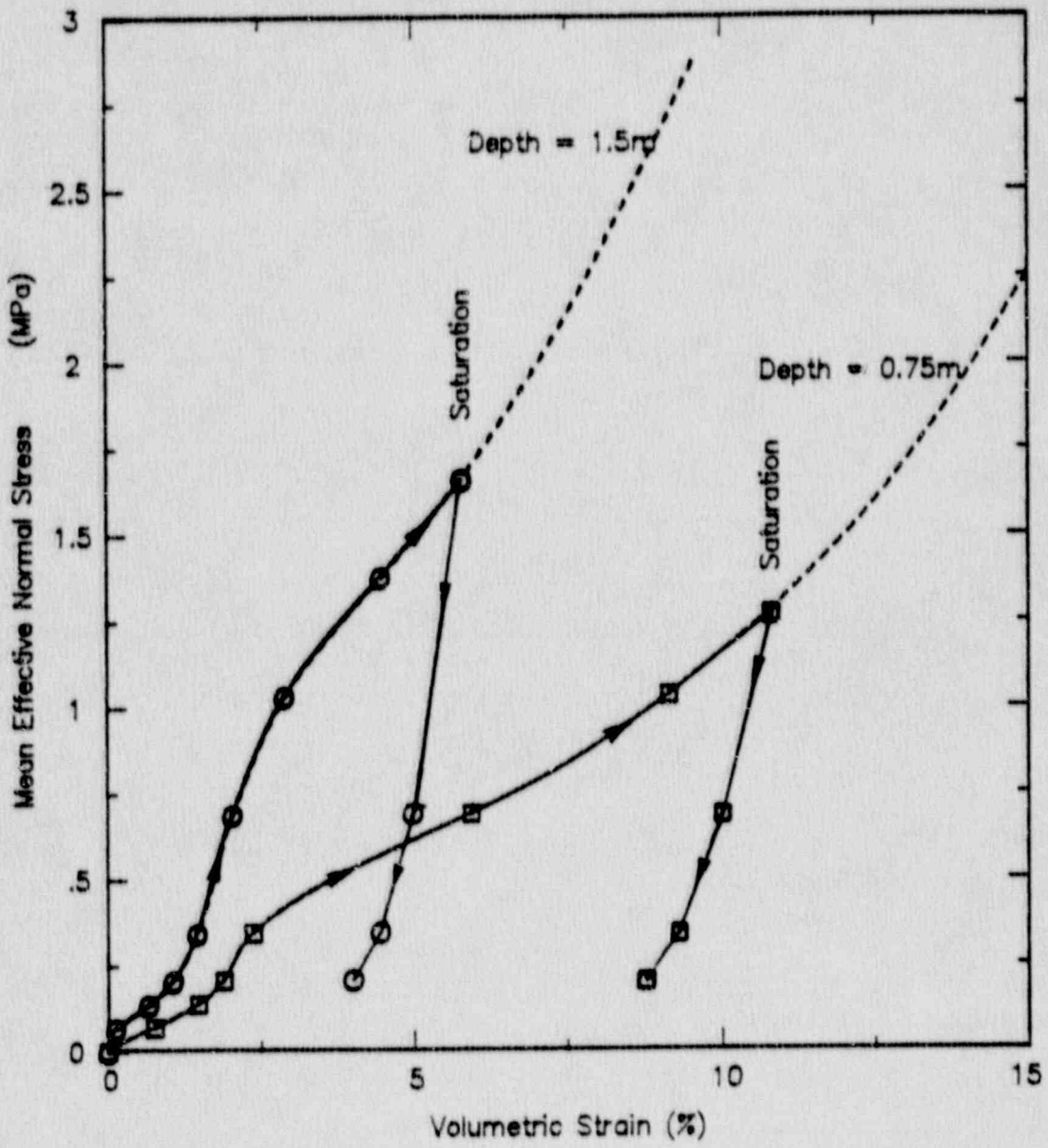

Fig. 4-11. Expected compressibility, saturation, and effective stress behavior during crash impact loading for depths of 0.75 and 1.5 m.

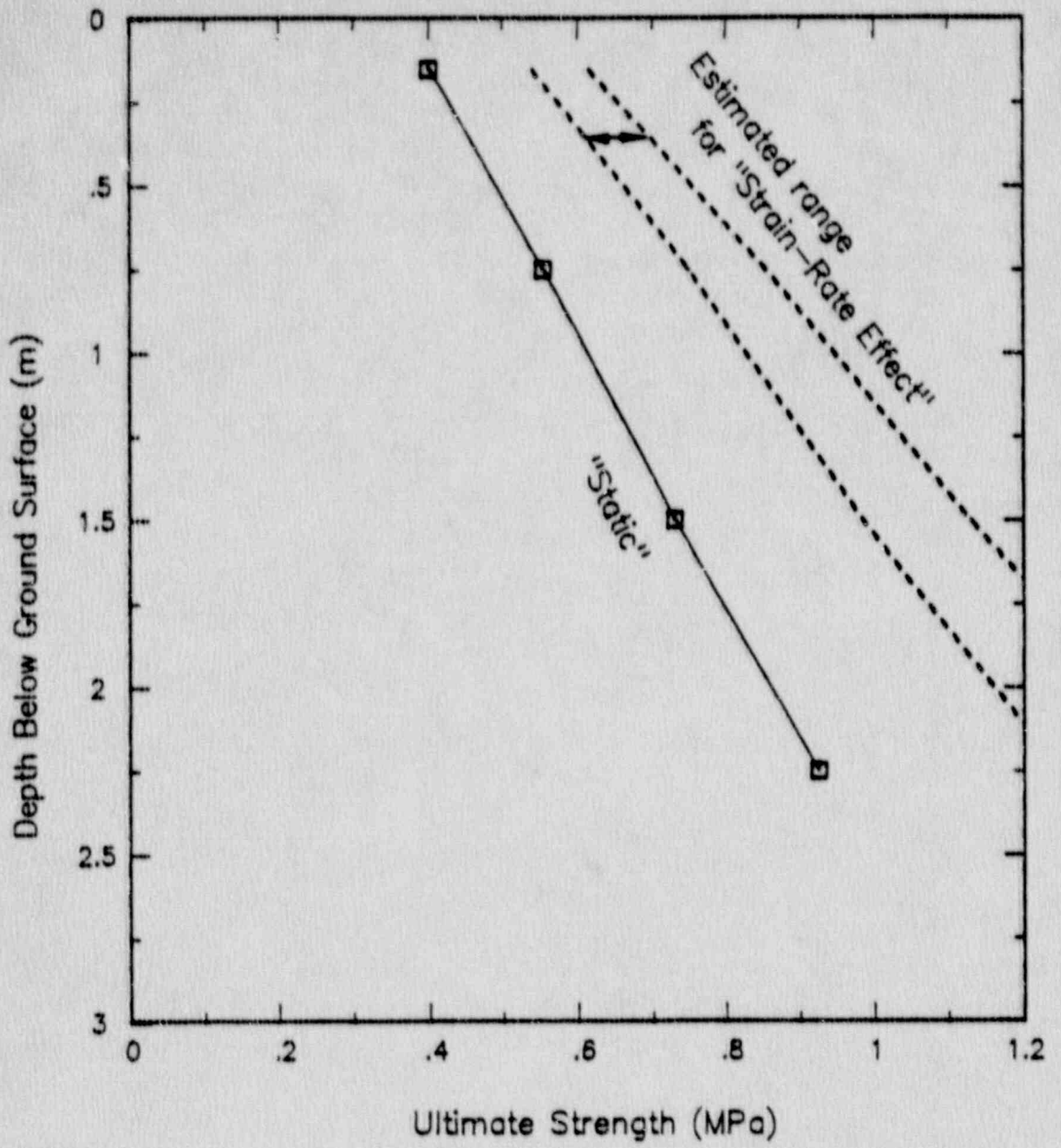

Fig. 4-12. Expected depth variation of ultimate strength behavior for crash impact loading conditions.

The parameters required for the Krieg model (model 5) developed for the PSA crash site soils described previously are summarized as follows:

Bulk density, γ_T:

For variations with depth, see Fig. 4-4.
Average value = 2090 kg/m^3 (130 lb/ft^3).
Coefficient of variation = 0.1.

Moisture content, w_c:

For variations with depth, see Fig. 4-4.
Average value = 16.2%.
Coefficient of variation = 0.3.

Unloading bulk modulus, K_e:

Values of K_e vary with mean effective stress level and the amount of unloading as shown in Figs. 4-11 and A-3. The range of values obtained from the test data is 2.1×10^5 to 0.5×10^5 kPa (0.3×10^5 to 0.07×10^5 psi) with an average value of 1.3×10^5 kPa (0.18×10^5 psi).

Ultimate strength, σ_u:

For variations with depth, see Fig. 4-12.
An average value calculated at 1.5 m depth is estimated to be 730 kPa (106 psi) for "as tested" slow rate of loading and 1060 kPa (154 psi) for impact loading.

Shear modulus, G:

Secant shear moduli of the site soil vary with stress level as shown in Fig. 4-10. For this study, values of shear modulus are defined at 50% stress level. The normalized shear modulus obtained from the undrained test data indicates that an average value of 11,600 kPa (1680 psi) may be expected for the slow rate of loading and 16,750 kPa (2430 psi) for impact loading.

Poisson's ratio = 0.45.

Slope of σ_y-versus-p curve, μ= 0.37.

Cohesive strength, $\tau_0 = 0$.

Tensile strength, $p_t = 0$.

Mean-normal-stress-versus-volumetric-strain curves: see Fig. 4-11.

5.0 CHARACTERIZATION OF MODEL PARAMETERS FOR OTHER SOIL CONDITIONS

5.1 General

To provide data for use in parametric studies, available test data for other soils have been gleaned from technical publications, books, journals and conference papers. These data include drained and undrained test results of clays, silts, sands, gravels and rock.

The test results reviewed are primarily from those obtained from static tests for the following reasons.

1. As previously mentioned in the literature review on strain-rate effect, test data of soils considering loading rate effect are not common.

2. Based upon test results of loading rate effect, the increase of strain rate causes primarily progressive strengthening of soil, and the effect perhaps can be covered by a strain-rate factor.

3. Because the basic features of soil behavior such as friction angle (failure envelope) and modulus variation are quite similar under either rapid loading or static loading, the data obtained for static conditions may be used as a basis for the numerical analysis.

4. The Krieg constitutive model (No. 5) used in DYNA3D is not a rate-dependent model, and the rate effect cannot be analytically incorporated without altering the model formulation.

The existing and available test data for a variety of soils obtained under undrained and drained loading conditions were deduced to develop parameter values required by the Krieg model (No. 5). The applicability of these parameter values for a specified site condition, of course, needs further examination in relation to the environment under consideration.

5.2 Parameter Values for Other Soils

Soil parameters for about 150 different soils have been compiled by J. M. Duncan, et al. (see Ref. 52). These parameters were developed for the nonlinear hyperbolic stress-strain model (Ref. 53). Due to the lack of original data, the parameters for the Krieg model (Ref. 3) were derived from the correlations between the Krieg model parameters and the hyperbolic model parameters of J. M. Duncan and C. Y. Chang (Ref. 53).

5.2.1 Correlations Between Duncan-Chang's Model and Krieg's Model

Before proceeding further, better understanding of the two models is warranted. The basic characteristics of these two models can be summarized as follows.

1. The hyperbolic relationship used by the Duncan-Chang model is a nonlinear elastic model, whereas the Krieg model is a linear-elastic, nonlinear-plastic model.

2. Consequently, Young's modulus and bulk modulus are dependent on confining pressure in the hyperbolic relationship, but shear modulus and bulk modulus of the Krieg model are constants for the input p-versus-v curve.

3. The mean-normal-pressure-versus-volumetric-strain curve (p-versus-v curve) is not a part of the hyperbolic relationship, but is an input data set required for the Krieg model.

4. The friction angle Φ in the hyperbolic relationship can be related to the slope of the yield surface, μ, in the Krieg model.

5. The cohesion value, c, in the hyperbolic relationship can be related to the cohesive strength, τ_0, in the Krieg model.

6. There is no ultimate strength concept in the hyperbolic relationship, so there is no definite way to derive σ_u values in the Krieg model.

A number of assumptions were made to convert parameter values from the Duncan-Chang model to the Krieg model, and they are listed in Table 5-1. The major drawback of this approach is the lack of p-versus-v curves in the report by J. M. Duncan, et al. (see Ref. 52), simply because hyperbolic relationships do not require such data. The mean-normal-pressure-versus-volumetric-strain relationships need to be developed using the actual test data.

5.2.2 Converted Parameters for Krieg's Model

The stress-strain parameters reported by J. M. Duncan, et al. (Ref. 52) for a variety of soils ranging from clays to sandy gravels under unconsolidated-undrained conditions were used to convert to the parameter values for the Krieg model using the correlations between the two models summarized in Table 5-1. The developed parameters for the Krieg model are shown in Table 5-2. It is noted that the ultimate strength for some of the materials are not available, but for frictional materials their values are expected to be large.

Table 5-1. Correlation formulation between Duncan-Chang's Model and Krieg's Model.

Parameters in Duncan-Chang's Hyperbolic Relationships	Parameters in Krieg's Model	Correlations Between Parameters
$\Phi = \Phi_0 - \Delta\Phi \log_{10}(\sigma_3/p_a)$ where: Φ_0 = friction angle for σ_3 = 1 atm (σ_3 = confining pressure), $\Delta\Phi$ = reduction in friction angle for a ten-fold increase in σ_3, p_a = atmospheric pressure.	μ = slope of σ_y-vs-p curve	$\mu = (6 \sin\Phi)/(3 - \sin\Phi)$ (See Appendix B)
c = cohesion intercept	τ_0 = cohesive strength	$\tau_0 = (6c \cos\Phi)/(3 - \sin\Phi)$
No ultimate strength	σ_u = ultimate strength	$\sigma_u \geq \tau_0 + \mu(p_m)$ where: p_m = test pressure
K_u = modulus number n = modulus exponent, unloading modulus $E_u = K_u p_a (\sigma_3/p_a)^n$	Elastic constants: G = shear modulus K_e = bulk modulus	Assume $\nu = 0.35$, then for a given σ_3: $G = (1/2.7) E_u$ $K_e = 1.11 E_u$
K_b and m are bulk modulus number and exponent $B = K_b p_a (\sigma_3/p_a)^m$ where: B = loading bulk modulus	For a linear p-vs-v curve: $K_1 = p/v$ = constant	For a given σ_3: $B = dp/dv = K_1$

Table 5-2. Stress-strain and strength parameters for soils tested under unconsolidated-undrained conditions.

[Converted from Table 6, J. M. Duncan, et al., 1980 (Ref. 52) to Parameters for Model 5, in DYNA3D.]

Soil Type	Class	S-No.*	ρ ($\times 10^{-4}$)	K_e ($\times 10^5$)	G ($\times 10^5$)	σ_u	μ	τ_0	p_t
Fat clay	CH	8-12	1.35	0.023	0.008	33.4	0.00	33.4	0
Silty clay	CL	4-8	1.60	0.089	0.030	82.1	0.45	62.3	0
Sandy clay	CL	4-8	1.72	0.033	0.011	102.0	0.45	64.7	0
Sandy clay	CL	4-8	1.60	0.14	0.048	84.6	0.69	12.7	0
Pittsburg Silty Clay	CL	4-8	1.69	0.095	0.031	131.8	0.94	25.1	0
Sandy Silt	ML	4-6	1.64	0.068	0.023	178.6	1.2	11.3	0
Silty Sand	SM	3-5	1.56	0.22	0.11	137.0	1.64	0	0
Poorly Graded Sand	SP	3-5	1.52	0.25	0.083	75.7	1.81	0	0
Sand Gravel	GC	5	2.09	0.19	0.064	289	0.11	285	0

* S-number estimate based on correlation with soil types developed by C. W. Young (Ref. 17).

Notes: ρ = density (lb/sec^2/in.^{4}).

K_e = unloading bulk modulus (psi) estimated using the relationship in Table 5-1 for assumed σ_3 = 100 psi.

G = shear modulus (psi) estimated using the relationship in Table 5-1 for assumed σ_3 = 100 psi.

σ_u = ultimate strength (psi).

μ = slope of σ_y-versus-p curve.

τ_0 = cohesive strength (psi).

p_t = tensile strength (psi).

Another set of parameters that were developed by using the actual test data obtained by J. V. Farr (Ref. 14) and W. F. Carroll (Ref. 54) for CARES-DRY (Yuma Clayey) sand, by J. V. Farr (Ref. 14) for Enewetak Beach sand and Flume sand, by C. S. Desai, et al. (Ref. 55) for McCormick sand, by R. J. Marsal (Ref. 56) for basalt rockfill materials, and by H. S. Chu and H. Brandt (Ref. 57) for limestone is summarized in Table 5-3. These data are from a variety of test conditions as indicated in Table 5-3, ranging from uniaxial impact loading tests to consolidated-undrained and consolidated-drained triaxial tests.

Table 5-3. Summary of soil/rock properties developed for Material Model 5 of DYNA3D analysis.

Material Type	ρ ($\times 10^{-4}$)	K_e ($\times 10^5$)	G ($\times 10^5$)	σ_u	μ	τ_0
Limestone (Rock)[a]	2.15	22.0	13.0	>50,000	1.20	3768
Basalt (Rock gravel)[b]	1.92	6.74	2.56	Large	1.96	0*
CARES-Dry Clayey Sand[c]	1.79	3.37-5.18	0.125-0.16	>870	1.59	33.4
Enewetak Sand[d]	1.59	3.68	1.41*	Large*	1.59*	0*
Flume Sand[d]	1.59	2.74	1.05*	Large*	1.29*	0*
McCormick Ranch Sand[e]	1.97	3.0	1.42	400*	0.38	170

* Estimated

Note:
- ρ = density (lb-sec^2/in.^{4}).
- K_e = unloading bulk modulus (psi)
- G = shear modulus (psi)
- σ_u = ultimate strength (psi)
- μ = slope of σ_y-versus-p curve
- τ_0 = cohesive strength (psi)

[a] Chu and Brandt (1987)—Triaxial test data.

[b] Marsal (1967)—Consolidated-drained triaxial test data.

[c] Farr (1986) and Carroll (1988)—Uniaxial impact tests and triaxial test data on unsaturated soils.

[d] Farr (1986)—Uniaxial impact test data on unsaturated soils.

[e] Desai (1984)—Consolidated-undrained triaxial test data.

For purposes of estimating the mean-normal-pressure-versus-volumetric-strain (p-versus-v) relationships for a variety of soil types, test data of 22 soil types presented in the references listed in Table 5-4 were compiled and summarized in Fig. 5-1. It is noted that the p-versus-v relationships vary considerably depending on soil types. However, a general trend of the data is apparent. The curves in the lower part of the figure representing more compressible behavior are generally associated with fine grained soils (i.e., silts and clays), and those in the upper part representing less compressive behavior are associated with coarse grained soils (i.e., gravels and sands). The data in Fig. 5-1 may be used for estimating possible ranges of the p-versus-v relationship for a given soil type when actual test data are not available.

Table 5-4. Test results for mean-normal-pressure-volumetric-strain curves cited in Fig. 5-1.

1.	Oroville Dam Material (N. D. Marachi, et al., Ref. 57).
2.	Crushed Basalt (Marachi, et al., Ref. 57).
3.	Pyramid Dam Material (N. D. Marachi, et al., Ref. 57).
4.	Qs-Colluvium, Sandy Clay-PSA Crash Site, DH2-2.
5.	CARES-Dry (Yuma Clayey) Sand (J. V. Farr, Ref. 14).
6.	Enewetak Beach Sand (J. V. Farr, Ref. 14).
7.	Flume Sand (J. V. Farr, Ref. 14).
8.	Vicksburg Loess (J. V. Farr, Ref. 14).
9.	McCormick Ranch Sand (C. S. Desai, Ref. 54).
10.	Limestone (H. S. Chu, et al., Ref. 56).
11.	Reid-Bedford Sand (A. A. Stephen, et al., Ref. 58).
12.	Reid-Bedford Sand (A. A. Stephen, et al., Ref. 58).
13.	Pittsburg Silty Clay (J. M. Duncan, et al., Ref. 51).
14.	Silty Clay (Canyon Dam) (J. M. Duncan, et al., Ref. 51).
15.	Silty Clayey Sand (Mica Dam Core) (J. M. Duncan, et al., Ref. 51).
16.	SP-4C, Sacramento River Sand ((J. M. Duncan, et al., Ref. 51).
17.	GW-2, Granitic Gneiss Rockfill (Mica Dam) (J. M. Duncan, et al., Ref. 51).
18.	GP-13, Sand Gravel (Rowallan Dam) (J. M. Duncan, et al., Ref. 51).
19.	Sandy Clay - PSA Crash Site, DH3-3.
20.	Sandy Clay - PSA Crash Site, DH4-1.
21.	Loose Sand (A. S. Vesic and G. W. Clough, Ref. 59).
22.	Dense Sand (A. S. Vesic and G. W. Clough, Ref. 59).

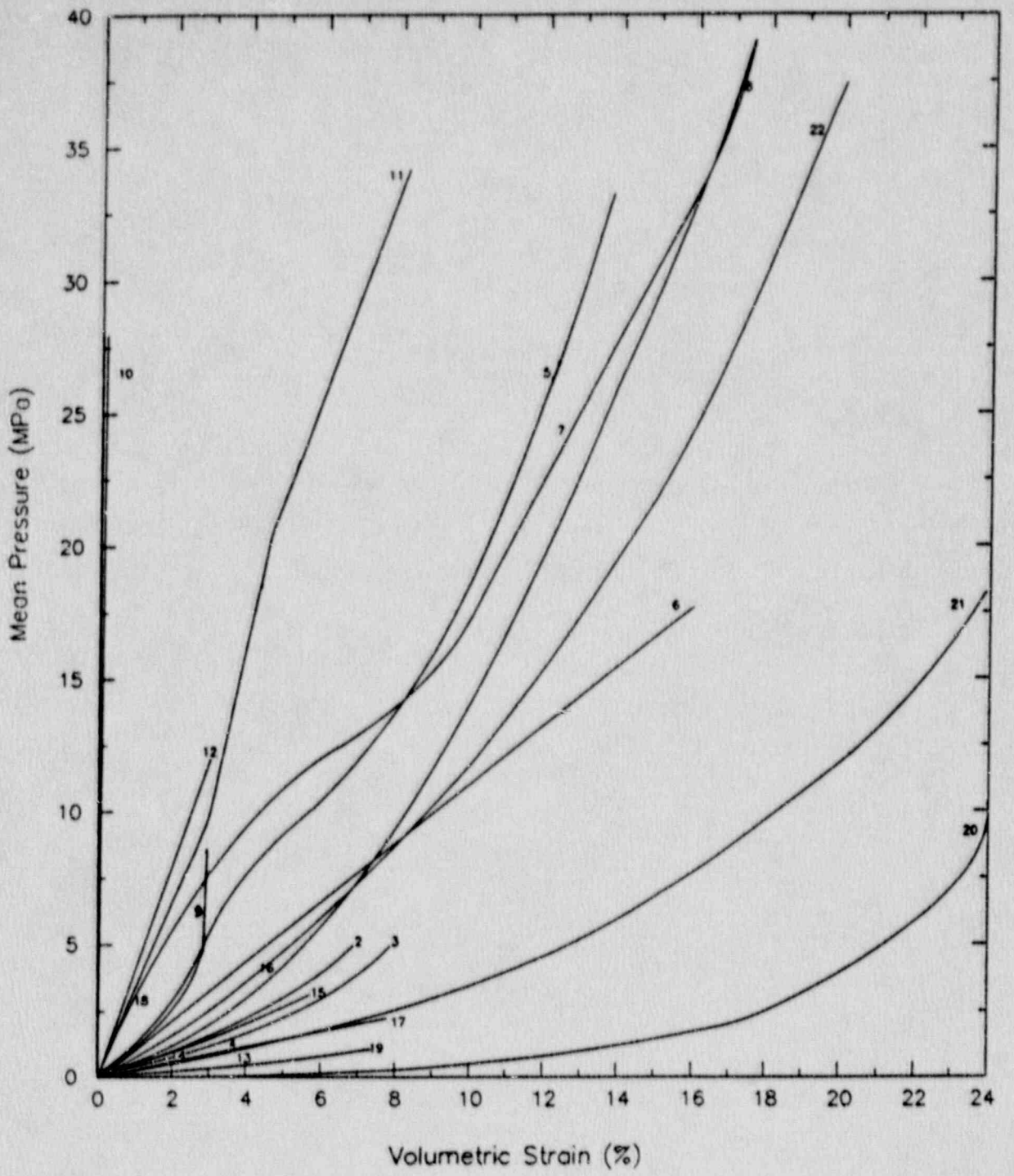

Fig. 5-1. Volumetric compressibility characteristics for a variety of soils.

6.0 SUMMARY OF RESULTS AND RECOMMENDATIONS

6.1 Summary of Results

The task of developing model parameters for in-situ soils at the PSA Flight 1771 crash site has been carried out as part of the verification study of soil/rock response to impact loading by using computer program DYNA2D (or DYNA3D).

The task includes: (1) a literature review on effects of loading rates and confining pressures on stress-strain, shear strength, and compressibility of soils; (2) laboratory testing on samples of undisturbed crash site soils, and (3) development of soil parameters appropriate for using Krieg's model of the DYNA3D code for analyses of the response of the crash site soils and other geologic materials under crash impacts.

The results of the literature review are summarized as follows:

- Strain-rate effect varies considerably with soil types. Generally, the percentage change in the strength of sands is less than that for clays for the same change of loading rate.

- Strain-rate effect also appears to vary with the stress history of a given soil. The effect increases with increasing overconsolidation ratio.

- Strain-rate affects stress-deformation behavior (modulus) of soils approximately in the same proportion as it affects soil strength.

- An increase in strain rate causes a progressive stiffening of soils. Compressibility of soils decreases as the strain rate increases.

- An increase in effective confining stress results in a decrease in overconsolidation ratio and an increase in compressibility.

- An increase in effective confining stress results in a decrease in the ratio of undrained shear strength to existing effective stress of clays (down to normally consolidated conditions) and in a decrease in the effective friction angle of coarse grained soils.

Characteristic stress-deformation and shear strength properties of the in-situ crash site soils were determined by using the results of laboratory testing on the drive soil samples recovered from the boreholes drilled at the site. The stress-deformation and shear strength characteristics of the soils were first interpreted under normal slow-loading-rate conditions performed in the laboratory and later extrapolated to crash impact loading conditions expected to prevail at the site.

Model parameters required for Krieg's model of the DYNA3D code were developed for both the in-situ crash site soils and other geologic materials.

6.2 Recommendations

Based on the results of the study on soil behavior under impact dynamic loads, the following recommendations were developed for modeling considerations in the crash-impact study.

- Soil characteristics at the crash site appear to vary with depth. It is desirable to account for this variation in the model. In addition, effects of strain rate, degree of saturation, and effective pressure on the stress-deformation and shear strength characteristics need to be incorporated in modeling the site soils.

- More comprehensive models for geological materials are available in the DYNA3D code (e.g., Models 16 and 25). These models are capable of incorporating (1) rate sensitivity and damage effects on yield stresses and (2) tensile fracture. Applicability of these models needs to be assessed with respect to the analysis results obtained using Model 5.

- We understand that the current numerical modeling using DYNA3D is primarily based on the framework of continuum modeling. The basic theory for the constitutive models in continuum modeling is plasticity. When a target site is underlain by a brittle, weathered rock mass near the ground surface, such as the PSA crash site, rock fracture or fragmentation and dynamic response of the fractured rock mass may play an important role in determining the dynamic response of a projectile penetrating into the rock mass. Recent studies on dynamic rock fragmentation (D. E. Grady, et al., Ref. 61) and the Discontinuous Deformation Analysis or Block Theory (G. H. Shi and R. E. Goodman, Ref. 62) may be useful in addressing this aspect of the problem.

7.0 REFERENCES

1. Blair, S. C., J. C. Chen, W. R. Ralph and D. W. Ruddle, 1989, "Mechanical Properties of Rocks from PSA Flight 1771 Crash Site," Lawrence Livermore National Laboratory, PATC-IR 89-05.

2. Hallquist, J. O., 1988, DYNA3D User's Manual (Nonlinear Dynamic Analysis of Structure in Three Dimensions), UCID-19592, Rev. 4, Lawrence Livermore National Laboratory.

3. Krieg, R. D , 1972, "A Simple Constitutive Description for Cellular Concrete," Rept. SC-DR-72-0883, Sandia National Laboratories, Albuquerque, N.M., 1972.

4. Sackett, S. J., 1977, "Geological/Concrete Model Development," Private Communication.

5. Simo, J. C., J. W. Ju, K. S. Pister and R. L. Taylor, 1988, "Softening Response, Completeness Condition, and Numerical Algorithms for the Cap Model," Intl. Journal Numer. Anal. Meth. Engr.

6. Vicat, 1833, "Recherches Experimentales sur les Phenomenes Physiques qui Precedent et Accompagnent la Rupture ou l'Affaissment d'une Certaine de Solides," Annales des Pont et Chaussees, pp. 201-268.

7. Collin, A., 1846, "Recherches Experimentales sur les Glissement, Spontanes des Terrains Argileux," Carilian-Goeung, Paris.

8. Whitman, R. V., 1957, "Testing Soils with Transient Loads," ASTM, STP232, pp. 242-254.

9. Whitman, R. V., 1957, "Behavior of Soils Under Transient Loadings," Proc. 4th International Conference on Soil Mechanics and Foundation Eng., London, Vol. I, p. 207-210.

10. Whitman, R. V., 1963, "The Response of Soils to Dynamic Loading, Report No. 17: Stress-Strain-Time Behavior of Soil in One Dimensional Compressions," Contract Report 63-25, U.S. Army Engineer Waterways Experiment Station, Vicksburg, Mississippi.

11. Whitman, R. V., 1970, "The Response of Soils to Dynamic Loading, Report No. 26: Final Report," Contract Report No. 3-26, U.S. Army Engineer Waterways Experiment Station, Vicksburg, Mississippi.

12. Crawford, C. B., 1959, "The Influence of Rate of Strain on Effective Stresses in Sensitive Clay," ASTM, STP 254, pp. 36-48.

13. Vaid, Y. P. and R. G. Campanella, 1977, "Time-Dependent Behavior of Undisturbed Clay," J. of the Geotechnical Engineering Division, ASCE, V.103, GT7, pp. 693-709, July.

14. Farr, J. V., 1986, "Loading Rate Effects on the One-Dimensional Compressibility of Four Partially Saturated Soils," Technical Report SL-86-46, U.S. Army Engineer Waterways Experiment Station, Vicksburg, Mississippi.

15. Farr, J. V. and R.P. Woods, 1988, "A Device for Evaluating One-Dimensional Compressive Loading Rate Effects," Geotechnical Testing Journal, GTJODJ, Vol. II, No. 4.

16. Young, C. W., 1969, "Depth Prediction for Earth-Penetrating Projectiles," Journal of the Soil Mechanics and Foundation Division, Proc. ASCE, p. 803.

17. Young, C. W., 1988, "Equations for Predicting Earth Penetration by Projectiles: An Update," Sandia National Laboratories Report SAVD88-0013, Advanced Projects Division II, Sandia National Laboratories, Albuquerque, NM, July.

18. Wang, W. L., 1971, "Low Velocity Projectile Penetration," Journal of the Soil Mechanics and Foundations Division, Proc. ASCE, Vol. 97, No. SM12, pp. 1635-1656.

19. Bishop, A. W., D. L. Webb and A. E. Skinner, 1965, "Triaxial Tests on Soil at Elevated Cell Pressures," Proceedings 6th International Conference on Soil Mechanics and Foundation Engineering, Montreal, Vol. 1, pp. 170-174.

20. Lambe, T. W. and R. V. Whitman, 1969, "Soil Mechanics," John Wiley and Sons, Inc., New York.

21. Mitchell, J. K., 1976, "Fundamentals of Soil Behavior," John Wiley and Sons, Inc.

22. Mitchell, J. K., 1964, "Shearing Resistance of Soils as a Rate Process," Journal of the Soil Mechanics and Foundation Division, ASCE, Vol. 90, No. SM1, pp. 29-61.

23. Bishop, A. W. and D. J. Henkel, 1962, "The Measurement of Soil Properties in the Triaxial Test," Edward Arnold, London, 2nd ed.

24. Casagrande, A. and S. D. Wilson, 1951, "Effect of Rate of Loading on the Strength of Clays and Shales at Constant Water Content," Geotechnique, Vol. 2, No. 3, pp. 251-263.

25. Bjerrum, L., N. Simons and I. Torblaa, 1958, "The Effect of Time in the Shear Strength of a Soft Marine Clay," Proceedings of the Conference on Earth Pressure Problems, Brussels, Belgium, Vol. I, pp. 148-58.

26. Crawford, K. E., C. J. Higgins and E. H. Bultmann, 1974, "The Air Force Manual for Design and Analysis of Hardened Structures," Report AFWL-TR-74- 102, Air Force Weapons Laboratory, Kirtland Air Force Base, New Mexico.

27. Whitman, R. V., and K. A. Healy, 1962, "Shear Strength of Sands During Rapid Loadings," J. of the Soil Mechanics and Foundation Engineering Division, ASCE, V.88, SM2, pp. 99-132, April.

28. Whitman, R. V., and K. A. Healy, 1962, "Shearing Resistance of Sands During Rapid Loadings, Report 9: The Response of Soils to Dynamic Loadings," U.S. Army Engineer Waterways Experiment Station, Vicksburg, Mississippi, May.

29. Richardson, A. M., Jr., 1961, "The Response of Soils to Dynamic Loads; Report 6: Effect of Rate of Strain on Stress-Strain Behavior of Saturated Soils," U.S. Army Engineer Waterways Experiment Station, Vicksburg, Mississippi, April.

30. Healy, K. A., 1962, "The Response of Soils to Dynamic Loadings, Report 11: Triaxial Tests Upon Saturated Fine Silty Sand," U.S. Army Waterways Experiment Station, Vicksburg, Mississippi.

31. Healy, K. A., 1963, "The Response of Soils to Dynamic Loadings, Report 13: The Dependence of Dilation in Sand on Rate of Shear Strain," U.S. Army Waterways Experiment Station, Vicksburg, Mississippi.

32. Healy, K. A., 1963, "The Response of Soils to Dynamic Loadings, Report 15: Undrained Strength of Saturated Clayey Silt," U.S. Army Waterways Experiment Station, Vicksburg, Mississippi.

33. Richardson, A. M., Jr., 1963, "The Response of Soils to Dynamic Loadings, Report 16: Effective Stress Versus Strength—Saturated Fat Clay," U.S. Army Engineer Waterways Experiment Station, Vicksburg, Mississippi, April.

34. Richardson, A. M., Jr., and R. V. Whitman, 1963, "Effect of Strain-Rate Upon Undrained Shear Resistance of a Saturated Remolded Fat Clay," Geotechnique, V.13, n.4, pp. 310-324.

35. Schimming, B. B., H. J. Haas, and H. C. Saxe, 1966, "Study of Dynamic and Static Failure Envelopes," J. of the Soil Mechanics and Foundations Division, ASCE, V.92, SM2, pp. 105-124, March.

36. Yong, R. N., and R. D. Japp, 1967, "A Flow Law for Clays in Dynamic Compression," Proceedings of the Symposium on Wave Propagation and Dynamic Earth Materials, ASCE, Albuquerque, New Mexico, pp. 183-188.

37. Lee, K. L., H. B. Seed, and P. Dunlop, 1969, "Effect of Transient Loading on the Strength of Sand," International Conference on Soil Mechanics and Foundation Engineering, Mexico City, pp. 239-247.

38. Perlow, M., Jr., and A. F. Richards, 1977, "Influence of Shear Velocity on Vane Shear Strength," J. of the Geotechnical Engineering Division, V.103, GTI, pp.19-32, January.

39. Vaid, Y. P., P. K. Robertson and R. G. Campanella, 1979, "Strain Rate Behavior of Saint-Jean-Viannay Clay," Canadian Geotechnical Journal, vol. 16, no. 1, pp. 34-42.

40. Casagrande, A. and W. L. Shannon, 1948a, "Research on Stress Deformation and Strength Characteristics of Soils and Soft Rocks Under Transient Loading," Soil Mechanics Series No. 31, Harvard University, Cambridge, MA, 148a.

41. Casagrande, A. and W. L. Shannon, 1948b, "Stress-Deformation and Strength Characteristics of Soils Under Dynamic Loads," Proceedings of the Second International Conference on Soil Mechanics and Foundation Engineer, Vol. V, pp. 29-34.

42. Casagrande, A. and W. L. Shannon, 1949, "Strength of Soils Under Dynamic Loads," Transactions ASCE, Vol. 114, pp.755-773.

43. Krizek, R. J., 1967, "Strain-Rate Response of a Bangkok Clay," Proceedings of the Third Asian Regional Conference on Soil Mechanics and Foundation Engineering, Haifa, Israel, pp. 289-292.

44. Egan, J. A., 1978, unpublished report.

45. Jackson, Jr., J. G., J. Q. Ehrgott and B. Rohani, 1979, "Loading Rate Effects on Compressibility of Sand," Miscellaneous Paper SL-79-24, U.S. Army Waterways Experiment Station, Vicksburg, Mississippi.

46. Felice, C. W., E. S. Gaffney, J. A. Brown and J. M. Olson, 1987, "Dynamic High Stress Experiments on Soil," Geotechnical Testing Journal, Vol. 10, No. 4, pp. 192-202.

47. Carpenter, D. W., J. C. Chen and G. S. Holman, 1989, "An Engineering Geologic Evaluation of the PSA Flight 1771 Crash Site Near Paso Robles, California," Lawrence Livermore Laboratory, PATC-IR 89-04.

48. Schmertmann, J. H., 1955, "The Undisturbed Consolidation Behavior of Clay," Transactions ASCE, vol. 120, pp. 1201-1233.

49. Mayne, P. W. and F. H. Kulhawy, 1982, "K_0-OCR Relationships in Soil," ASCE, Journal of the Geotechnical Engineering Division, GT6, pp. 851-872.

50. Deere, D. U., 1974, cited in Mitchell, 1976.

51. Deere, D. U., and F. D. Patton, 1971, "Slope Stability in Residual Soils," Proceedings 4th Pan-American Conference on Soil Mechanics and Foundation Engineering, San Juan, ASCE, Vol. 1, pp. 87-170.

52. Duncan, J. M., P. Byrne, K. S. Wong and P. Mabry, 1980, "Strength, Stress-Strain and Bulk Modulus Parameters for Finite Element Analyses of Stresses and Movements in Soil Masses," Report No. UCB/GT/80-01.

53. Duncan, J. M. and C.-Y. Chang, 1970, "Nonlinear Analysis of Stress and Strain in Soils," Journal of the Soil Mechanics and Foundations Division, ASCE, Vol. 96, No. SM5, September, pp. 1629-1653.

54. Carroll, W. F., 1988, "Rate Effects in Shear for Cares-Dry Soil," Technical Report SL-88-9, U.S. Army Engineer Waterways Experiment Station, Vicksburg, Mississippi.

55. Desai, C. S. and H. J. Siriwardane, 1984, Constitutive Laws for Engineering Material, with Emphasis on Geologic Material, Prentice-Hall, Inc.

56. Marsal, R. J., 1967, "Large Scale Testing of Rockfill Materials," Journal of the Soil Mechanics and Foundations Division, ASCE, Vol. 93, No. SM2, pp. 27-43.

57. Chu, H. S. and H. Brandt, 1987, "Constants for an Elastic-Plastic Cap Model for Limestone," International Journal for Numerical and Analytical Methods in Geomechanics, Vol. 11, pp. 193-202.

58. Marachi, N. D., C. K. Chan, H. B. Seed, and J. M. Duncan, 1964, "Strength and Deformation Characteristics of Rockfill Materials," Report No. TE69-5, University of California, Berkeley.

59. Stephen, A. A., A. R. Paul and J. Q. Ehrgott, 1986, "WES High-Pressure Uniaxial Strain and Triaxial Shear Test Equipment," Miscellaneous Paper SL-86-11, U.S. Army Engineer Waterways Experiment Station, Vicksburg, Mississippi.

60. Vesic, A. S. and G. W. Clough, 1968, "Behavior of Granular Material Under High Stresses," Journal of the Soil Mechanics and Foundations Division, ASCE, Vol. 94, no. SM3, pp. 661-688.

61. Grady, D. E. and M. E. Kipp, 1989, "Dynamic Rock Fragmentation," Fracture Mechanics of Rock, edited by B. K. Atkinson, Academic Press Geology Series.

62. Shi, G. H. and R. E. Goodman, 1985, "Two Dimensional Discontinuous Deformation Analysis," Int. J. Numer. Anal. Meth. Geomech., vol. 9, pp. 541-556.

APPENDIX A. LABORATORY TESTING PROGRAM AND TEST RESULTS

A.1 Introduction

The laboratory testing portion of the soil characterization program was intended to provide information regarding the identification and classification, volumetric compressibility, and shear strength and stress-deformation characteristics of the soils at the PSA crash site. Visual classification, water content, plasticity, and unit weight evaluations provided indices to identify and classify the soils. One-dimensional consolidation tests provided volumetric stress-strain characteristics, as well as a means to estimate the existing soil stress history. Measurements of undrained shear strength and stress-deformation characteristics were obtained from unconsolidated undrained triaxial tests.

As indicated by the soil descriptions contained in Table A-1, the five boreholes drilled at the site encountered a variety of soil types and conditions. The testing program involved seven soil samples from among the four holes (DH2 through DH5) located outside the crash crater area (see Section 4, Fig. 4.1) in an effort to characterize pre-crash conditions. Samples tested were obtained from depths down to six feet below ground surface. Soils from hole DH1, located within the crater area, were not tested. A summary of the samples tested during this program is presented in Table A-2.

Brief descriptions of the testing procedures and the results for each of the tests are presented in the following sections.

Table A-1. Soil description.

Location	Depth (ft)	Classification	Description
DH1	0-5	Clayey silt (ML-CL)	Wood, metallic debris
	5-9.8	Clayey silt (ML-CL)	Predominantly rock fragments in soil, debris noted
DH2	0-0.6	Silty-clay (CL)	Rock fragments, brown
	0.6-6	Sandy-clay (CL)	Stiff, decomposed from shale, light to dark brown, dry to moist, trace of roots
	6-7	Fine silty sand (SM)	Very dense, decomposed from sandstone, orange brown, damp
DH3	0-0.5	Sandy silt (ML-SM)	Estimate 50% slightly plastic fines, 30% sand, 20% rock fragments, dark brown, dry, contains roots
	0.5-10	Shale, predominantly lean clay (CL) and silty clay (CL-ML)	Interbedded shale and sandstone, decomposed to damp, moderately plastic clay, brown
DH4	0-0.7	Clayey silt (ML-CL)	Slightly plastic, 25% sand and siltstone fragments, dark brown, dry, contains roots
	0.7-1.8	Silty sand (SM), sandstone	Sandstone, fine, silty, decomposed to yellow-brown, damp, silty sand
DH5	0-0.5	Sandy silt (ML)	Slightly plastic, abundant shale fragments, dark brown, damp, contains roots
	0.5-2	Dense silty sand (ML)	Decomposed from sandstone, orange
		Hard, lean clay (CL), sandstone predominant	Decomposed from shale, brown

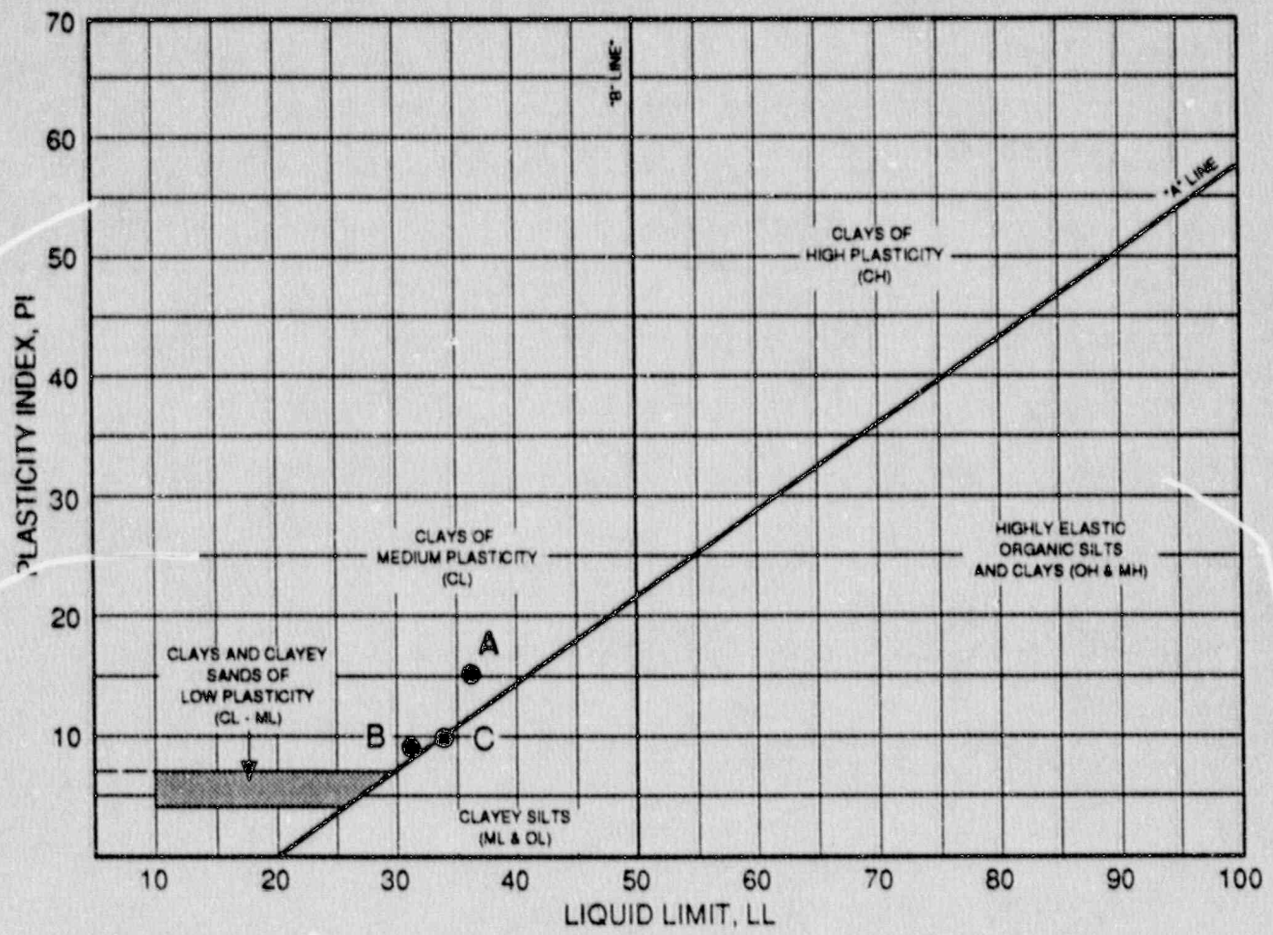

SAMPLE IDENTIFICATION				ATTERBERG LIMITS		
LETTER DESIG'N	BORING NO.	SAMPLE NO.	DEPTH, FT.	LIQUID LIMIT	PLASTIC LIMIT	PLASTICITY INDEX
A	DH2	2	5.4 - 5.9	36	21	15
B	DH3	3	5.0 - 5.5	33	24	9
C	DH3	4	5.5 - 6.0	34	24	10

Fig. A-1. Plasticity classification.

Table A-2. Data of undisturbed samples from crash site.

Sample Number	Depth (ft)	Soil Type	Liquid Limit (LL)	Plasticity Index (PI)	Content (%)	Unit Weight (pcf) Wet	Unit Weight (pcf) Dry	Type of Test[a]
DH2-2	5.4-5.9	Sandy clay	36	15	16.6	137	118	UU
DH3-2	1.6-2.1	Sandy clay	- - -	- - -	20.7	118	98	UU
					18.9	129	108	CS
DH3-3	5.0-5.5	Silty sandy clay	32	8	19.9	134	112	UU
DH3-4	5.5-6.0	Sandy clay	34	10	18.0	132	112	UU
					18.8	138	117	CS
DH4-1	0.25-0.75	Silty sandy clay	- - -	- - -	17.8	117	100	CS
DH4-1	2.25-2.75	Silty sand/sandstone	- - -	- - -	11.4	129	116	NA
DH5-2	0.8-1.3	Sandstone	- - -	- - -	6.3	139	131	NA

[a] Test type designation: UU = unconsolidated undrained triaxial; CS = one-dimensional consolidation; NA = not applicable.

A.2 Identification and Classification Tests

Identification and classification indices, including visual classification, water content, Atterberg limits, and unit weights, were determined during the laboratory test program. The procedures followed for performing each of the tests were in general accordance with recommended American Society for Testing and Materials (ASTM) standards (1988). The procedure standards referenced were the following:

TEST	PROCEDURE STANDARD
Visual classification	ASTM D 2488-84
Water content	ASTM D 2216-80
Liquid and plastic limits	ASTM D 4318-84

The results of the identification and classification tests for each sample tested are summarized in Table A-2. Plasticity data are illustrated in Fig. A-1.

A.3 One-Dimensional Consolidation Tests

Three one-dimensional consolidation tests were performed on intact soil specimens from two boreholes.

For a one-dimensional consolidation test, the soil specimen encased in the sampling tube was directly placed in a steel ring. This procedure was necessary because of difficulties in extruding the specimens due to their rocky nature. Specimen dimensions were approximately 1.4 inches in diameter and 1.7 inches in height. The steel ring prevents lateral deformation of the specimen so that all volume change under vertical stress results in a change of specimen height.

Vertical effective stresses were generally increased incrementally by doubling the previous stress; except at higher stresses where smaller increments were used. For each stress level, the specimen was allowed to consolidate for a time period of about 90 percent of primary consolidation (t_{90}) plus one hour, or until volume change equilibrium if reached first, before applying a subsequent stress increment. A rebound (unloading) cycle was performed for each specimen from the maximum consolidation stress.

A summary of pertinent test specimen data and results is presented in Table A-3. The one-dimensional consolidation-stress-versus-volumetric-strain curves are illustrated in Fig. A-2.

Table A-3. One-dimensional consolidation test results summary.

Sample Number	Depth (ft)	σ_{v0} W_n (%)	σ_{vm} (psi)	OCR (psi)	$(\sigma_{vm}/\sigma_{v0})$	$C_c/(1 + e_0)$	$C_s/(1 + e_0)$
DH4-1	0.25–0.75	17.8	0.4	45	~110	0.165	0.011
DH3-2	1.6–2.1	18.9	1.6	145	~90	0.115	0.011
DH3-4	5.5–6.0	18.8	5.0	300	~60	0.093	0.010

Notes:
W_n = natural moisture content.
σ_{v0} = in-situ overburden pressure.
σ_{vm} = preconsolidation pressure.
OCR = overconsolidation ratio.
e_0 = void ratio.
C_c = compression index.
C_s = rebound index.

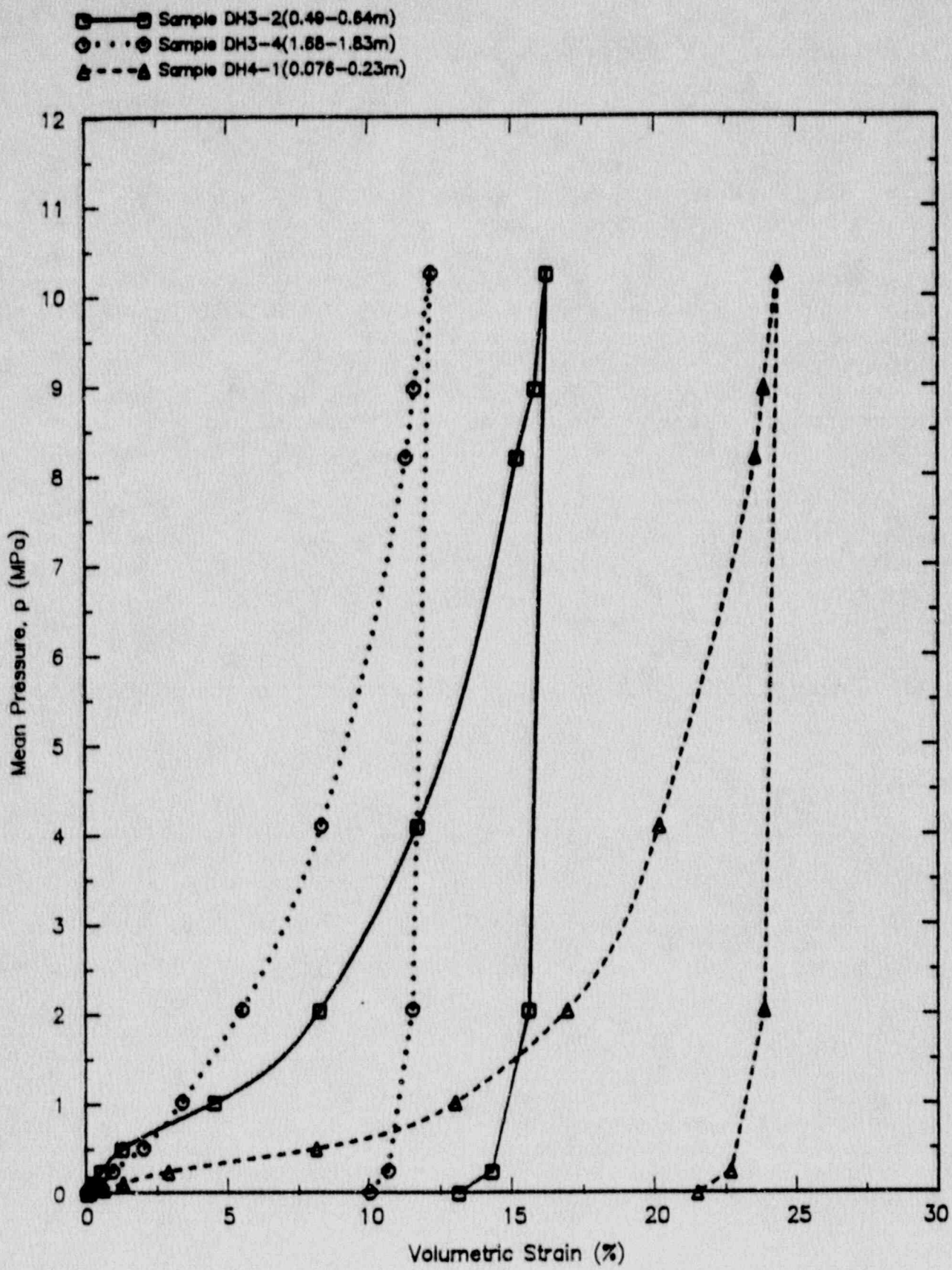

Fig. A-2. One-dimensional consolidation tests: compression curves.

A.4 Unconsolidated Undrained Triaxial Compression Tests

Four unconsolidated undrained triaxial compression (UU) tests were performed on intact soil specimens from three holes.

The reference standard for the testing procedure was ASTM Designation D 2850-70. The cylindrical specimens, approximately 1.4 inches in diameter by 2.15 to 3.7 inches in length, were enclosed in rubber membranes and subjected to lateral confining stresses of either 100 or 150 psi for shearing. Prior to shearing, the specimens were subjected to a loading-unloading-reloading cycle of confining stress to measure undrained volume change behavior. The specimens were then sheared monotonically to failure at a constant axial strain rate of approximately two percent per minute. No drainage was allowed either before or during shear. Axial load and axial deformation were monitored during shear using a calibrated load cell and deflection dial indicator, respectively.

Pertinent test specimen data and test results are summarized in Table A-4. The confining-stress-versus-volumetric-strain curves for the tests are illustrated in Figs. A-3 and A-4. The respective undrained shear-stress-vs-strain curves are illustrated in Fig. A-5.

Table A-4. Unconsolidated undrained triaxial compression tests summary.

Sample Number	Depth (ft)	LL (%)	PI (%)	W_n (%)	σ_{v0} (psi)	σ_c (psi)	ε (%)	q (psi)	Deformation Rate (in./min)
DH3-2	1.6-2.1	- - -	- - -	20.7	1.7	150	12.0	159	0.042
DH3-3	5.0-5.5	32	8	19.9	4.7	100	16.0	112	0.054
DH3-4	5.5-6.0	34	10	18.0	5.1	100	10.0	100	0.055
DH2-2	5.4-5.9	36	15	16.6	5.0	150	12.0	62	- - -

Notes:
- LL = liquid limit.
- PI = plasticity index.
- W_n = natural moisture content.
- σ_{v0} = in-situ overburden pressure.
- σ_c = confining pressure.
- ε = axial strain.
- q = deviatoric stress.

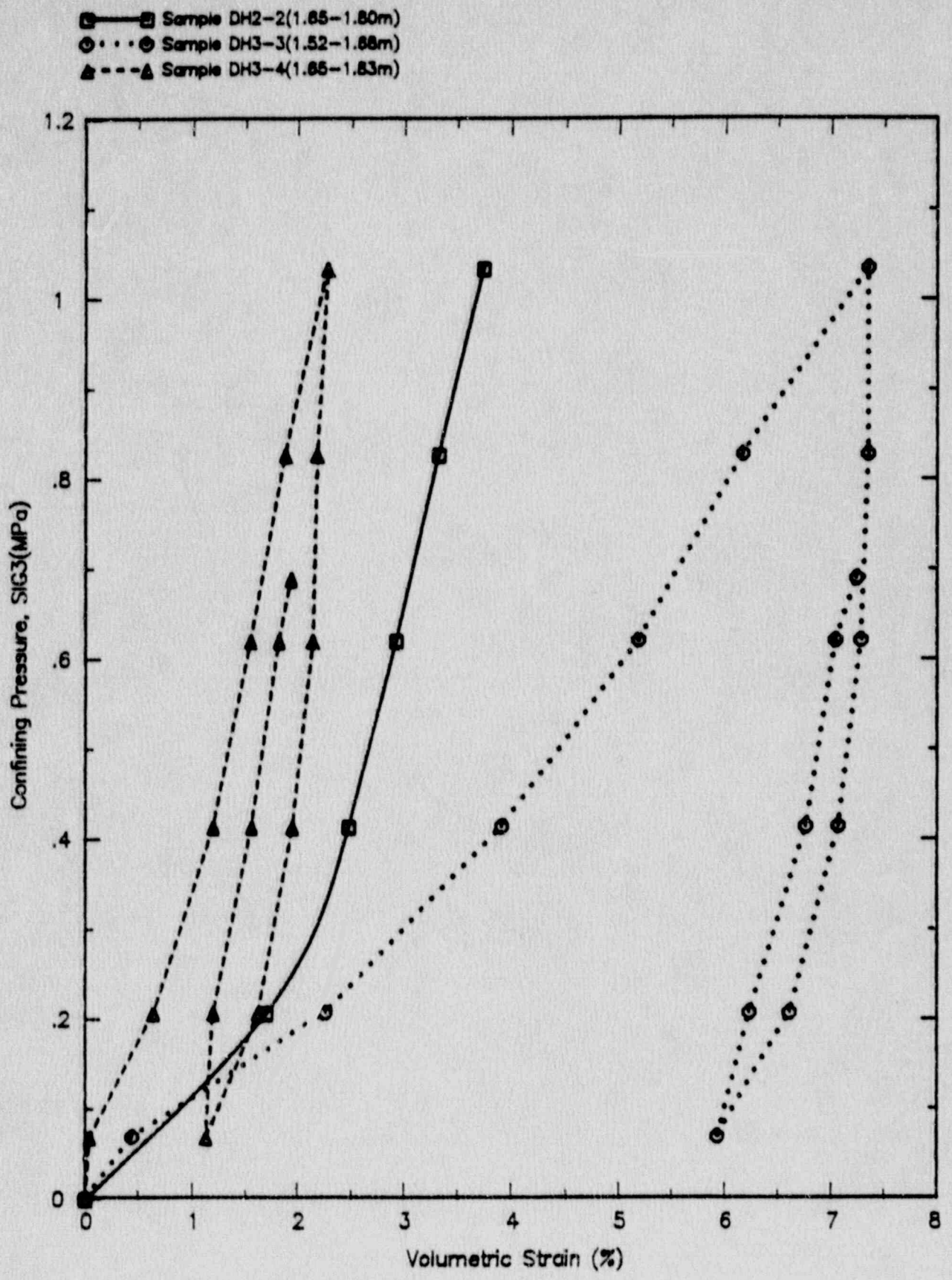

Fig. A-3. UU tests: volumetric compression curves.

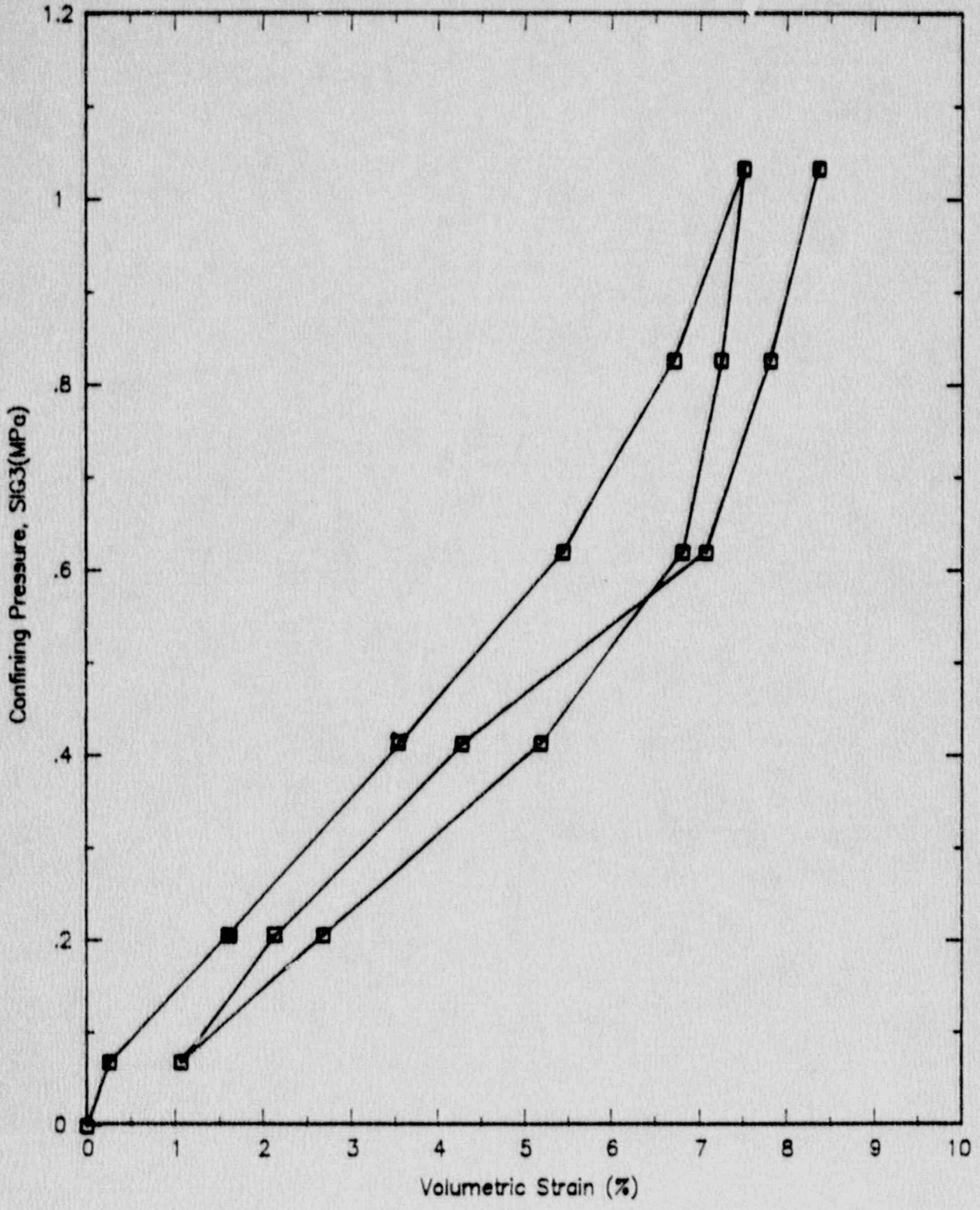

Fig. A-4. UU test DH3-2: volumetric compression curve.

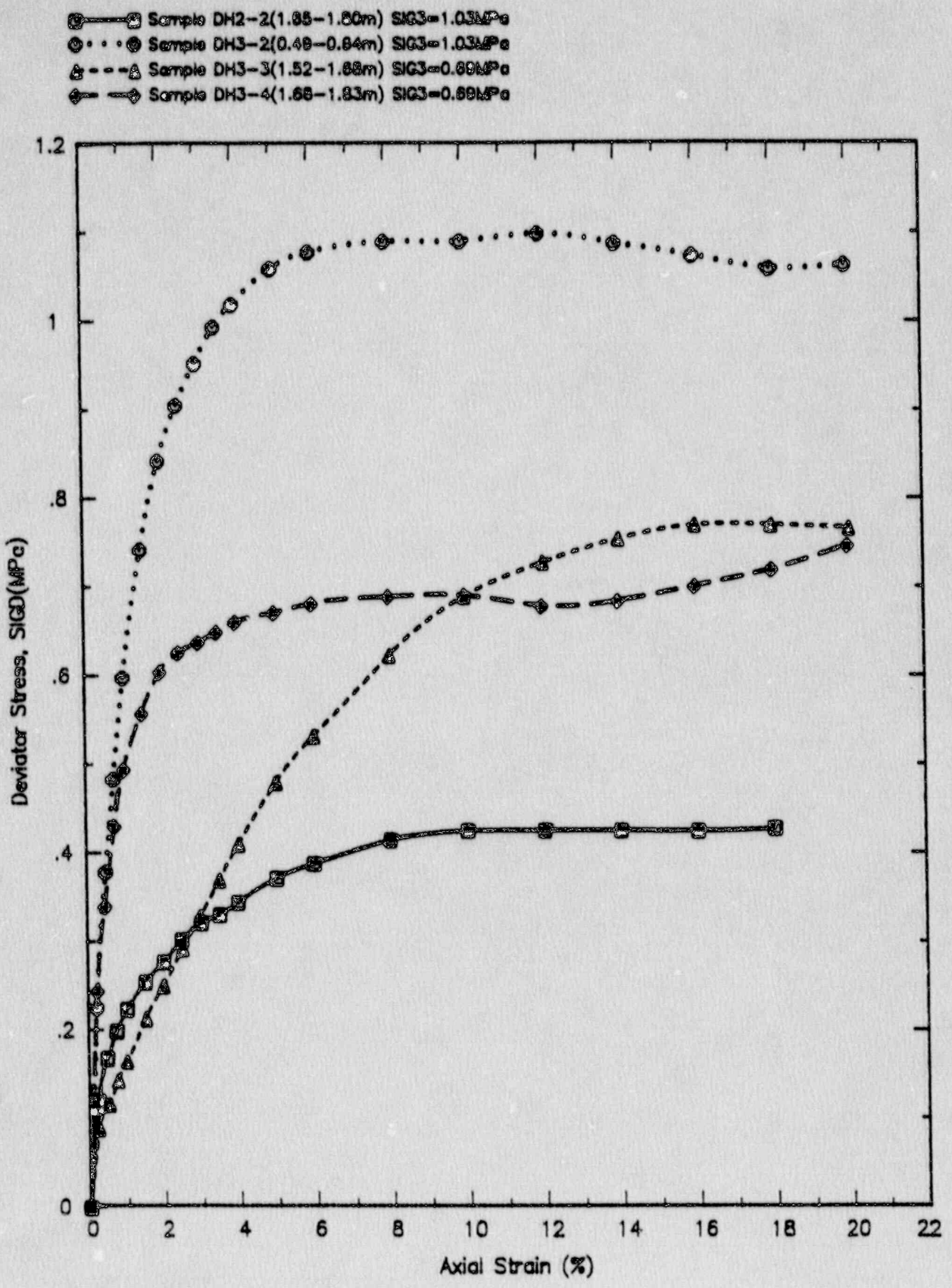

Fig. A-5. UU tests: strain-strain response curves.

APPENDIX B. FORMULATIONS FOR KRIEG'S MODEL SOIL PARAMETERS

B.1 Basic Formulations in Model

Yield surface for deviatoric behavior:

$$\Phi_s = 1/2\ S_{ij}\ S_{ij} - (a_0 + a_1 p + a_2 p^2),$$

where:

p	=	$1/3\ \sigma_{kk}$
a_0	=	$\tau_0^2/3$,
a_1	=	$2/3\ \tau_0\ \mu$,
a_2	=	$1/3\ \mu^2$,
τ_0	=	cohesive strength in psi,
μ	=	slope of σ_y-versus-p curve.

Volumetric yielding is determined by a tabulated pressure-versus-volumetric-strain curve.

B.2 Relationship for Triaxial Variables

We define $q = \sigma_v - \sigma_h$ and $p = 1/3\ (\sigma_v + 2\sigma_h)$ in triaxial space p-q. Because:

$$S_{11} = \sigma_v - (\sigma_v + 2\sigma_h)/3 = 2/3\ q,$$

$$S_{22} = S_{33} = \sigma_h - (\sigma_v + 2\sigma_h)/3 = 1/3\ q.$$

Then:

$$J_2 = 1/2\ S_{ij}\ S_{ij} = 1/3\ q^2,$$

$$\Phi_s = 1/3\ q^2 - (a_0 + a_1 p + a_2 p^2),$$

or

$$3\Phi_s = q^2 - (\tau_0^2 + 2\tau_0 \mu p + \mu^2 p^2).$$

In Krieg's model, the symbol $\sigma_v = q$ and at $p = 0$, $q = \tau_0$.

In critical-state soil mechanics, for $\tau_0 = 0$ and critical state line $q - \mu_p = 0$, the slope $M = \mu$ corresponds to the slope of the σ_v-versus-p curve in Krieg's model.

The parameters μ (or M) and τ_0 can be expressed in terms of failure parameters from the Coulomb failure envelope,

$$S = c + \sigma_n \tan \Phi.$$

If

$$\tau_m = (\sigma_1 - \sigma_3)/2 \text{ and } P_a = (\sigma_1 + \sigma_3)/2,$$

then (Carroll, 1988, Ref. 53 in the main text)

$$\tau_m = d + P_a \tan \beta,$$

in which

$$\sin \Phi = \tan \beta,$$
$$d = c \cos \Phi,$$
$$s = \tau_m \cos \Phi,$$
$$\sigma_n = P_a - \tau_m \sin \Phi.$$

Now, we need variables:

$$q = 2\tau_m = \sigma_1 - \sigma_3,$$

$$p = (\sigma_1 + 2\sigma_3)/3 = P_a - \tau_m/3,$$

and

$$q = \tau_0 + \mu p \quad (q = \sigma_y \text{ in Krieg's model}).$$

Substituting for P_a and τ_m in the above equation, one gets:

$$\mu = (6 \sin \Phi)/(3 - \sin \Phi), \quad \tau_0 = c\mu \cot \Phi = (6c \cos \Phi)/(3 - \sin \Phi).$$